CHAPTER 1

INTRODUCTION

1.1 Background

Corrosion is a natural phenomenon involving degradation of materials (metals, plastics, polymers etc). Corrosion of metals, which is of more concern to engineers and scientists throughout the world, is an electrochemical process. It involves the oxidation of metals which results in metal loss. There are two basic types of corrosion; uniform corrosion and localized corrosion. Uniform corrosion as its name suggests refers to the corrosion that is uniform throughout the corrosion-affected metal surface. Whereas, localized corrosion is confined to a small area on the metal surface where it attacks more vigorously as compared to uniform corrosion. Corrosion affects metallic equipment efficiency resulting in undesirable situations.

1.1.1 Adverse Effects of Corrosion

Corrosion appears to be naïve to a common man or a common household. However, it is a constant threat to various industries dealing with metallic equipment on a larger scale. Statistics show that metallic corrosion has caused economic as well as human loss. For instance the annual direct cost of corrosion in US in 2001 was 3.1% of gross domestic product (GDP). Similar studies conducted in countries like United Kingdom, Japan, Australia, and Kuwait showed that the total annual cost of corrosion ranged between 1% to 5% of each country's gross national product (GNP). This is huge amount of economic assets that is being claimed by corrosion [1], [2].

Economic assets aside, here is a brief look at the failure statistics of corrosion. Pipelines have been a major source of transportation through ages. Since most, of the pipelines are

made of metal they too are not safe from corrosion especially oil and gas pipelines [3]. Failure statistics collected by US department of transportation indicates that 17% of reportable gas pipelines and 27% of reportable liquid pipelines failures are caused by corrosion [4].

Economic loss can be recovered but not the loss of human life. Corrosion has lead to many unpleasant incidents ranging from supply shutdowns to the extreme case of human casualties. Sewer explosion on April 1992, in Mexico killed 215 and injured 1500 people. The cause of accident was gas pipeline leakage due to corrosion, leading to an explosion. Another natural gas pipeline exploded in New Mexico on August 2000 due to severe internal corrosion of pipeline; number of casualties was 12 and damage to three vehicles [5]. Internal corrosion of pipelines is found to be the main cause of pipeline failures because it is always easier to detect and monitor external corrosion of pipelines as compared to internal corrosion. This results in unattended internal corrosion. Internal corrosion can be either uniform or localized or both. However, localized corrosion offers more damage to the pipelines and other metal equipment because it proceeds at a higher rate as compared to uniform corrosion and its is also concentrated to small regions which result is pipeline wall punctures leading to disastrous incidents mentioned earlier. There are many other examples in which corrosion played havoc by retarding the carrier ships resulting in massive oil spills in the ocean or making complete plant shutdowns due to equipment failures.

1.1.2 Monitoring Techniques

The situation presented in section 1.1.1 showed a grim picture of corrosion. However, humans are not completely helpless in this respect. By applying appropriate corrosion detection and monitoring techniques, preventive measures and awareness of corrosion related issues, the damaging effects of corrosion can be minimized.

Numerous corrosion monitoring and detection techniques have been established. Each having an edge over another in certain respects. Corrosion monitoring is the practice of acquiring information on the progress of corrosion-induced damage to a material or on

the corrosivity of the environment surrounding the material. As research over the corrosion phenomenon progressed, the advancement in the corrosion monitoring techniques and preventive measures also evolved greatly. A few of the established corrosion monitoring techniques reviewed in this research are described below (later to be reviewed in detail in Chapter 2).

- Coupons are the conventional method to determine the corrosion rate of metal by assessing the weight loss caused by corrosion to the coupons. Although widely used but coupons lack the ability to provide real time corrosion rates and also it is limited to provide uniform corrosion rates.

- Electrical resistance (ER) also measures corrosion rate based on the weight loss due to corrosion. However, this weight loss is translated in change in resistance of the monitoring probe and used to calculate the corrosion rate. Although being comparable to coupons the ER probes outshines it by providing real time corrosion rates. Though, ER probes can be very useful to provide real time uniform corrosion rates but in case of localized corrosion rates it has its limitations and cannot detect localized corrosion rates.

- Linear polarization resistance (LPR) is an electrochemical based technique. It determines the corrosion rate through the polarization resistance resulting due to application of small voltage to the electrode. LPR provides real time corrosion rates but this technique has its limitations too. LPR is widely used because of its ability to provide quick corrosion rates but it is confined to uniform corrosion rates only. In addition, for LPR measurements the monitored electrolyte has to be sufficiently conductive with low resistivity, otherwise LPR fail to produce accurate results.

- Electrochemical impedance spectroscopy (EIS) is also a very established corrosion rate measurement technique. Essentially its setup is similar to LPR with the exception that alternating voltage is applied as the excitation to the working

electrode and the resulting impedance is observed. The advantage of EIS over LPR is that it differentiates between the solution and the polarization resistance and hence it can be used to monitor corrosion rates in high resistivity electrolytes.

- Electrochemical noise (EN) provides estimated corrosion rates by observing the noise produced due to small voltage or current applied to the working electrode. Although EN has emerged as a promising technique to identify the type of corrosion and to some extent can identify localized corrosion however, it is still not a signature localized corrosion monitoring technique.

- Coupled multielectrode array sensor is an electrochemical based corrosion monitoring technique (details of CMAS are provided in Chapter 2). For the past decade coupled multielectrode array sensors (CMASs) have gained recognition based on their ability to detect and monitor real time online localized corrosion rates. CMAS has proved to work in diverse corrosive environments providing real time online localized corrosion rates and other corrosion related parameters [19]. However, its typical long cylindrical probe style design proves to be a hindrance in application in confine probe restricted areas.

1.2 Motivation

Until now it is seen that corrosion and in particular localized corrosion can lead to metallic equipment failure. Numerous corrosion monitoring techniques are developed and still are developing. CMAS is an emerging technique in monitoring localized corrosion. However, the commercially available CMAS are typically bulky and to use them in confine spaces e.g. very small pipes, small planar surfaces, valves etc. is not very feasible.

This motivated us to design and implement a cost effective, planar and miniaturized multielectrode array sensor (MAS). The aim is to operate this miniaturized planar MAS like the CMAS by monitoring real time localized corrosion rates. At the same time design it to be truly planar to become an easy solution for use in confine spaces.

1.3 Objective

The objectives of this work are:

1. To design and fabricate miniaturized and planar PCB-based MAS.
2. To assess PCB-based MAS corrosion detection capabilities by characterizing the fabricated sensor in different corrosive environments.
3. To assess the reliability of PCB-based MAS.

1.4 Scope of Study

The study can be categorized into (1) design and fabrication (2) characterization and (3) validation and repeatability.

- In the design and fabrication, the scope of the research will be confined to designing the sensor layout using CAD tools. Actual fabrication is done with the help of technician in PCB lab.
- As for the characterization. It is only done in controlled laboratory environment using equipments certified to measure low current. No read out circuit is considered in this work.
- Validation of reliability and repeatability is done by taking correlation of measured corrosion rates from samples of PCB-based MAS.

1.5 Thesis Outline

A brief outline of the following chapters is described in this section.

In Chapter 2 the basic phenomenon of corrosion is discussed in detail. This is followed by the review of various corrosion monitoring techniques which include weigh loss method (coupons), ER probes, LPR, EIS and EN. These techniques are discussed in

details with their governing equations and illustrations. After discussing theses techniques emphasis is laid on the background of multielectrode array sensing technique by discussing the first published work on the technique and then how it evolved into the present real-time corrosion rate sensors. This is followed by the working principle of CMAS and a detailed discussion of the corrosion rate equation used to deduce the corrosion rates, parameters governing this equation and then a brief introduction of PCB-based MAS sensor.

Chapter 3 will discuss the overall methodology that we adopted throughout the project. This will include the design of PCB-based MAS, its fabrication, experimental setup, characterization and data acquisition. The designing steps including the design criteria, software and schematic and board layouts are discussed in detail with the description of potential designs. In addition, the fabrication steps are also explained with the help of a flow chart and illustrations of the fabricated sensors. All experimental setups are discussed with the help of figures of the actual setups. Furthermore, the characterization including the data acquisition and analysis done are discussed. The equipment used for data acquisition is also shown and discussed with the help of figures. The equations used to analyse the data are also presented and explained in detail in this chapter.

Results obtained from detailed characterization of PCB-based MAS will be discussed in Chapter 4. This chapter is divided in three parts. The first section presents the results obtained with bare as well as with coated Cu traces that show the corrosion detection capability of PCB-based MAS in the form of anodic currents. These anodic currents are used to calculate the corrosion rates. These obtained corrosion rates in different corrosive environments are then analyzed and compared with the published data. The second section of this chapter includes the effects of conformal coatings on PCB-based MAS performance by analyzing the results from PCB-based MAS coated with different conformal coatings in different corrosive environments. These results are further validated by comparing it with the results obtained by using the electrochemical impedance spectroscopy EIS technique. Finally, the third section provides results to assess the ability of PCB-based MAS to produce reliable and repeatable results. A

complete discussion is provided with every result and at the end of each section of Chapter 4.

Finally Chapter 5 will present the conclusion and recommendations.

CHAPTER 2

LITERATURE REVIEW

2.0 Overview

In this chapter, basic phenomenon and types of corrosion is initially reviewed. This is followed by an overview of corrosion monitoring techniques. Multielectrode corrosion monitoring technique is reviewed in detail afterwards. Then the evolution of real time corrosion monitoring sensors called coupled multielectrode array sensor (CMAS) is presented. The working principle and the governing parameters of CMAS are also discussed in detail. PCB-based MAS is introduced briefly at the end of the chapter.

2.1 Corrosion

The word corrosion comes from the Latin word “corrodore” meaning to “gnaw away” [6]. There is a general opinion that only metals corrode. In contrast to this it is interesting to note that almost everything in nature is subject to corrosion including metals, ceramics, polymers and even our teeth. However, metallic corrosion is known to have relatively more adverse effects. This is why it has been a focus of interest for scientists and engineers for many years. Metallic corrosion, in general is electrochemical in nature. An electrochemical process is one in which electrons are produced as a result of a chemical reaction. According to corrosion experts, four components are essential for the onset and continuation of metallic corrosion. These are given as follows.

1. Anode
2. Cathode
3. Electrolyte
4. Metallic conductor

If either one of these factors is missing then corrosion would not take place. Scientists and engineers are usually interested in eliminating one or few of these factors to eliminate corrosion altogether. However, in most practical situations it is not possible. Returning to corrosion phenomenon, refer to Fig. 2.1. When metal dissolves in the corrosive solution it leaves electrons behind. These electrons move from the corroding electrode that is the anode to the less corroding electrode that is the cathode producing a current called corrosion current. If this current can be measured then the rate at which the metal is corroding or detoriating can be calculated. However things are not as easy as they first appear to be. Usually the anodic and cathodic sites on the corroding metal cannot be distinguished easily as they are randomly located on the metal surface.

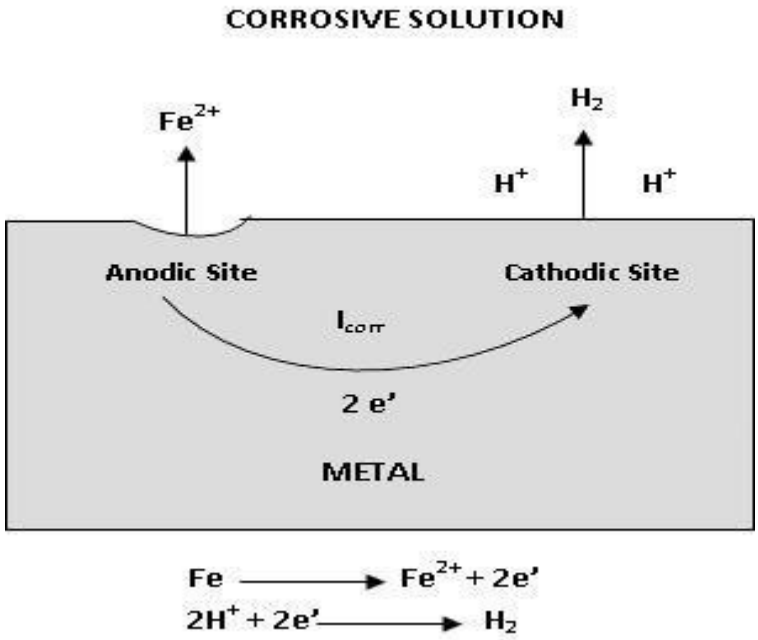

Fig. 2.1 Corrosion phenomenon is shown. Electrons produced at the anodic sites move towards the less corroded electrode. This flow of electrons produces corrosion current.

This was a general overview of corrosion. To have more clear insight of corrosion it can be compared to reactions in an electrical battery, in which electrical current is generated by immersing two dissimilar metals, called electrodes in a chemical solution (electrolyte) and connecting them with an external conducting wire, referred to as the return current path. This is called a galvanic cell. Fig. 2.2 shows the typical battery or a galvanic cell. The basic electrochemical reactions called redox (reduction oxidation) reactions occurring in a galvanic corrosion cell are fairly simple. In the cell shown in Fig. 2.2, the iron (Fe) anode on the left is corroding. Some of the iron atoms release electrons which travel across the electronic path and enter the cathode. This current is called the corrosion current. The loss of electrons changes the iron atoms from elemental iron (Fe^{0}) to ferrous iron (Fe^{2+}) and then to ferric iron (Fe^{3+}), leaving them with a strong positive charge. Some of the molecules of the electrolyte, in this case (H_20), are naturally separated into hydrogen ions (H^{+}) with positive charges and hydroxyl ions (OH^{-}) with negative charges. The positively charged iron atoms are attracted to negative OH^{-} ions. The attraction causes the iron atoms to leave the anode and enter the electrolyte, where they combine with OH^{-} ions. As atoms are lost, the metal surface of the anode deteriorates. This deterioration is corrosion. Note that the products of corrosion, $Fe(OH)_2$ and $Fe(OH)_3$, may accumulate on or near the corroded surface.

At the cathode, the negatively charged electrons arrive from the electronic path. The electrons are attracted to the positively charged H^{+} ions in the electrolyte. The attraction causes the electrons to leave the cathode and combine with the H^{+} ions, forming hydrogen gas (H_2). The gas may accumulate on the surface of the cathode. Note that the metal of the cathode does not corrode. In fact the reactions within the corrosion cells actually protect the cathode from corrosion. This fact forms the basis for cathodic protection. When different materials are used for the electrodes and electrolytes, the chemical reactions will be slightly different [7].

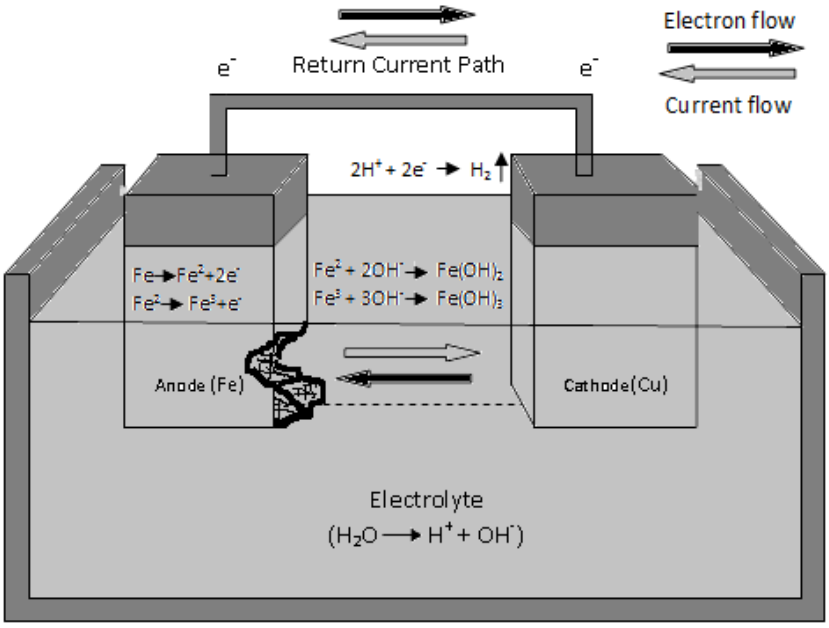

Fig. 2.2 A typical galvanic cell is shown along with the chemical reactions. The battery works on the same principle. When one electrode (anode) corrodes its sends current in the conductive path keeping the other electrode (cathode) intact.

The type of galvanic cell just described has two different metals immersed in a single uniform electrolyte. A second type of galvanic cell occurs when two pieces of the same metal are immersed in an electrolyte of uneven composition, as shown in the Fig. 2.3. Because of the uneven nature of the electrolyte a corrosion cell can develop. One piece of metal will become anode – it will corrode and feed electrons into the electronic path. The other piece of metal acts as the cathode – it will be protected from corrosion and will feed electrons into the electrolyte.

Figure 2.4(a) shows the same configuration as Fig. 2.3 - two electrodes of the same metal in a non-uniform electrolyte (corrosive solution). In Fig. 2.4(b), the two electrodes have been placed in direct contact with each other, eliminating the connecting wire. In Fig. 2.4(c), the two separate electrodes have been replaced by a single block of metal which has one area acting as cathode, another as an anode, with electrons flowing through the block and the metal block acts as the current path also [7]. Although in this illustration only one anode and one cathode is shown however in actual corroding metal there are numerous random anodic and cathodic sites.

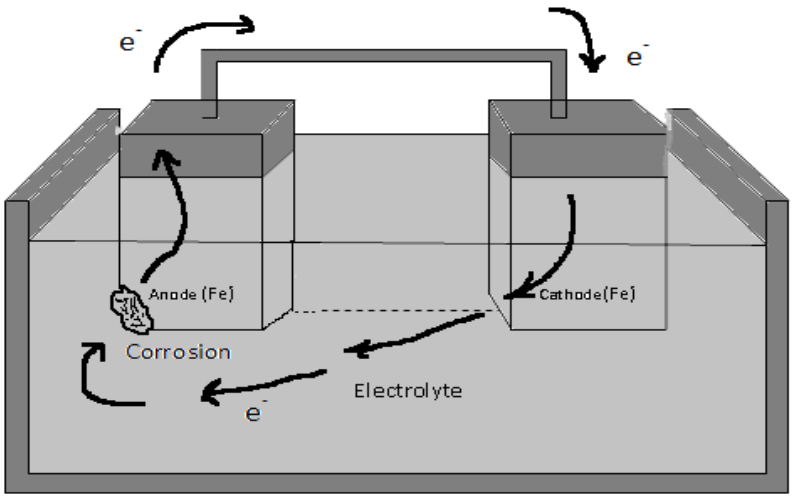

Fig. 2.3 Galvanic cell formed with corrosive electrolyte and electrodes of a single metal.

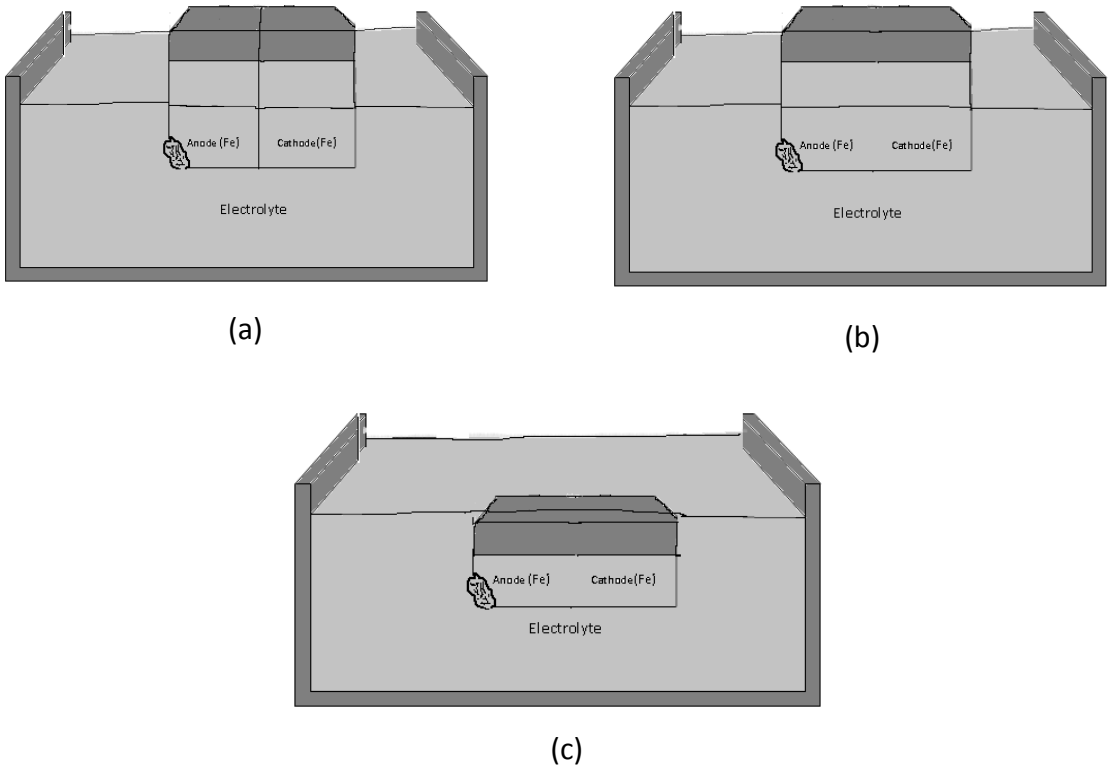

Fig. 2.4 (a) Corrosion of a metal piece is shown with respect to a galvanic cell. (b) the anode and cathode appear on the single metal piece. (c) the corroding metal in a corrosive environment with anode and cathode and the metal acting as the conductive path itself.

2.1.1 Faraday's Law

The current entry into and exit from an electrolyte is consequently always associated with electrode reactions which will be manifested as changes in the electrode materials or the environment. The quantities converted during electrode reactions are proportional to the amount of current which passes through the electrode surface. This relationship is expressed in Faraday's Law. It states that 96,500 Coulombs of charge transfer will oxidize or reduce One Gram Equivalent Weight of material involved in the electrochemical reaction. Hence the corrosion rate expressed as rate of uniform penetration for metals and alloys, from the measured current density by using Faraday's Law is give by Eq (1)

$$CR = \frac{iE_w}{F\rho} \tag{1}$$

In Eq (1), CR is the corrosion rate, i is the current density in μA/cm^2, E_w is the equivalent weight in g, F is the Faraday constant, equal to 96485 C/g-equivalent and ρ is the density of the metal in g/cm^3. The corrosion rate is commonly given in mils per year (mpy), millimeters per year (mm/yr) or in units of weight change per unit area per unit time (mg/cm^2.s) [6].

2.1.2 Types of Corrosion

Corrosion can be classified into two main types, uniform corrosion and localized corrosion. These main types can further be classified into various types according to the nature and properties of each type e.g. pitting corrosion, crevice corrosion, stress corrosion, galvanic corrosion and many more.

2.1.2.1 Uniform Corrosion

Uniform corrosion attacks the metal surface uniformly. In other words the corrosion proceeds at relatively same rate over the whole metal surface exposed to the corrosive environment.

In uniform corrosion, it is not possible to distinguish between the anodes or cathodes which are randomly emerging as a result of electrochemical process. The most common example of general corrosion is rusting of iron which occurs as a result of oxidation of iron metal. Fig. 2.5 shows the uniform corrosion of steel door [8].

Fig. 2.5 Corrosion of a ferritic stainless steel door in a sulphur-containing atmosphere Source: [8].

2.1.2.2 Localized Corrosion

Localized corrosion is one that is more concentrated or isolated to a certain area of metal surface exposed to corrosive environment. Pitting is the most common type of localized corrosion [6]. In localized corrosion the anodic and cathodic are clearly visible. As seen in Fig. 2.6 the pit is the anode surrounded by the cathodic sites. Localized corrosion and

pitting in particular is relatively more dangerous than uniform corrosion as it can produce more structural damage. What makes it even more dangerous is that sometimes the pits are not visible as they are covered by corrosion products but they continue to perforate the metal surface. Therefore, continuous localized corrosion monitoring is extremely important for metal equipment integrity.

Fig. 2.6 Pitting corrosion along the seam-weld, induced by chloride ions, caused failure of this stainless steel.

2.2 Review of Corrosion Monitoring Techniques

Due to time and space limitation, it is not possible to review each and every corrosion monitoring technique. Instead, few of the established techniques were reviewed and studied to have a clear insight on how corrosion can be monitored efficiently. This review helped to prepare a strong ground for this research. The reviewed corrosion monitoring techniques are classified under two categories; physical corrosion monitoring techniques and electrochemical corrosion monitoring techniques. The former technique monitors corrosion based on physical parameters and principles while the latter works on electrochemical principles to monitor corrosion.

2.2.1 Physical Monitoring Techniques

2.2.1.1 Weight Loss Method (Corrosion Coupon)

A very established corrosion rate measurement technique is weight-loss method in which a metallic coupon (see Fig. 2.7 taken from [9]) is weighed before it encounters the corrosive environment and then left to corrode. After some specific time the corroded coupon is weighed again. The difference in weight is used to calculate the corrosion rate by employing Eq (2).

$$CR = W_0 - W_1 / A \times T \quad (2)$$

In Eq (2), W_0 is the weight of the coupon before encountering corrosive environment. W_1 is the weight of the coupon after its corroded. A is the area of the coupon in square meter (m^2) and T is the time (in h) for which the coupon was left to corrode. The units for CR are g/ m^2h [10], [11].

This is by far the easiest way to calculate the corrosion rate. However, weight-loss method is limited to uniform corrosion detection only. Without visual inspection and applying other characterization techniques the nature of the corrosion, cannot be determined. In addition, this method does not provide real time data to determine corrosion rates. This is because the coupons have to be left in the corrosive environment for a particular time and after that the rate is determined. In other words the measurements are not frequent or real-time in case of weight-loss method.

Fig. 2.7 Corrosion Coupons. Source: [9].

2.2.1.2 Electrical Resistance (ER)

Electrical Resistance (ER) probe is another physical corrosion monitoring technique. Typical ER probes are shown in Fig. 2.8 (taken from [12]). ER probes outshine weight loss method because it provides real time data for corrosion rate detection. The ER probe is relatively easy to use and their maintenance is also low. The ER probe works on a principle that when a metal corrodes, metal loss occurs. This leads to a decrease in the cross-sectional area of metal and consequently an increase in its resistance. This relationship of cross sectional area and resistance is given in Eq (3).

$$R = \rho l/A \tag{3}$$

In Eq (3), ρ is the resistivity of the metal, l is the length and A is the cross-sectional area of metal. ER probe made of the same metal whose corrosion rate is to be determined, is exposed to the corrosive environment. A small current is applied across it and then the resulting potential drop is measured. By knowing the current and voltage, Ohm's Law is used to calculate the resistance. This resistance is compared with the resistance of the

original non corroded probe. The difference in resistance with respect to time is used to determine the corrosion rate.

ER probes are widely used because they measure the metal loss directly. This makes this technique comparable to weight loss or coupon method with an advantage of real time data acquisition. However, this technique has its limitations too. Although ER probes provide real time data but this technique is limited to uniform corrosion rate only. In case of non uniform corrosion like pitting, crevice or stress corrosion, ER probes produce erroneous results. This is because of the non uniform metal loss of the sensing probe [13]-[15]. This limitation restricts ER probes application in non uniform or localized corrosion monitoring conditions.

Fig. 2.8 Typical ER Probes. Source: [12]

2.2.2 Electrochemical Monitoring Techniques

Until now a couple of non electrochemical corrosion monitoring techniques are discussed. Since, metallic corrosion is an electrochemical process most of the corrosion

detection techniques work on electrochemical principle. Following is a review of some of the electrochemical corrosion monitoring techniques.

2.2.2.1 Linear Polarization Resistance (LPR)

Linear polarization resistance (LPR) is an electrochemical based corrosion monitoring technique. Its working principle is simple. An electrochemical excitation is applied to an electrode and response of this electrode against a reference electrode is used to measure the corrosion rate (see Fig. 2.9 taken from [16]). The excitation can either be voltage excitation or current. In the case of voltage excitation a small voltage is applied to the electrode in increasing steps and the resulting current response is measured. The electrode potential moves away from the corrosion potential hence it is polarized. The resulting resistance is called polarization resistance R_p. R_p is the slope of the current potential plot around the corrosion potential and Stern and Geary found that this slope is essentially linear. This is how this technique is called linear polarization resistance. Once R_p is calculated, it is used to obtain corrosion current I_{corr} using Eq (4) in which B is a constant. Equation for calculating B is widely available in literature.

$$I_{corr} = B/R_p \tag{4}$$

LPR being an electrochemical based monitoring technique provides corrosion rate much faster than ER. However, again LPR is limited to uniform corrosion detection only. Localized corrosion makes the LPR measurements complicated. Another limitation of LPR is that it requires a sufficient conductive liquid for corrosion monitoring. This condition makes LPR not suitable for less conductive corrosive environments e.g. corrosion under thin films or under coatings etc [15], [17], [18].

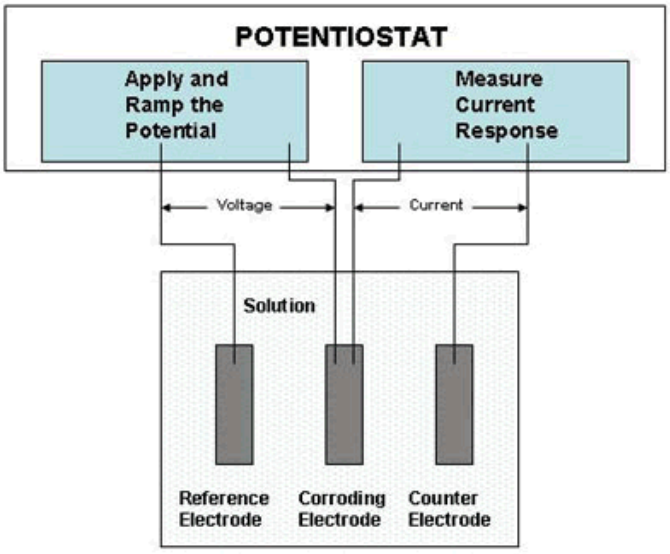

Fig. 2.9 Schematic of LPR measurement. Source: [16].

2.2.2.2 Electrochemical Impedance Spectroscopy (EIS)

Electrochemical impedance spectroscopy as its name suggest is also an electrochemical based technique. Its measurement setup is similar to LPR with the exception that the sensing element or the working electrode is polarized by application of an alternating potential that in turn produces an alternating current response. For corrosion monitoring, the frequency range of the applied ac polarization is typically between 0.1 Hz to 100 kHz with the polarization level within 10mV to 50mV. As result of ac polarization EIS measures the resultant impedance which caters the solution and polarization resistance separately [19] as seen in Fig. 2.10

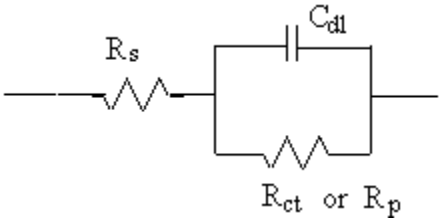

Fig. 2.10 Schematic of the impedance measured by EIS.

This makes EIS outshine LPR because due to its inability to differentiate between solution and polarization resistance LPR can only work in high conductive, low resistive corrosive electrolytes. In contrast to this EIS can measure corrosion rates efficiently even in high resistive and low conductive electrolytes. The Eq (5) shows the impedance calculated by EIS.

$$Z_{(\omega)} = R_s + \frac{R_p}{1 + (j\omega R_p C_{dl})} \tag{5}$$

In Eq (5) $Z_{(\omega)}$ is the impedance, R_s is the solution resistance, R_p is the polarization resistance, ω is the ac polarization frequency and C_{dl} is the double layer capacitance which appears between metal surface and the electrolyte. EIS also make use of Stern Geary equation mentioned above (see Eq (4)) to obtain corrosion rates. Although EIS is a very established technique, its use in field tests is still limited mainly due to the large and sophisticated data acquisition and analysis equipments [20].

2.2.2.3 Electrochemical Noise (EN)

Another electrochemical corrosion monitoring technique is electrochemical noise (EN). EN detects and monitors the fluctuation in potential, electrochemical potential noise (EPN) or current, electrochemical current noise (ECN) on the corroding electrode and determines the electrochemical noise resistance R_n. This R_n is used to estimate the corrosion rate. Besides corrosion rate EN is known to identify the type of corrosion. In some systems EN is also used along LPR to identify the onset of localized corrosion [21]. However, EN measurements are complicated and lengthy. In addition, although EN can provide the information regarding localized and pitting corrosion but it does not quantitatively provides the localized corrosion rates, hence it is not a signature localized corrosion monitoring method [22], [23].

2.3 Overview of Multielectrode Array Corrosion Monitoring Technique

Mulielectrode array systems have been used in various fields of science. They have application in field of medicine where they are used as DNA sensors for electrochemical gnotyping or as hypodermic continuous glucose monitoring systems [24], [25].

In the field of corrosion monitoring, detection, study of corrosion processes and in particular localized corrosion, Multielectrode array systems have been a milestone. The first multielectrode system for corrosion monitoring emerged only two decades ago. This technique then advanced rapidly and for the past decade it has evolved as real time corrosion monitoring sensors known as CMAS. A summary of the advancement of multielectrode array from the time of their start to the currently available CMAs is discussed below.

Evidence of usage of coupled multielectrode systems for corrosion monitoring for the first time goes back to 1991 when a patent was issued in US by Peter Schiessl. He claimed a corrosion measuring cell for structural or reinforcing steel embedded in a concrete part having an exterior surface [26]. Fig. 2.11 shows the multielectrode system used by Schiessl to monitor steel corrosion in concrete. This system consisted of a number of electrodes (anodes) made of steel and a cathode made of a corrosion resistant material. The electrodes in this system were distinguished as anodes because they were made of the same material whose corrosion had to be monitored which was steel. The sole electrode distinguished as cathode was made of corrosion resistant material. In corrosion process metal loss occurs at anode and cathode remains intact. Similarly in this system the corrosion would affect the steel electrodes i.e. the anodes and the corrosion resistant electrode i.e. cathode would remain intact thus simulating the actual steel corrosion. These anodes and cathodes were placed inside the concrete structure at different distances from the surface as seen in Fig. 2.11. Each anode was connected to the cathode separately through a resistor (this system is called coupled multielectrode system because all the electrodes were connected to each other all the time). The voltage across each resistor was measured to derive the current flowing between each anode and cathode [27].

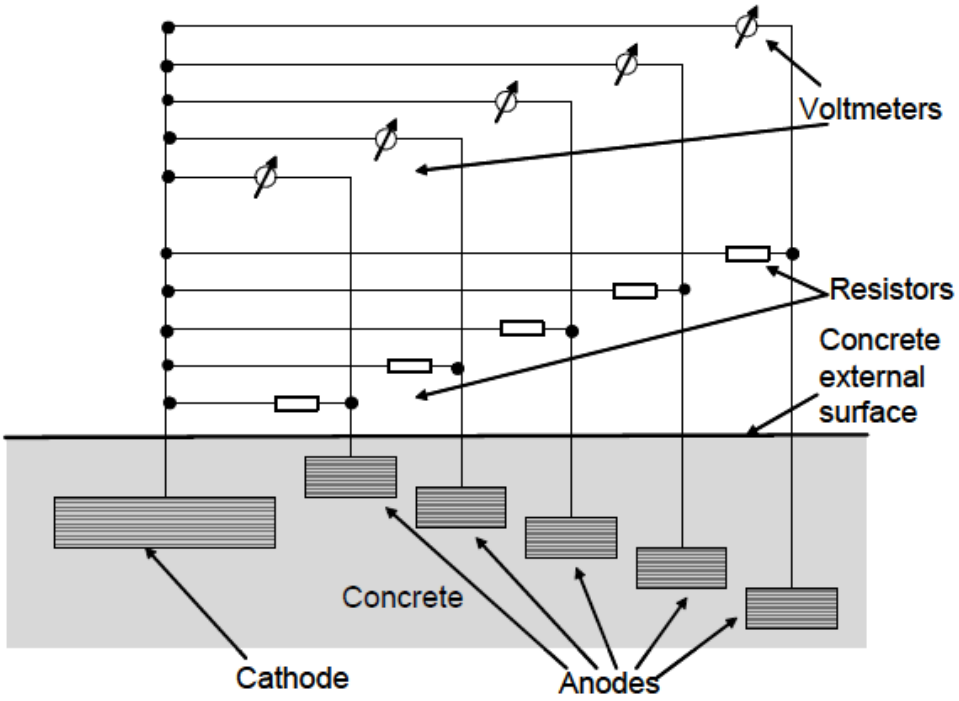

Fig. 2.11 Multielectrode system used by Schiessl to monitor corrosion of steel in concrete. This system consisted of multiple carbon steel anodes all coupled separately to a corrosion resistant cathode made of special steels or alloys. Source: [27]

L. Yang and N. Sridhar [27] reported that Steinsmo and coworkers published their work of using galvanically coupled multielectrode systems to study crevice corrosion of steel in sea water. This system was galvanically coupled because the anode and cathode were made of different materials. It is worth highlighting that the mentioned work was based on multielectrode systems not multielectrode array systems, because although it included multielectrodes but the electrodes were not arranged in a fixed pattern.

This system being the first multielectrode system for corrosion monitoring could detect the onset of general or localized corrosion but fail to determine the actual general or localized corrosion rates because of the large size of anodes.

In [27], it is also shown that in 1991 Tan and Tan, et al. reported the first uncoupled multielectrode array also called wire beam electrode (WBE) to study the corrosion behavior of carbon steel under oil based coatings. This uncoupled WBE consisted of wires of metal /alloy (of diameter in the range 0.5-2 mm) acting as electrodes arranged in

a square shape. The wires were isolated from each other by flush mounting them in epoxy with the cross-section of electrodes being exposed to corrosive environment. Open circuit potential of each electrode and current or resistance between selected pair of wires was used to study the corrosion processes.

L. Yang and N. Sridhar [27] also reported that later in 1996 Fei, et al. reported the first coupled multielectrode array for the first time to study the spatiotemporal behavior of iron metal in sulphuric acid solution. The system used by Fei was almost similar to the system used by Tan and Tan. et al, with electrodes/ wires flush mounted in epoxy. The electrodes were arranged in a fixed pattern or arrays with different shapes like square, hexagon etc simulating a single piece of metal. As seen in Fig. 2.12 this system was different because the current flowing through each electrode was measured independently using a multichannel zero resistance ammeter (ZRA) as opposed to measurement between selected pair of wires in Tan and Tan et al. The common coupling point of this system was connected to the potentiostat as working electrode (WE) to study the electrochemical spatiotemporal pattern of the electrodes at different potentials. These kind of coupled multielectrode arrays have been used significantly to study the corrosion processes of various metals.

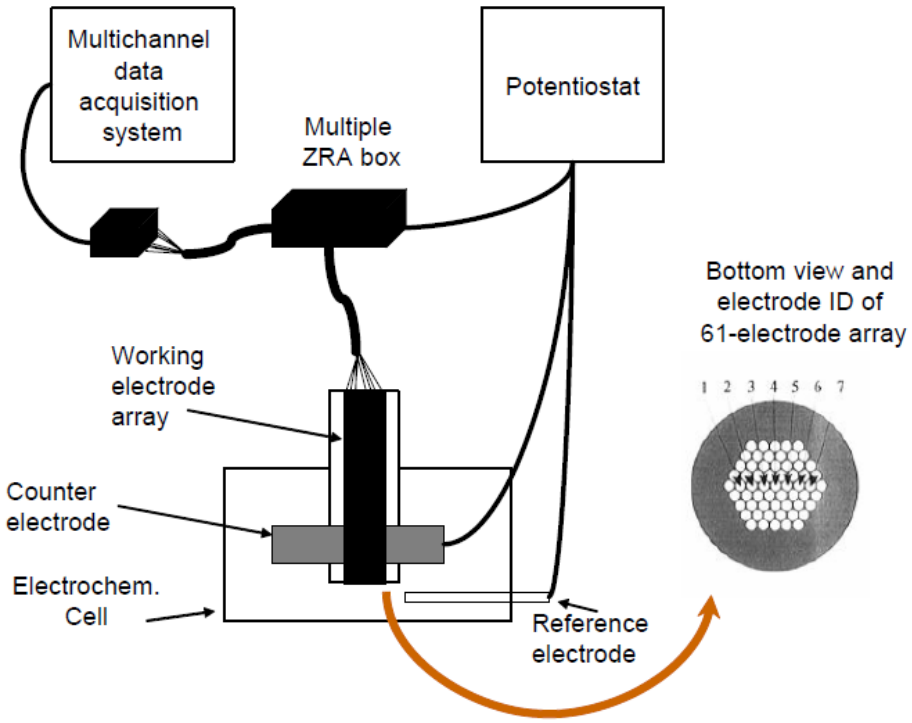

Fig. 2.12 Coupled multielectrode array used by Fei, et al. to study the spatiotemporal behavior of iron metal in sulphuric acid. The current of each electrode was measured independently using a zero resistance ammeter box. Source: [27]

In 1997 Tan [28], [29] published his work in which he used coupled WBE to study localized corrosion current and potential for carbon steel electrodes. As shown in Fig. 2.13 the current through each electrode was measured by temporarily decoupling it from the common coupling point. Similarly the potential of each electrode was measured against a reference electrode using a voltmeter. They used Eq (6) derived from Butler Volmer equation to calculate the corrosion current of each electrode.

$$I_{ka} = I_{kcouple} / \left\{1 - \exp\left[-\left(\frac{2.3}{b_{ka}} + \frac{2.3}{b_{kc}}\right)\left(E_{coup} - E_{kopen}\right)\right]\right\} \qquad (6)$$

In Eq (6) I_{ka} is the anodic current from k electrode, $I_{kcouple}$ is the coupling current from electrode k while b_{ka} and b_{kc} are the anodic and cathodic tafel slopes respectively. E_{kopen} is open circuit potential of electrode k and E_{coup} is the coupling potential of all electrodes. WBE have been used extensively to study localized corrosion behaviour.

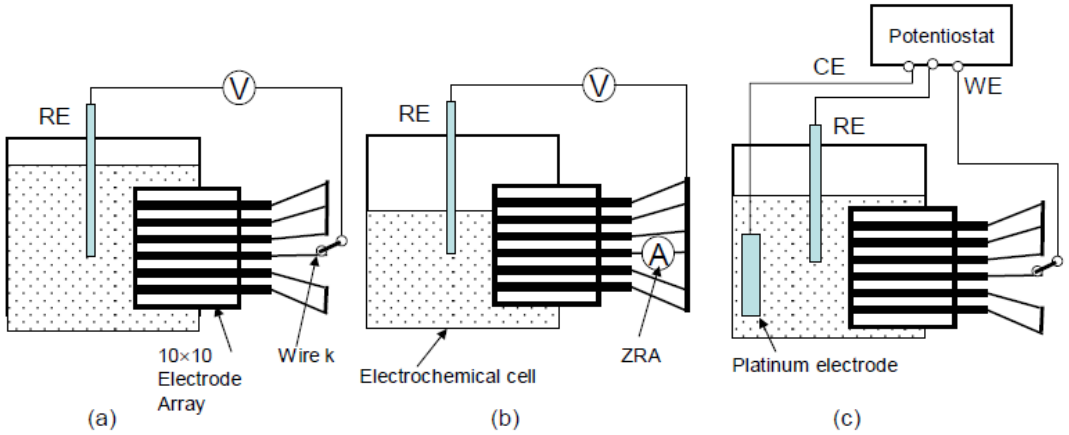

Fig. 2.13 Coupled multielectrode array system used by Tan. (a) shows the measurement of open circuit potential of each electrode. (b) The current measurement of each electrode. (c) measurement of tafel slopes of each electrode. Source: [27]

All these multielectrode array systems either coupled or uncoupled, have proved to provide a valuable assistance in understanding and monitoring the corrosion phenomenon. However all the techniques presented in the overview required lengthy and complicated measurement of more than one parameters to either study or monitor corrosion.

L. Yang [30]-[32] and his co-workers made use of the coupled multielectrode arrays and came up with a real time localized corrosion monitoring sensor called CMAS shown in Fig. 2.14. CMAS probes are made by using array of same metal/alloy whose corrosion rate has to be monitored with diameter typically in the range of 0.5-2 mm. These electrodes are flush mounted in epoxy to isolate them from each other. Although the electrodes are electrically isolated from each other, however, they are externally connected or coupled to a common coupling point through resistors as seen in Fig. 2.15.

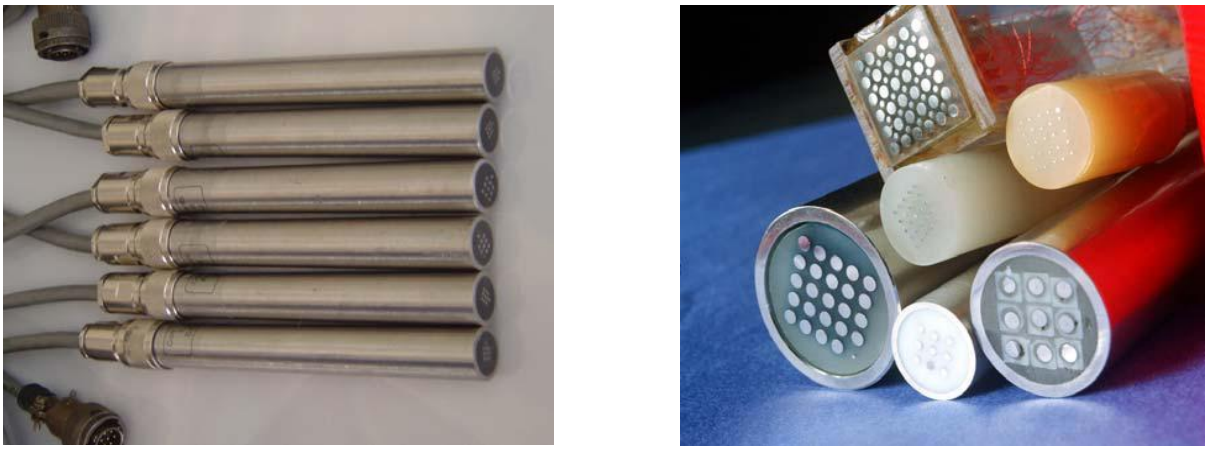

Fig. 2.14 Typical CMAS probes. Source: [27]

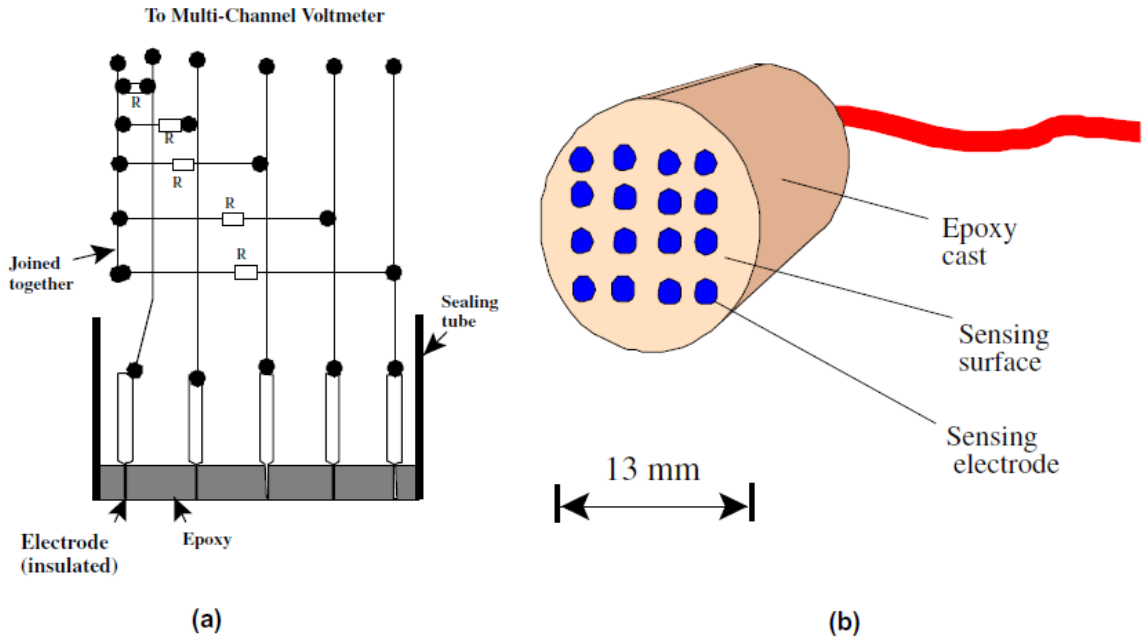

Fig. 2.15 (a) Electrodes of CMAS isolated from each other and connected externally through resistors. (b) Schematic of a CMAS probe Source: [31]

The CMAS is revolutionary in the respect that it has simplified corrosion monitoring especially for industrial application where most of the operators are not familiar with corrosion. The corrosion rate measurement is made easy by focusing on one parameter which is the most anodic current. In addition, CMAS has the ability to detect and monitor localized corrosion rates under numerous corrosive environments ranging from corrosion under cathodic protection conditions to corrosion in high pressure simulated natural gas systems [33]-[40]. The following sections describe the working principle, corrosion rate equations and parameters in detail.

2.4 Working Principle of CMAS

When CMAS encounters a corrosive environment, its electrodes which are of the same metal whose corrosion rate has to be monitored simulate a single metal piece (see Fig. 2.16). Randomly some of the electrodes become anodic and some become cathodic. By simulating a single metal piece it is meant that as anodic and cathodic sites appear in a metal when it encounters corrosion, the use of array of electrodes is meant to simulate those electrodes. The formation of anodic and cathodic sites is based on the nano level structural differences in the composition of metal. As mentioned earlier that the onset of anodic and cathodic sites produces a current flow between these electrodes. As the electrodes are isolated from each other (in case of a metal piece the electrodes are connected to each other through the metal itself, see Fig. 2.4) the current flows through the external circuitry. It is worth mentioning that this corrosion current moves into the anode (due to release of electrons from anode) and out of the cathode, this is because anode release electrons due to metal loss and we know current moves opposite to the direction of electrons. Therefore, anodic current is *negative* while cathodic current is *positive*. This current flow produces a very small potential drop across the resistors which is measured and converted to current using Ohm's law. This current is the determining factor in calculating the corrosion rate. The corrosion rate equation is discussed in detail in the next section. CMAS is particularly focused on detecting and monitoring localized (pitting, crevice) corrosion rates. When CMAS encounters corrosive environment usually there is an electrode which is significantly more anodic than rest of the electrodes. This

simulates a localized corroded metal piece where the pit or crevice is highly anodic while the surrounding is cathodic. This is why the corrosion current (most anodic current) from this significantly anodic electrode act as the pivotal parameter to determine the localized corrosion rate.

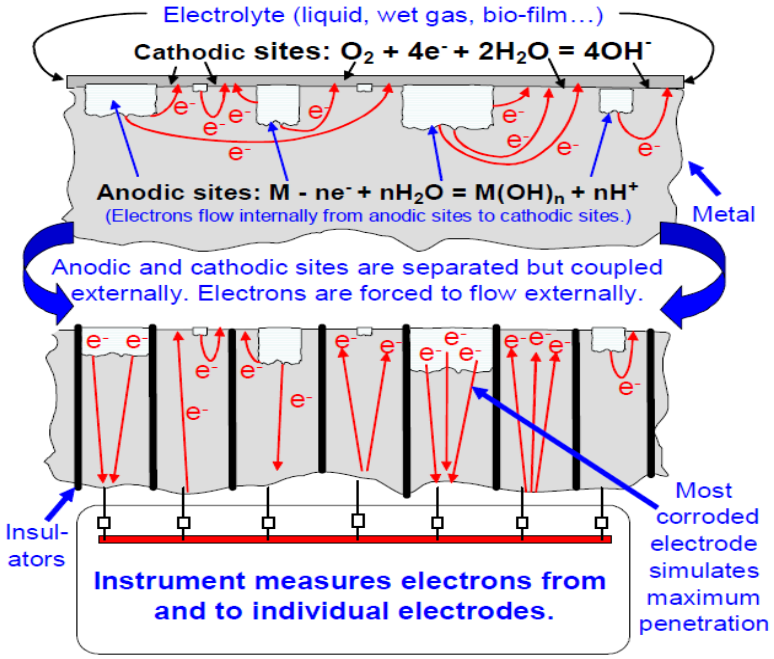

Fig. 2.16 The localized corrosion of metal is shown where the current between anode and cathode flows within the metal surface. CMAS consist of electrodes isolated from each other but connected externally through resistors. Source: [27]

2.5 Maximum Localized Corrosion Rate Equation and Parameters

The Faraday's Law shown by Eq (1) relates the uniform corrosion rate to the current density. However, to find localized corrosion rate the standard Faraday's Law could not be used used. Therefore, Eq (7) is used to calculate the maximum localized corrosion rate. It is derived from Faraday's Law by the pioneers of CMAS [27], [30]

$$CR_{max} = (1/\epsilon)\, I^{a}_{max}\, W_e/(F\rho A) \tag{7}$$

In Eq (7), CR_{max} is the maximum penetration rate, ε is the current distribution factor (fraction of the electrons produced on the most corroding electrode that flows to the other

electrodes through the coupling circuit), F is the Faraday constant (96485 C/mol), A is the surface area of the electrode (cm^2), ρ is the density of the alloy or electrode (g/cm^3), and the W_e is the equivalent weight (g/mol). I^a_{max}, on the other hand, is the maximum anodic current determined either by taking only the maximum measured anodic current or three times the standard deviation of all measured anodic currents to increase the confidence level of the measured corrosion rate [27], [30], [40]. In addition, ε is taken to be unity based on the assumtion that the electrode will corrode uniformly due to its very small size (the electrode size in CMAS is relatively 2 to 3 orders smaller than typical LPR electrodes, therefore this assumption is valid) [30].

Eq (7) was derived from the Faraday's Law by introducing one new parameter which was ε and instead of using current density, the most anodic current I^a_{max} and the surface area of the electrode are used. The ε and I^a_{max} make this derived equation specialized for localized corrosion rates because in localized corrosion only the pit produces most anodic current while rest of the surrounding surface of the metal produces cathodic current. Therefore the maximum anodic current in Eq (7) will represent the pit or the localized corrosion effected metal area with surface area as that of the electrode A. Although ε also plays important role in corrosion rate equation, however, reasearch is underway to study its effect on the corrosion rate [30]. Until its effects are completely analyzed and it is assumed unity in all the experimental setups.

Although Eq (7) uses the most anodic current I^a_{max} as the determining parameter of corrosion or penetration rate. However, sometimes the most anodic electrode is not completely corroded which results in the presence of some cathodic sites (see Fig. 2.17). This is also true in case of cathodic electrodes. They may also contain some anodic sites but the focus of interest are the anodic electrodes mainly. It is believed that all the current flow between the anodic and cathodic electrodes in CMAS is through external circuitry. However, due to the presence of some cathodic sites on less corroded anodic electrodes, some of the current start to flow within the electrode rather than flowing through the external circuitry. This small current flowing within the electrode is called internal current expressed in Eq (8).

$$I_a = I_a^{ex} + I_a^{in} \quad (8)$$

Equation (8) shows that the total anodic current of an anodic electrode is the sum of the external anodic current (flowing through the external circuitry) and the internal anodic current (flowing within the anodic electrode due to local cathodic sites).

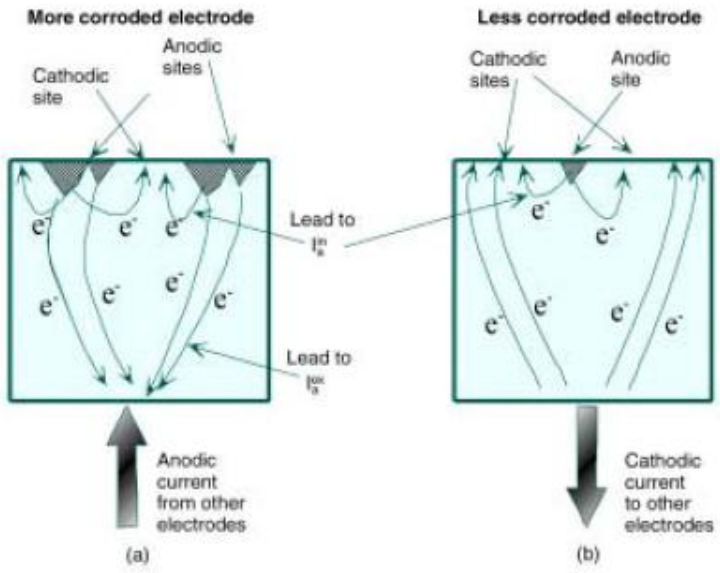

Fig. 2.17 (a) Partially corroded electrode with local cathodic sites. (b) Slightly corroded electrode with local anodic sites. Source: [30]

Although the presence of cathodic sites on the anodic electrodes cannot be eliminated altogether. However, L. Yang and his co-worker came up with an instrument that polarizes the common coupling point in CMAS in a way that the anodic current flows entirely through the external circuitry [38]. Actually the potential through the most cathodic electrode is measured and considered to be the highest cathodic potential among all the electrodes in the CMAS. The common coupling point is polarized to a potential slightly higher than this most cathodic potential. This way all the anodic current flows

through the external circuitry rather than flowing internally. This way internal current flow is reduced to a greater extent.

According to L. Yang and et al. in [30] the anodic current may also be expressed as in Eq (9)

$$I_a = I_a^{ex}/\varepsilon \tag{9}$$

As menioned earlier that ε is the current distribution factor. Its value varies between 0 to 1. If the electrode is completely corroded all the current will flow through the external circuitry and the value of ε will be close to 1. If there are some local cathodic sites, there will be internal current flow then ε will be close to or equal to 0.

However, in most of the CMAS experiments ε was considered unity based on the assumption that the electrode corroded completely. This assumption is taken due to the small size of CMAS electrodes ~ 2 to 4 times smaller than typical LPR or EN electrodes.

Another important point is that to increase the confidence level of the corrosion rate measurements L. Yang and et al. prefered using a statistical parameter like 3 times standard deviation of all anodic or both anodic or cathodic currents. 3 times standard deviation define a confidence level of 99.86% for normal distribution [30], [32], [42].

2.6 Introduction to Planar PCB-based MAS

As discussed earlier the existing CMAS probes have a limitation to be used in confine spaces so a planar PCB- based MAS is demonstrated in this work. We have called it MAS rather than CMAS because although the electrodes are coupled in our sensor but due to experimental limitations we will have to decouple the electrodes to measure the current so we prefer to call it MAS. Its working principle is the same as that of CMAS. The detailed look at how the existing concept of circular linear CMAS probes are designed in a planar sensor with the same working principle intact, how PCB is used for fabrication and later the detailed characterization is presented in the next chapters.

2.7 Summary

In this chapter, corrosion phenomenon is discussed in detail. In addition, uniform and localized corrosions are also discussed with illustrations to help in understanding the working principles of various kinds of multielectrode arrays. The corrosion monitoring techniques both physical and electrochemical techniques are reviewed. The multielectrode array overview reflects that multielectrode arrays have been a useful tool in studying and monitoring localized corrosion. Moreover, CMAS have proved to simplify corrosion monitoring to a greater extent. Its working principle, corrosion rate equations and parameters are discussed in detail because they have to be used later in this research. Finally, a brief introduction of PCB-based MAS is provided to show how it is related to the existing CMAS technology.

CHAPTER 3

METHODOLOGY

3.0 Overview

In this chapter design, fabrication and characterization processes of PCB-based MAS will be discussed. Software used in this work and the sensor layout will also be described. This will be followed by the fabrication steps. Finally the experimental setup and data acquisition procedure will be explained in detail.

3.1 Designing the Planar PCB-based MAS

As mentioned earlier, the objective of this research is to develop a planar and miniaturized multielectrode array sensor. To meet this objective, several criteria need to be considered when designing the PCB-based MAS.

3.1.1 Design Criteria

CMAS probes typically have long metallic wires as electrodes. These wires are flush mounted in epoxy and electrically isolated from each other. To monitor corrosion, the cross-section of these wires is exposed to corrosive environments while the rest of the surface is completely secured in epoxy.

This linear cylindrical design had to be made planar. In order to achieve this goal, two technologies were considered. These techniques are the CMOS and PCB. Employing CMOS technology it was thought that planar electrodes could be

deposited over a silicon substrate with SiO_2 working as the insulator between the electrodes. However, with CMOS being chosen as the fabrication technique there were a few challenges. One, this planar MAS for corrosion monitoring was being fabricated for the first time and there were chances of error in the design. Second, the the facility of CMOS fabrication is lacking at the moment which means that the designs had to be sent somewhere else to be fabricated. For optimum design the fabrication probably had to be done many times. Therefore, keeping these points in view PCB was chosen for a few reasons. One, it was cost effective as compared to CMOS. Second, the PCB fabrication facilities are available in the university. This would be helpful in making as many designs as possible without being worried about the time as in case of CMOS if designs are sent somewhere else.

Once, PCB was chosen as the fabrication technique, design steps were worked upon. The first criterion for PCB-based MAS design was the electrode size or diameter. Since PCB-based MAS is the miniaturized version of CMAS. The electrode diameter should be in the same range of 0.5mm to 2mm. This is the optimum range of electrode size defined in the literature for CMAS probes [27] [30]. Hence remaining in this optimum range, the electrode size was chosen to be 1.5mm in this research. Optimization of electrode size is considered out of the scope of this research.

Since, the electrodes have to be of some metal or alloy and PCB boards are widely available with copper (Cu). Therefore, Cu was chosen as the sensing element.

In CMAS the path for corrosion current to the external circuitry is the electrode itself (see Fig. 3.1). However, in planar design, a conductive path was required between the planar electrodes and external circuitry for current measurement. Since Cu is a good conductor of electricity and also to make our design simple, it was decided that both the electrodes and the conductive path would be fabricated of Cu.

The minimum trace width (trace is the Cu path) achievable in our PCB laboratory is 10 mils (equals to 0.01 inches). Since the corrosion current produced during the corrosion monitoring is very small, it was assumed that the width of the trace had no

effect on the current flow. Therefore, the trace width was chosen to be as minimum as possible, to miniaturize the design, which is 10 mils.

Finally, for the external circuitry it is seen that in CMAS the anodic current or cathodic current was measured by measuring the potential across each resistor using a multi channel nano voltmeter (see Fig. 2.15). This potential is then converted to current. This approach is very practical regarding a system level solution. However, for research purposes and simple approach it was decided to measure the current directly rather than measuring the potential first and then convert it to current. Therefore resistors were not incorporated in the design.

One important point to highlight over here is that the PCB-based MAS can be compared with the galvanic cell shown in Chapter 2 (see Fig. 2.3). In that galvanic cell there was only one anode and one cathode connected to each other through a conductive path for current flow. Now PCB-based MAS can be visualized in the same manner but since it contains several electrodes so now there will be several galvanic cells all of them coupled through the conductive path, in our case we call it the common coupling point. So randomly, some of the electrodes would be anodic and some would be cathodic. The current from each half cell of galvanic cell (electrode) will be measured by temporarily decoupling it from the common coupling point and placing the ammeter in series to measure the current flowing due to that particular electrode into the common coupling current path. Out of these electrode currents the most anodic (negative current) will be used to calculate corrosion rate.

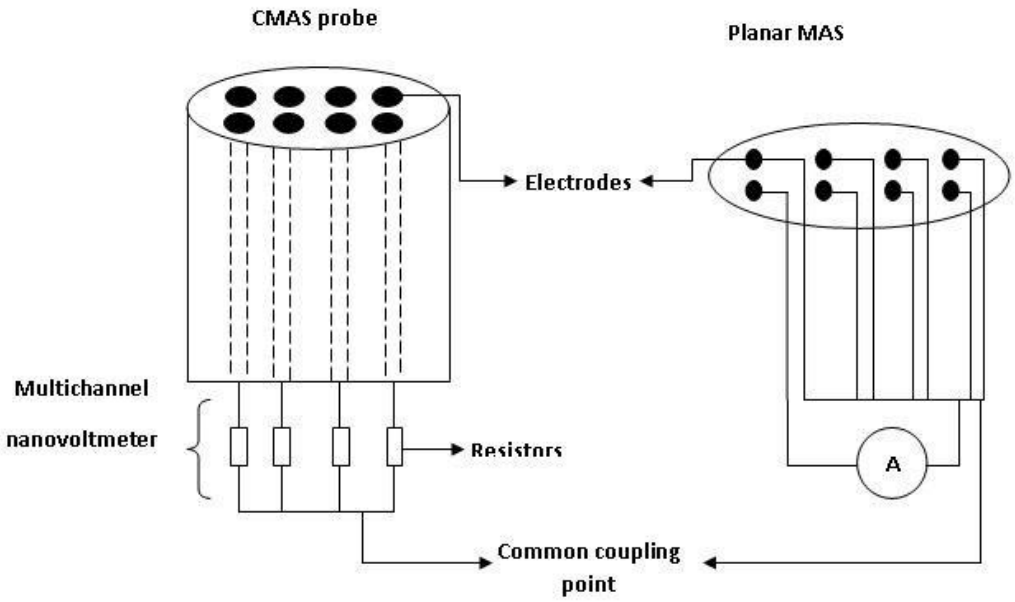

Fig. 3.1 The conversion from cylindrical to planar design is shown. The electrodes in a CMAS probe are connected directly to the resistors. However, in planar design a conductive path is required between the electrodes and the current measurement device

3.1.2 Software Tool

Eagle software 5.0.1 is used to design the schematic and board layout for PCB-based MAS. This software is widely used for designing PCB circuits and is very user friendly. It can be run on Windows, Linux or Mac OS.

Fig. 3.2 shows the Eagle schematic layout editor window. The command tool bar is on the left side of the window. It contains separate tabs for each command. The most common commands like component library access, cut, copy, paste, move, name, value (e.g. resistors values), text etc. are all performed by using different tabs in the command tool bar. The wire is also selected from this tool bar. The action tool bar containing tabs for zoom in, zoom out, undo, redo, schematic conversion to board layout etc. is present on the upper side of the window. The coordinate measurements (x, y) are also shown with respect to the movement of the mouse below the action

tool bar. It should be noted that a circuit cannot be simulated using Eagle software. In order to simulate the circuits other simulator software can be used.

The general rule of designing PCB circuit in Eagle is that initially the schematic is designed using this schematic editor window. Once the schematic containing all the components is prepared it is converted to the board layout using the tab in the action tool bar. Fig. 3.3 shows the Eagle board layout editor window. It has the similar action and command tool bars.

The basic difference between schematic and board layouts is that the schematic shows the actual components in the circuit. However, the board layout only shows the foot print of the components as they would appear on the actual PCB board.

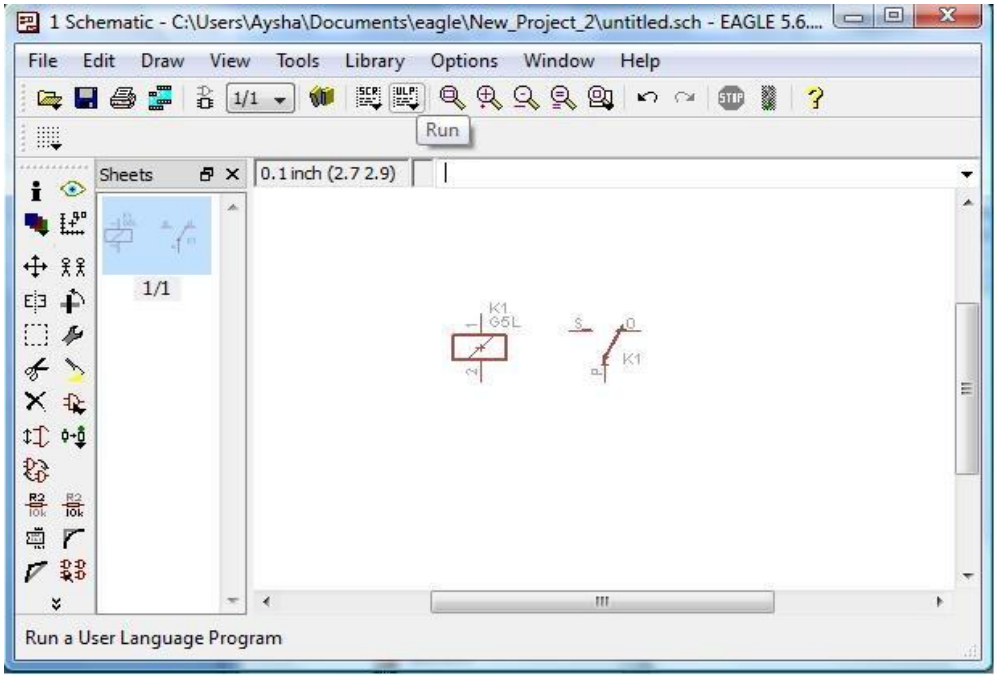

Fig. 3.2 The schematic layout editor window of Eagle software has the action tool bar on the upper side while the command tool bar on the left side. Schematics can be easily drawn by using different tabs in the tool bars. A simple relay is shown as an example.

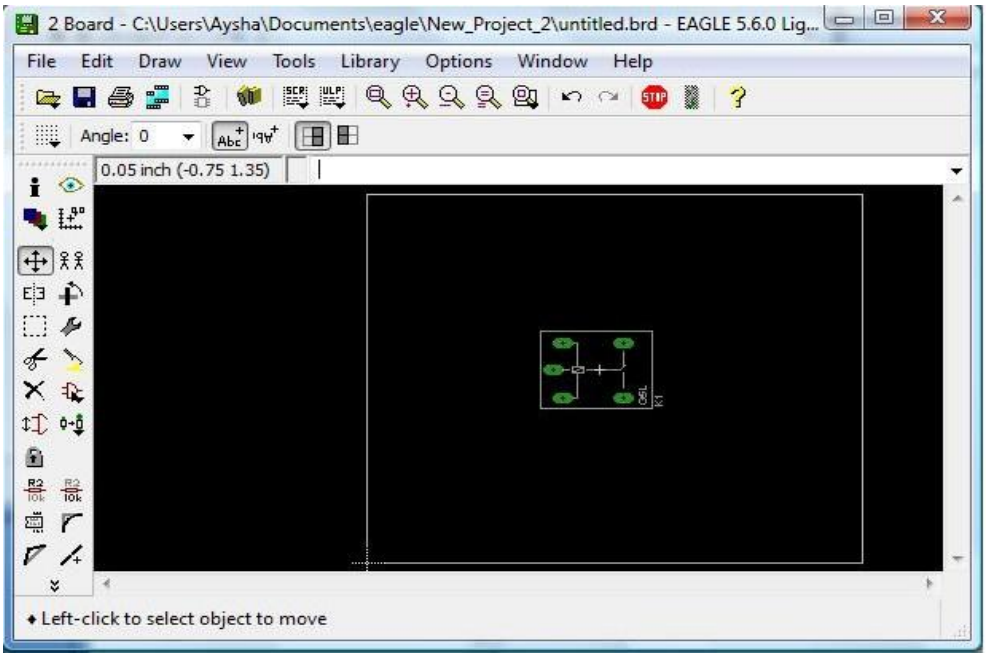

Fig. 3.3 The board layout editor window in Eagle software is similar to the schematic layout editor window with almost similar tool bars. The exception is that in the board layout only the foot prints of the components appear in the circuit. As the five pins of the relay can be seen in this board layout.

3.1.3 Schematic Layout of PCB-based MAS

For a typical circuit the schematic consists of the electronic components (e.g. resistors, capacitors, ICs etc) and the wires connecting these components. However, for design of PCB-based MAS there are no components involved. The requirement is to pattern copper in a particular configuration with contact pads for connecting these electrodes externally. Three schematic layouts of PCB-based MAS were designed for fabrication. Fig. 3.4, Fig. 3.5 and Fig. 3.6 show these three schematics. Each Cu electrode or contact pad was represented by a pin hole in the schematic. One pin hole represents the foot print of an IC pin in the board layout. The design configuration is more clearly visible in the board layouts.

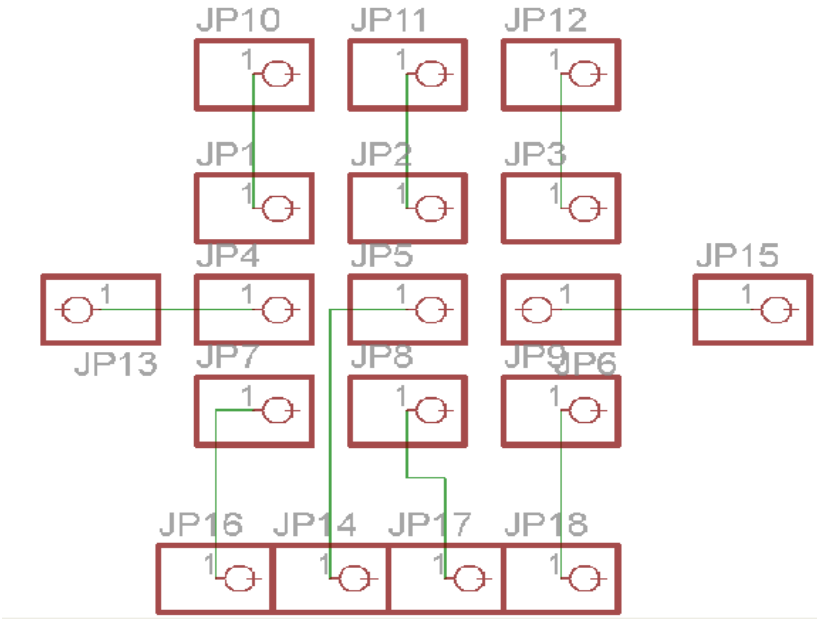

Fig. 3.4 The schematic of Design 1 of PCB-based MAS. Pin heads are used to schematize the electrodes and the contact pads.

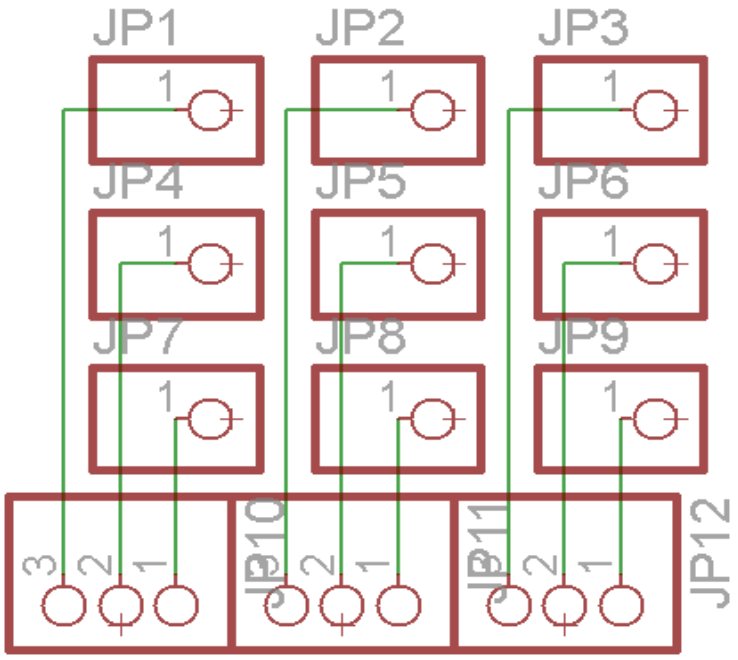

Fig. 3.5 Schematic layout of Design 2 of PCB-based MAS

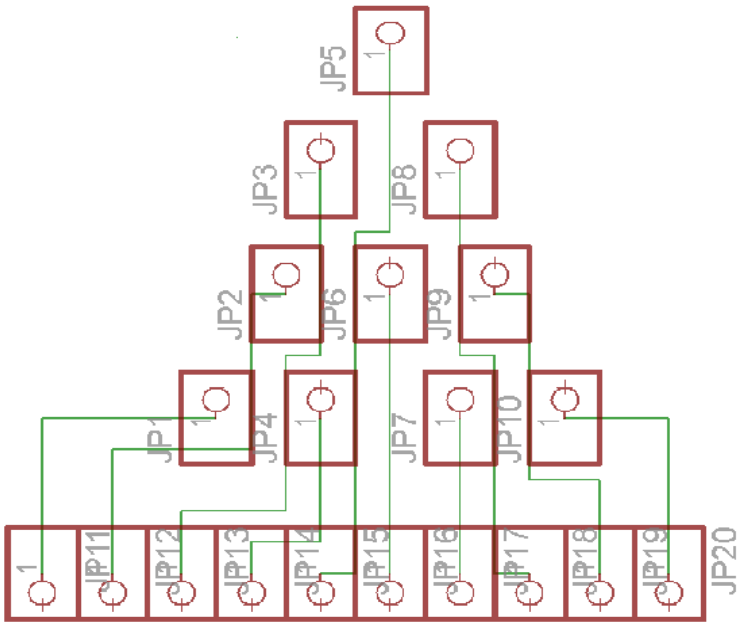

Fig. 3.6 Schematic layout of Design 3 of PCB-based MAS

3.1.4 Board Layout of PCB-based MAS

Fig. 3.7, Fig. 3.8 and Fig. 3.9 show the board layouts of the above mentioned schematics respectively. All the designs are approximately in the range of 2x2 inches in area.

Design 1 (see Fig. 3.4 and Fig. 3.7) contains 9 electrodes in a square configuration. JP1 to JP9 represent the contact pads while JP10 to JP18 represent the electrodes. This design was perceived on the basis that if only a drop of corrosive solution is place on the 9 electrodes rather than immersing the whole sensor in the corrosive solution. This way the corrosive solution would only cover the 9 electrodes leaving out the contact pads. The percentage of Cu trace coming in contact with the corrosive solution along with the electrodes was also calculated. It was only ~5% of the total length of the Cu traces in this design.

Another square configuration of electrodes was designed in Design 2 but in a slightly different manner (see Fig. 3.5 and Fig 3.8). JP1 to JP9 represents the electrodes while the

contact pads are at the bottom of the electrodes arranged linearly. If all the 9 electrodes in this design were to be immersed in the corrosive solution, it was calculated that ~45% of the Cu would come in contact with the solution.

Finally, the Design 3 contained electrodes in a triangle configuration with 10 electrodes (see Fig. 3.6 and Fig. 3.9). JP1 to JP10 represent the electrodes while JP11 to JP20 represent the 10 contact pads. The percentage of Cu trace exposed to corrosive environment was calculated to be ~16% in this design.

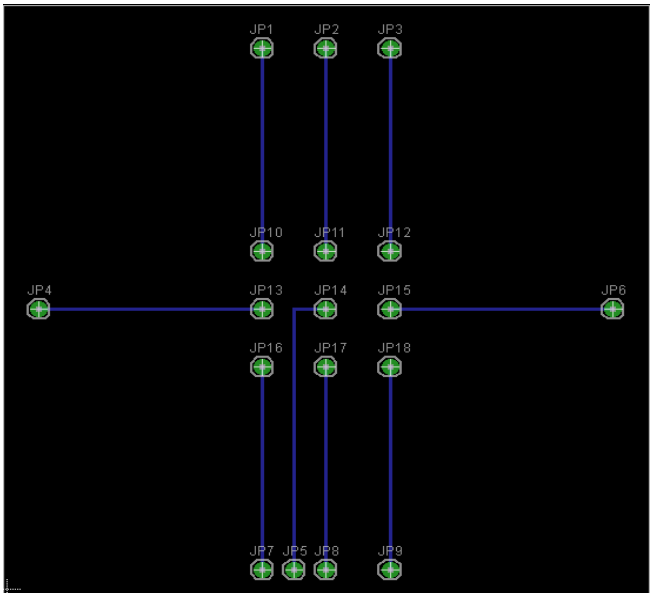

Fig. 3.7 Board layout of Design 1. JP10-JP18 represents the electrodes of the sensor while JP1-JP9 represents the contact pads.

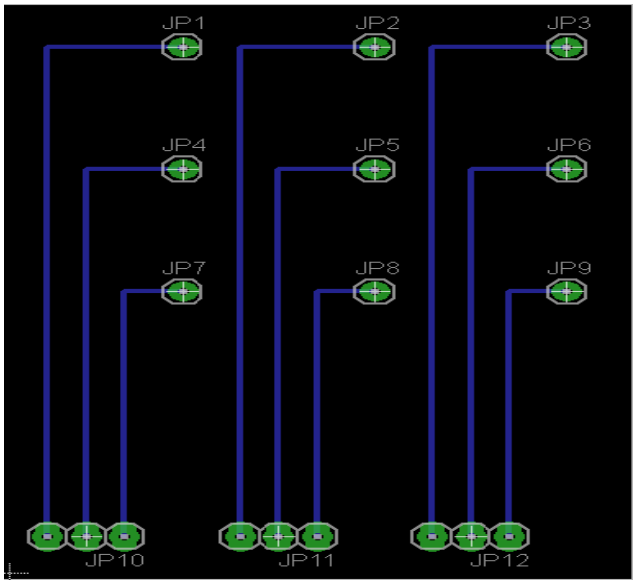

Fig. 3.8 Board layout of Design 2. JP1-JP10 represents the electrodes of the sensor while JP10-JP12 represents the contact pads.

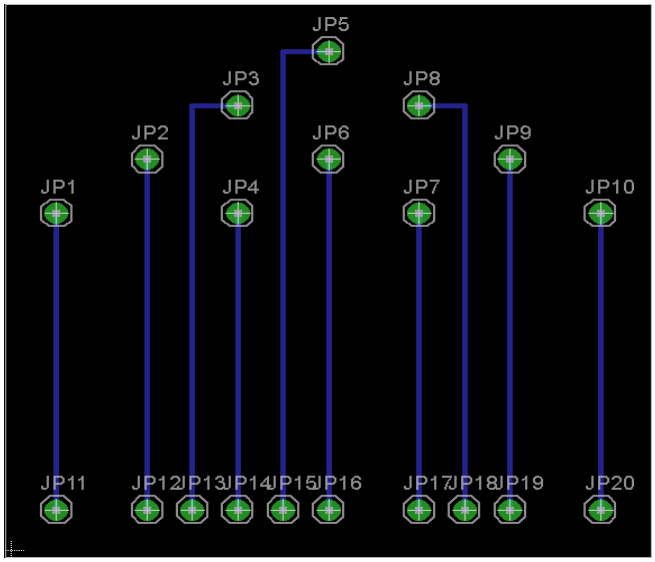

Fig. 3.9 Board layout of Design 3. JP1-JP10 represents the electrodes of the sensor while JP11-JP20 represents the contact pads.

Although from design perspective Design 1 appears to be the optimum design with the least Cu trace exposed percentage. However, from characterization point of view Design 3 was most suitable for experimental setup and testing. This is discussed in detail under the characterization section.

3.2 Fabrication of Planar PCB-based MAS

The designs mentioned in previous sections were fabricated using typical PCB processes [43], [44]. The flow chart in Fig. 3.10 constitutes all the PCB fabrication steps.

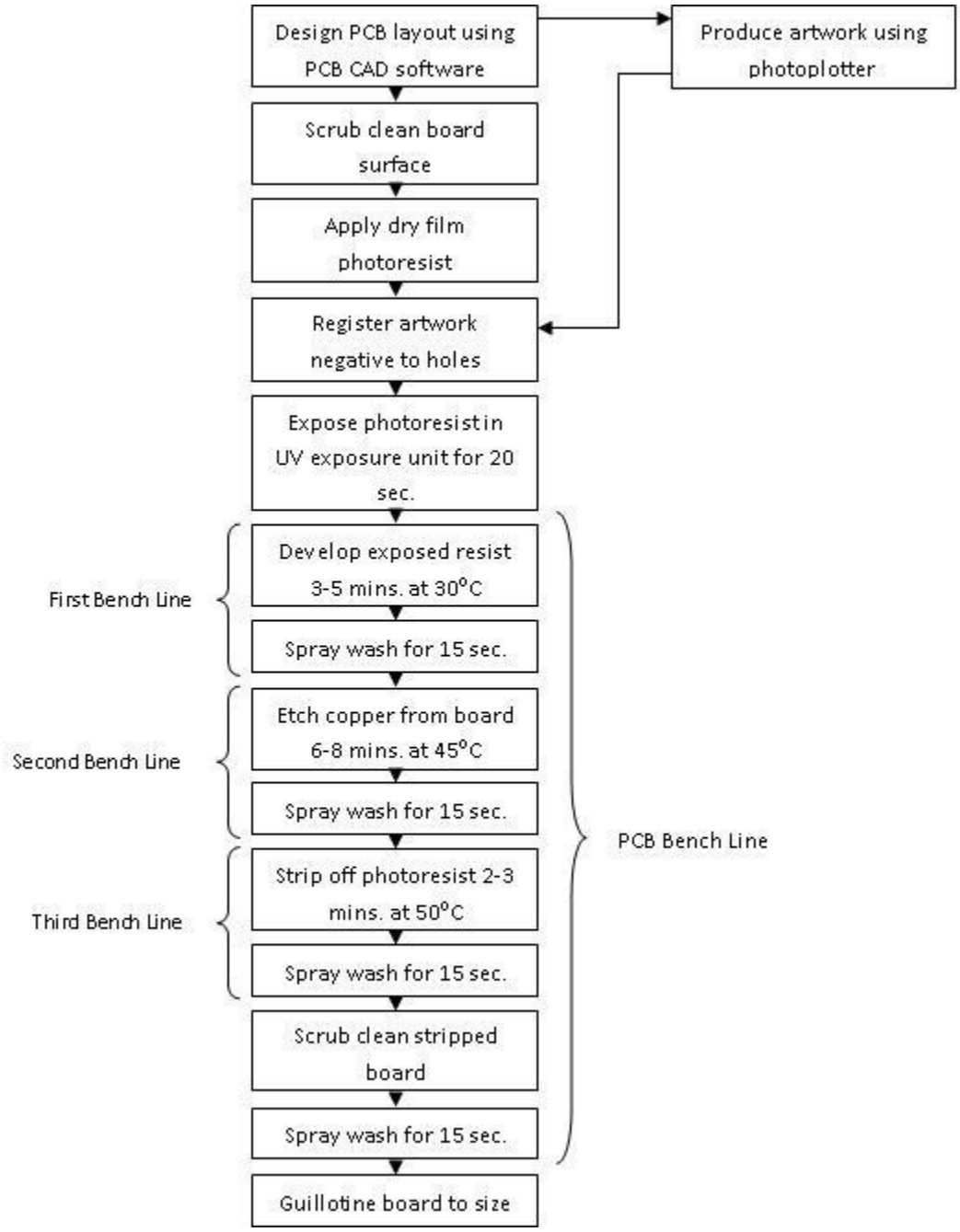

Fig. 3.10 Flow chart for PCB fabrication.

Once the board layout is completed, a file with .brd extention is created. This file is converted to .sol (solder) file using multisim software. This .sol file is converted to .gwk format using GC power station software. In this file the electrode diameter, pad size, pad and diameter shape and trace width are defined. This file is converted to Gerber file with .gbx extension. Gerber file is exported to the photo plotter for making artwork. Negative artwork is used in this work. Artwork is made of a piece of photographic film with black where Cu has to be removed and blank where the Cu is desired to be on the finished board. This kind of artwork is called negative artwork.

In the mean while the board is cleaned using brush cleaning machine. After scrub cleaning, the positive photoresist film is applied to the clean board through laminator. The prepared artwork is then manually fixed on the photoresist clad board. This is exposed to the ultra violet (UV) light for 20 sec. The photoresist exposed to the UV light through the artwork hardens. The board is then developed using Potassium Carbonate (K_2CO_3) for 3 to 5 min at 30°C. This way the hardened photoresist becomes harder while the unexposed photoresist peels off leaving the Cu exposed. The board is spray washed with deionized water to remove residues of peeled off photoresist. This is called 1^{st} PCB bench line. Until this point the desired Cu pattern is under the hardened photoresist layer while the unwanted Cu is exposed. Now comes the 2^{nd} PCB bench line. The unwanted Cu is etched away by immersing the board in Ferric Chloride (Fe_2Cl_3) for 2 to 3 min. it is heated to 45°C to speed up the etching process. Fe_2Cl_3 quickly eats away all the exposed Cu leaving behind only the Cu pattern under the resist film. The board is again spray washed with deionized water. Finally in the 3^{rd} PCB bench line the resist layer is etched off using stripper solution. Once the resist layer is etched off the board is finally spray washed, scrubbed clean and spray washed again. The finished board can then be cut to required size using Guillotine board.

Fig. 3.11, Fig. 3.12 and Fig. 3.13 show the fabricated PCB-based MAS. The electrode size in each design is 60 mils (1.5mm) and the trace width is 10 mils (0.254mm). The total area of each fabricated sensor is ~2x2 inches.

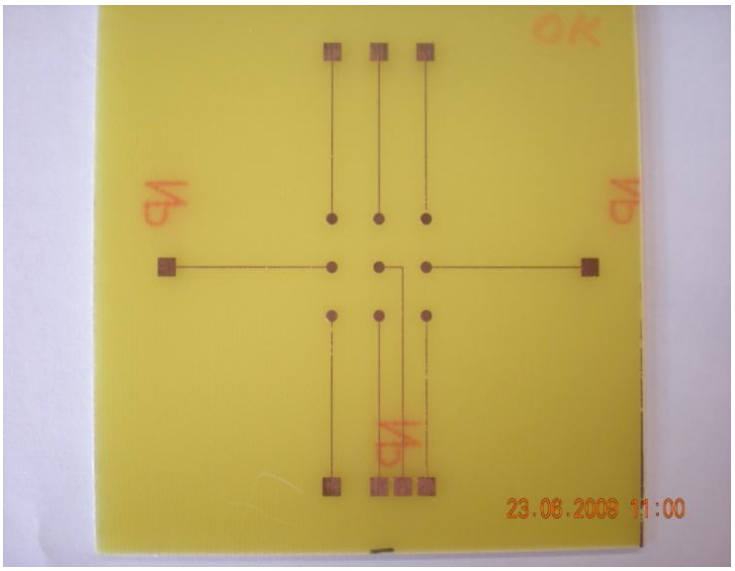

Fig. 3.11 Fabricated PCB of Design 1

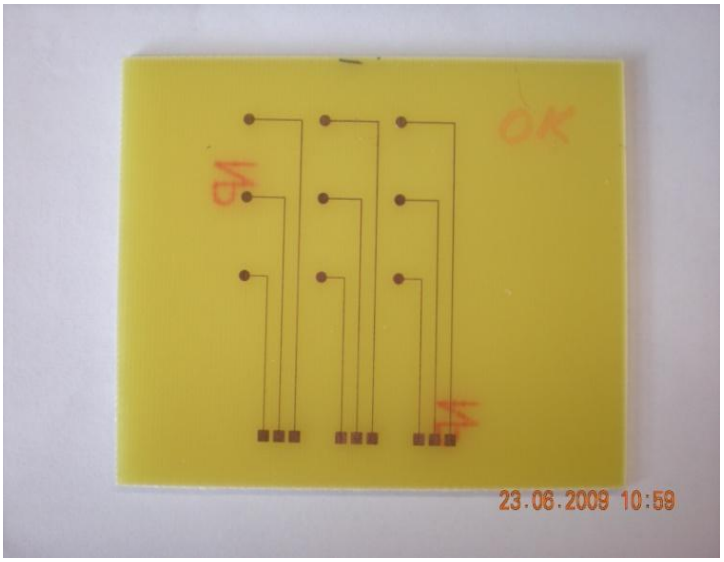

Fig. 3.12 Fabricated PCB of Design 2

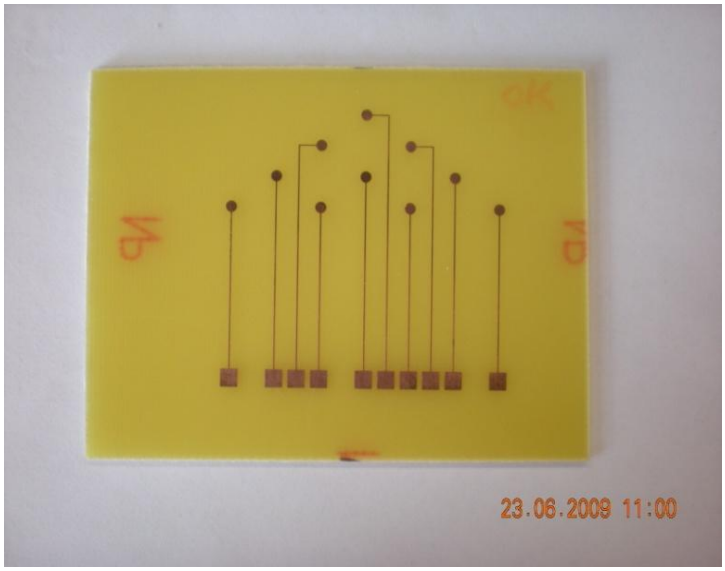

Fig. 3.13 Fabricated PCB of Design 3

3.3 Characterization of PCB-based MAS

The characterization of PCB-based MAS mainly consists of two parts. First, the experimental setup and secondly, the data acquisition and analysis.

3.3.1 Experimental Setup

Three types of experiments were conducted to assess the PCB-based MAS performance. These three experiments will be discussed categorically but first some pre-experimental steps are discussed.

The most important pre-test requirement was the optimum design of the PCB-based MAS. As described earlier Design 1 appeared to be the best choice. Although Design 1 is a potential design for PCB-based MAS. However, considering the experimental conditions in this research, it was not considered for testing. The main reason for abandoning Design 1 was that it was decided that for this research all the experiments will be run using sufficient amount of corrosive solutions (because it simulates a

corrosive environment better e.g. stagnant corrosive solution at the bottom of a pipeline) . This means that all the electrodes in the sensor must be completely immersed in the solution. Design 1, however, lacked the ability of complete immersion because it was designed for a drop of corrosive solution. Furthermore, the contact pads were far apart from each other in Design 1 and their coupling and decoupling was not very feasible during tests.

Now, the choice remained between Design 2 and Design 3 of PCB-based MAS. Since both the designs were capable of immersing completely in the solution and the contact pads were also feasible for easy coupling and decoupling. Therefore, the choice criterion between Design 2 and Design 3 was mainly the percentage of exposed Cu traces. As calculated Design 3 had ~16% of Cu traces exposed as opposed to ~45 % of Design 2. Therefore, Design 3 was chosen to be tested in all the experimental setups.

3.3.1.1 First Experimental Setup

The first experiment was run to test the corrosion detection capability of planar PCB-based MAS. It was tested to assess whether its performance was comparable to the existing CMAS probes or not. 3%wt sea salt solution was used as the corrosive solution. It was prepared by adding 3 gm of sea salt to 100 ml of deionized water and stirred. Then the electrodes were completely immersed in the said solution. The electrodes were externally coupled to each other through contact pad (see Fig. 3.14). Before exposing the sensor electrodes to the corrosive environment, the oxide layer on the Cu electrodes was polished using a fine sand paper. Once immersed in the said solution, each electrode was temporarily decoupled from the common coupling point. The picoammeter was connected to the decoupled electrode and the common coupling point to measure the electrode current. The corrosion currents were measured and recorded at predefined time intervals for 10 days using Keithley 6487 Picoammeter. The measured corrosion rates were very misleading and only 7 electrodes gave corrosion current (explained in results and discussion chapter). It was found by close visual inspection there were small cracks in the Cu traces connecting the three non-functioning electrodes to the contact pads.

Therefore, there was no connectivity of the Cu electrodes with the contact pads which caused no current to flow. In addition, for the misleading corrosion rate, the reason was found to be the exposed Cu traces. Although very small in width as compared to the electrodes, the Cu traces were also corroding along with the electrodes producing erroneous results. These two points were very important regarding the experimental setup. Therefore, a similar experimental setup was placed with the exception that this time the connectivity of each electrode to the contact pad was checked with a multimeter. In addition, the Cu traces of PCB-based MAS were covered with acrylic conformal coating. Acrylic conformal coating is widely used in PCB circuits to protect them against environmental effects. The rest of the experimental procedure was the same as before. The corrosion currents were measured and recorded at predefined time intervals for 10 days using a Keithly 6487 Picoammter. The soultion concentration was changed on Day 8 from 3% wt to 6% wt and 9% wt. This allowed us to check if the sensor efficiently detected change in corrosive environment.

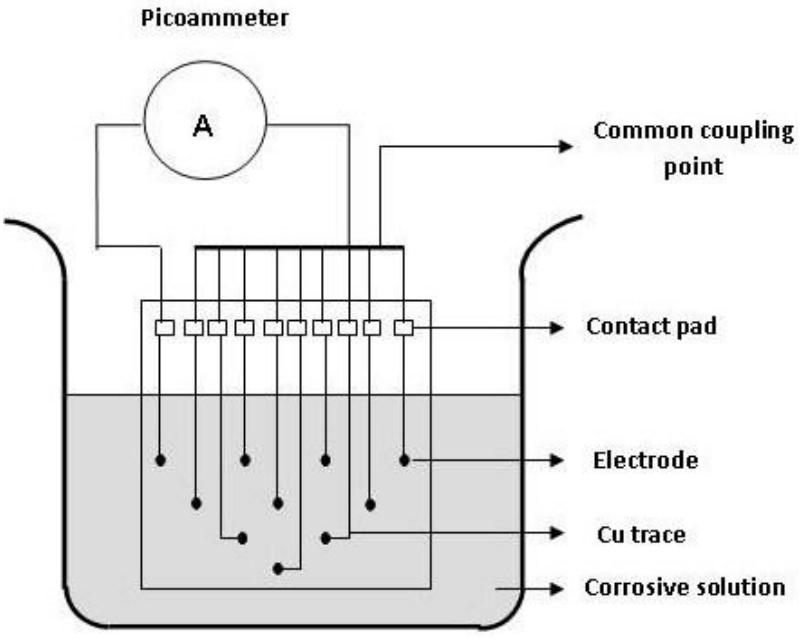

Fig. 3.14 Schematic of the measurement setup. The Cu electrodes were immersed in sea salt solution and allowed to corrode. Corrosion current is then measured using Keithley 6487 Picoammeter attached to contact pads and common coupling point.

3.3.1.2 Second Experimental Setup

This experiment was aimed to determine the effect of conformal coatings on PCB-based MAS performance. In addition, its corrosion detection capability is tested in acidic (HCl) and basic (NaCl) solutions using three types of conformal coatings namely; acrylic, cyanoacrylate and epoxy see (Fig. 3.15). It was believed that acrylic may not withstand the harsh corrosive environment like HCl. Therefore, cynaoacrylate and epoxy which are considered good insulators were used as conformal coatings besides acrylic. In addition, since epoxy is known to inhibit corrosion it was also believed that epoxy may prolong the sensor life. The conformal coatings were applied over the Cu traces leaving only the electrodes exposed. Furthermore, the solution concentrations were changed according to the Table 1**.** Fig. 3.16 shows the actual experimental setup. A total of six samples of PCB-based MAS were used in this experiment, three in HCl solution and other three in NaCl solution each coated with the mentioned respective conformal coating.

Table 3.1 HCl and NaCl corrosive solutions were used in second experiment. The highlighted boxes represent the number of days for a particular concentration.

Concentration		8 days	16 days	24 days	28 days
HCl	NaCl				
0.5M	0.5M				
2M	2M				
4M	4M				
6M	6M				

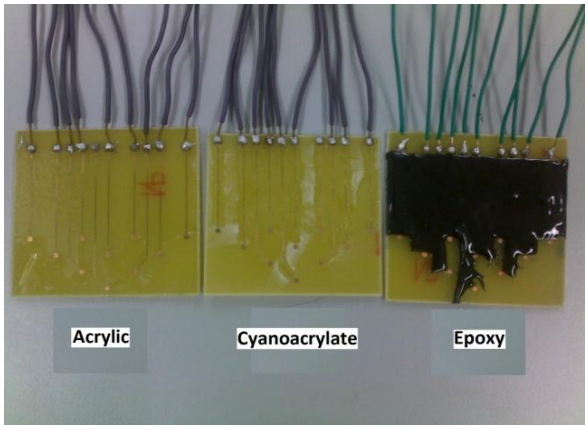

Fig. 3.15 Three samples of PCB-based MAS each coated with acrylic, cyanoacrylate and epoxy conformal coatings respectively.

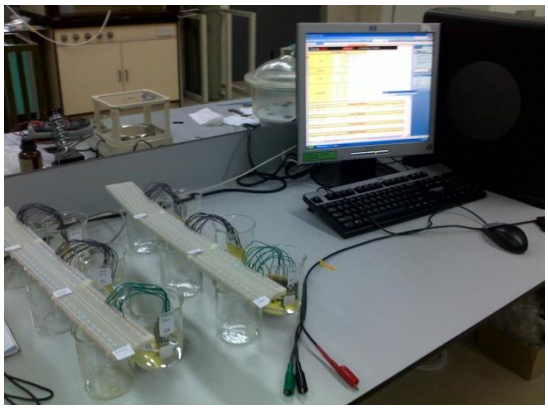

(a)

(b)

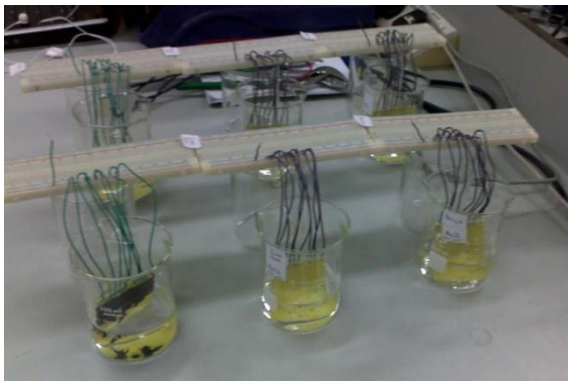

(c)

Fig. 3.16 (a) Experimental setup for testing the effects of conformal coatings on PCB-based MAS performance in HCl and NaCl solutions. (b) Keithley 6487 Picoammeter interfaced with computer. (c) Six samples of PCB-based MAS immersed in corrosive solution.

Similarly, as in the first experimental setup (see Fig. 3.14), the Cu electrodes of the sensor are initially polished to remove any oxide layer before immersing it in the mentioned solution. The Cu contact pads, on the other hand, were connected to a common coupling point. To measure the corrosion current, each contact pad was temporarily decoupled from the common coupling point and then hooked up to Keithley 6487 Picoammeter. The electrode currents were recorded at an 8-hour interval daily.

3.3.1.2.1 EIS Setup for Results Validation

Results obtained from second experimental setup were compared with the corrosion rate obtained using EIS. The actual setup used for EIS measurements is shown in Fig. 3.17. PCB FR486 UV Cu clad laminate was used as the working electrode as can be seen in Fig. 3.17 (a), while the counter electrode was Pt and reference electrode was Ag/AgCl. WEIS 510 equipment by WonTech Company was used for measurements and data acquisition. The data acquisition unit along with the PC is seen in Fig. 3.17 (b). The connections were made as seen in Fig. 3.17 (c). A voltage of 30mV was applied to the working electrode tested in both NaCl and HCl with different solution concentration as mentioned in Table 3.1. The current response as a result of applied alternating voltage is plotted on the PC automatically through WEIS 1.7 software. The data obtained is then extracted and put into IVMAN software. It then linearly fits the graph extrapolates it and by using tafel slopes finds the corrosion rate. This process is repeated several times with different solution concentration to obtain a comparison for results from second experimental setup.

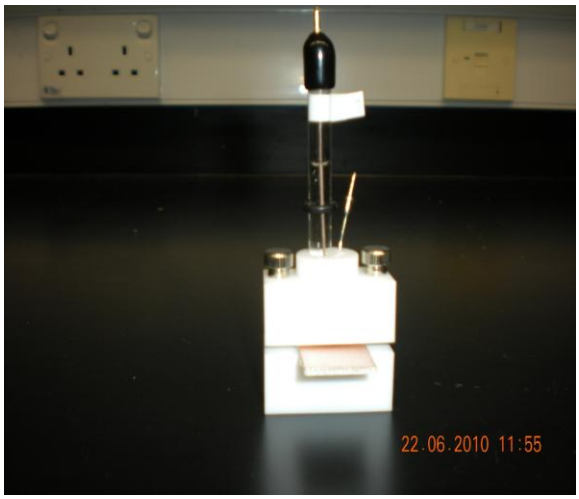

(a)

(b)

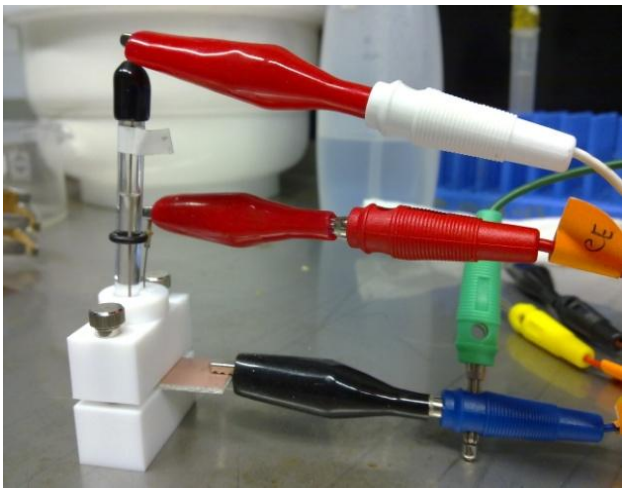

(c)

Fig. 3.17 (a) EIS cell containing the working elecrtrode, the PCB board, reference and counter electrode. (b) Data acquisition unit with four channels interfaced with a PC. (c) connections made for reference electrode, counter electrode and working electrode with the data acquisition unit.

3.3.1.3 Third Experimental Setup

The third experimental setup was put up to determine the reliability and reproducibility of PCB-based MAS. Three PCB-based MAS were used in this experiment with each sensor having the Cu traces coated with acrylic conformal coating. Each sensor was tested in 3%wt sea salt solution and the solution concentration was changed to 9 %wt sea salt solution on Day 8 to check the response of PCB-based MAS to the change in corrosive environment. The electrodes were polished before immersing in the solution and the electrode current was measured similarly as in the previous two experimental setups. Fig. 3.18 shows the experimental setup for this experiment.

(a) (b)

Fig. 3.18 (a) Experimental setup to check the repeatability of PCB-based MAS. (b) Picoammeter probes connected to one of the sensor for current measurement.

3.3.2 Data Acquisition and Analysis

Keithley 6487 Picoammeter was used to measure the corrosion currents as mentioned in the experimental setup section. This picoammeter is a high resolution device with a visual display as well as computer interfacing capabilities (see Fig. 3.19). For a small number of measurements the reading can be noted directly from the display of the picoammeter.

However, for a large number of data like measurement of electrode currents from 10 electrodes at various intervals for many days using display could be cumbersome. In order to avoid confusion and to acquire reliable data, Keithley 6487 picammeter was interfaced with the computer using a GPIB cable. This way picoammeter was completely controlled through the computer.

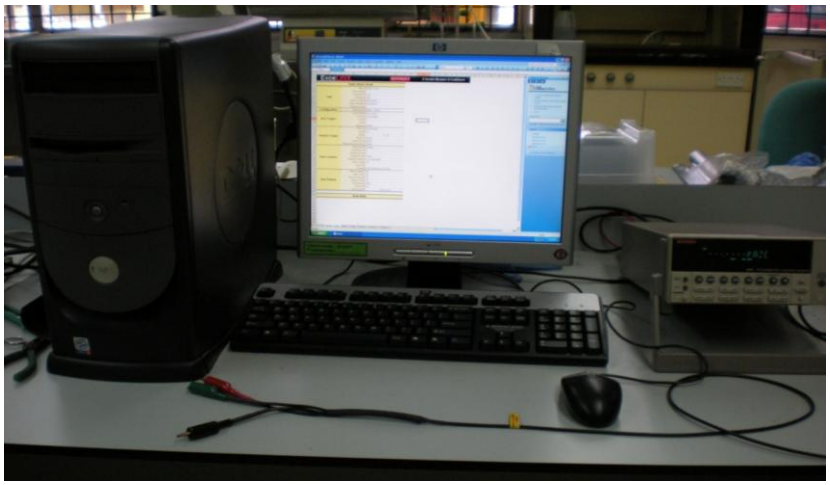

Fig. 3.19 Keithley 6487 Picoammeter interface with the computer through ExceLinx program. All the control parameters for picoammeter measurements are selected through computer.

For measuring the current of each electrode the red wire of the picoammeter was attached to that electrode while the black wire is attached to the common coupling point as shown in Fig. 3.20. The sample rate is selected to be 10 in the Scan Meter sheet and excel sheet is selected for the data to be stored. Sample rate is chosen to be 10 so that 10 values of each measurement are acquired. This makes the data more reliable. The mean of these 10 values is taken using Eq (8) to get the electrode current.

$$Mean = \frac{\sum_{i=1}^{n} X_i}{n} \tag{10}$$

In Eq (8), X_i is the sample value, and n is the total number of reading which is 10. If the measurement is stable all these 10 readings for one measurement are very close to each other and therefore their mean is also same. The currents of rest of the electrodes are measured similarly.

Fig. 3.20 Connection of picoammeter probes is shown. One probe is connected to the common coupling point and the other probe is connected to the electrode.

Fig. 3.21 shows the recorded electrode currents. For each electrode the current is measured 10 times and its mean is calculated (shown by the bold digits). This means 100 readings are recorded at one time measurement. This procedure is repeated twice or thrice a day to monitor the corrosion rate. The currents obtained are either positive or negative. As mentioned earlier that positive currents are cathodic and negative currents are anodic.

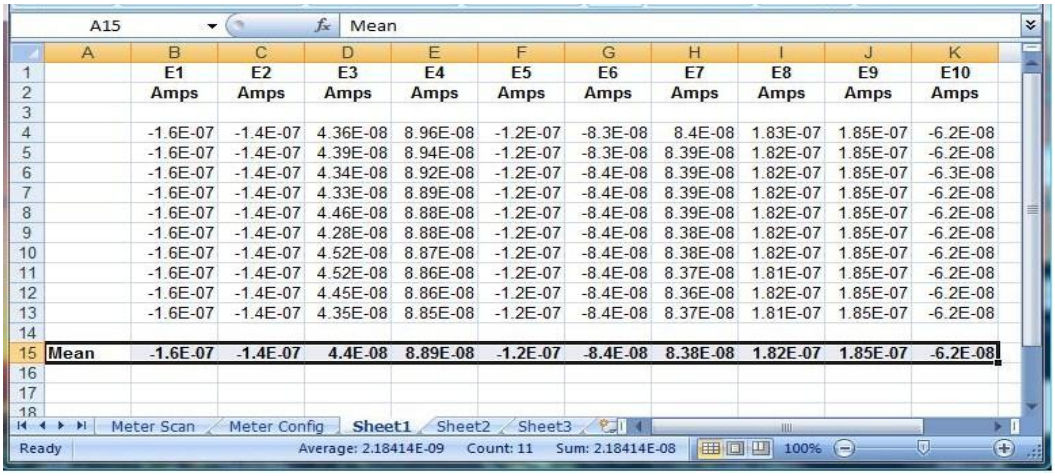

A15 | Mean

	A	B	C	D	E	F	G	H	I	J	K
1		**E1**	**E2**	**E3**	**E4**	**E5**	**E6**	**E7**	**E8**	**E9**	**E10**
2		**Amps**	**Amps**	**Amps**	**Amps**	**Amps**	**Amps**	**Amps**	**Amps**	**Amps**	**Amps**
3											
4		-1.6E-07	-1.4E-07	4.36E-08	8.96E-08	-1.2E-07	-8.3E-08	8.4E-08	1.83E-07	1.85E-07	-6.2E-08
5		-1.6E-07	-1.4E-07	4.39E-08	8.94E-08	-1.2E-07	-8.3E-08	8.39E-08	1.82E-07	1.85E-07	-6.2E-08
6		-1.6E-07	-1.4E-07	4.34E-08	8.92E-08	-1.2E-07	-8.4E-08	8.39E-08	1.82E-07	1.85E-07	-6.3E-08
7		-1.6E-07	-1.4E-07	4.33E-08	8.89E-08	-1.2E-07	-8.4E-08	8.39E-08	1.82E-07	1.85E-07	-6.2E-08
8		-1.6E-07	-1.4E-07	4.46E-08	8.88E-08	-1.2E-07	-8.4E-08	8.39E-08	1.82E-07	1.85E-07	-6.2E-08
9		-1.6E-07	-1.4E-07	4.28E-08	8.88E-08	-1.2E-07	-8.4E-08	8.38E-08	1.82E-07	1.85E-07	-6.2E-08
10		-1.6E-07	-1.4E-07	4.52E-08	8.87E-08	-1.2E-07	-8.4E-08	8.38E-08	1.82E-07	1.85E-07	-6.2E-08
11		-1.6E-07	-1.4E-07	4.52E-08	8.86E-08	-1.2E-07	-8.4E-08	8.37E-08	1.81E-07	1.85E-07	-6.2E-08
12		-1.6E-07	-1.4E-07	4.45E-08	8.86E-08	-1.2E-07	-8.4E-08	8.36E-08	1.82E-07	1.85E-07	-6.2E-08
13		-1.6E-07	-1.4E-07	4.35E-08	8.85E-08	-1.2E-07	-8.4E-08	8.37E-08	1.81E-07	1.85E-07	-6.2E-08
14											
15	**Mean**	**-1.6E-07**	**-1.4E-07**	**4.4E-08**	**8.89E-08**	**-1.2E-07**	**-8.4E-08**	**8.38E-08**	**1.82E-07**	**1.85E-07**	**-6.2E-08**
16											
17											
18											

Meter Scan | Meter Config | Sheet1 | Sheet2 | Sheet3

Ready | Average: 2.18414E-09 | Count: 11 | Sum: 2.18414E-08 | 100%

Fig. 3.21 The current measured from picoammeter is recorded in Excel sheet. To make data more reliable 10 readings are taken for each electrode current measurement. Mean of these 10 readings is highlighted in bold.

The highest negative current is observed and used in Eq (7) to calculate the CR_{max} of Cu. In addition, three times standard deviation of all the anodic currents in one time measurement is also calculated and used in Eq (7) to calculate the CR_{max} of Cu. This means that I^a_{max} in (5) is taken to be equal to two parameters as shown in (11) and (12).

$$I^a_{max} = I_{max} \tag{11}$$

$$I^a_{max} = 3\sigma \tag{12}$$

In Eq (11), I^a_{max} is equal to the maximum anodic current recorded while in (10), I^a_{max} is equal to the 3 times standard deviation of all the anodic currents at that instant. If CR_{max} is calculated using Eq (11) and Eq (12) the confidence level increases because if the measurements are correct the resultant CR_{max} should be similar. In Eq (7), I^a_{max} is the determining parameter for corrosion rate. However, other parameters used in Eq (7) are also calculated according to our design. The surface area A is calculated using Eq (13).

$$A = \pi r^2 \tag{13}$$

As mentioned earlier the electrode diameter is 1.5mm (0.15 cm) making the surface area to be 0.0176 cm^2. For density ρ, as Cu is used as the sensing element therefore, the density of Cu 8.96 g/cm^3 is used. Faraday constant F is 96485 C/mol and current distribution factor ε, is assumed as unity as in previous works [30]. Equivalent weight W_e as defined in [30] is given by Eq (14).

$$W_e = \frac{1}{\sum(m_i z_i / W_i)} \tag{14}$$

In Eq (14), m_i is the mass fraction, z_i is the oxidation state and W_i is the atomic weight of the component i in the electrode alloy. Since Cu was used in this work and it is a metal not an alloy therefore, Eq (14) was modified as Eq (15).

$$W_e = \frac{W_c}{z_c} \tag{15}$$

In Eq (15), W_c is the atomic weight of Cu and z_c is the oxidation state of Cu. Using Eq (15) the equivalent weight of Cu was calculated to be 63.546 g/mol.

3.3.3 Switching Circuit

As mentioned in previous sections, the electrode current is measured by temporarily decoupling the electrode from the common coupling point and inserting the picoammeter between the electrode and the common coupling point. This coupling and decoupling of electrodes was done manually each time. In order to make current measurements more efficient and easy, a switching circuit was designed and developed. The circuit was first simulated in Crocodile software and then designed in Eagle software to be fabricated on PCB. Fig. 3.22 shows the simulated design of the switching circuit in Crocodile software.

In order to simulate the current produced from the electrodes of PCB-based MAS sensor. The electrodes were taken as current sources. Each current source is connected to a common point through a corresponding switch and a single core double pole relay. This connection is made in such a way that the input of the each relay is connected to the corresponding current source. Out of two poles, the normally closed pole of each relay is connected to the common coupling point, while the normally open pole is connected to a lamp. In addition the core of each relay is connected to the power supply through a switch to control the switching of the relay. All the currents (from current sources) flows to the common coupling point through normally closed pole of the relay. Whichever current (from current source) is required to flow to the LED (simulating the picoammeter), the switch connected to that current source's corresponding relay is turned on. This switch operates the relay and the current is made to flow to the LED. The turning on of the lamp indicates that the switching is performed. Since the pole of the relay is a metallic contact, the current measured at the output (lamp) during simulation is the same as that of the current source. This shows that this circuit can be used as a switching circuit to make the measurements easy.

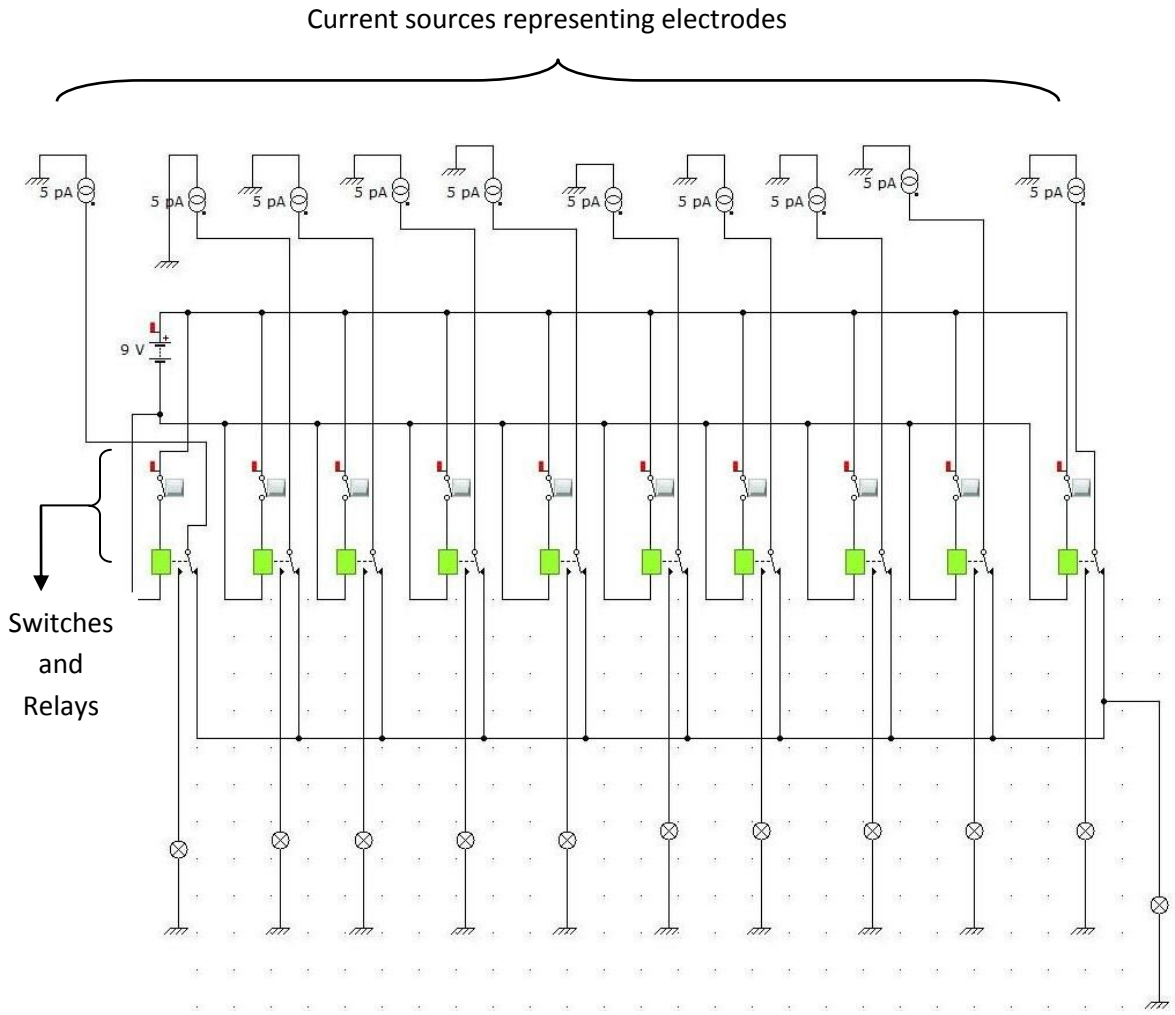

Fig. 3.22 Switching circuit for electrode current measurement was designed and simulated in Crocodile software. The electrodes are simulated as current sources, while the LEDs indicates the current flowing to the picoammeter.

Fig. 3.23 show the fabricated version of the easy switching circuit. 10 relays are used along with a dip switch package of 10 on off switches. The electrodes are connected to the relays. The picoammeter probes are permanently attached to the output of the relays. Each electrode current is measured easily by just turning on the corresponding switch.

This circuit was designed and implemented along the on going experiments. Therefore, this was not used during the experiments. However, this circuit has simplified the switching for electrode current measurement and will prove useful for future works.

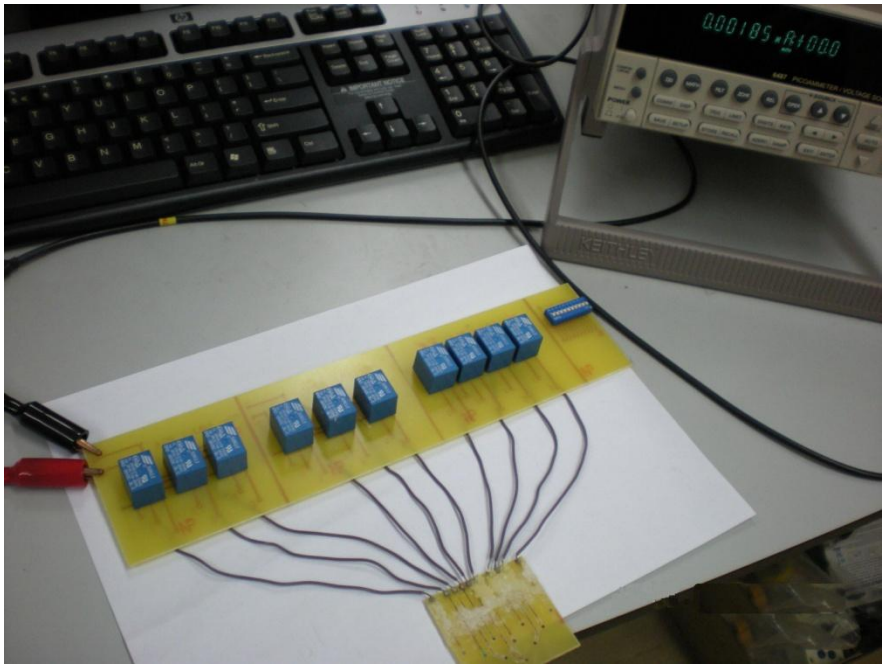

Fig. 3.23 The fabricated switching circuit. 10 relays and a 10 on off dip switch package was used to achieve easy switching for electrode current measurement. Each electrode is selected for current measurement by just turning on the switch.

3.4 Summary

This chapter highlights the complete methodology adopted to achieve the objectives of this research. This includes the design, fabrication and charcterization of PCB-based MAS. For designing, initially a few design criteria like requirements for planar design, electrode size, trace width etc. were defined. Eagle software is used to design the layouts of the sensor later to be fabricated using PCB. The PCB fabricating steps are described with the help of flow chart and illustrations. The experimental setups for different kind of experiments and the data acquisition is described in detail. The equations and formulas used for the analysis of the acquired data are also discussed. Finally, the design and implementation of an easy switching circuit for electrode current measurement is also presented.

CHAPTER 4

RESULTS AND DISCUSSION

4.0 Overview

This chapter presents the results obtained from the three experiments described in the previous chapter. The first experiment was aimed to obtain results depicting the corrosion detection capability of PCB-based MAS and ability to detect change in corrosive environment. The second experiment focused on the effects of conformal coatings on the sensor's performance with results compared with corrosion rates obtained from EIS. Finally, the third experiment was done to assess the reliabilty and repeatibility of PCB-based MAS. The detailed discussion over the obtained results is provided at the end of each section.

4.1 Corrosion Detection Capabilities of PCB-based MAS

4.1.1 Bare PCB-based MAS in Sea Salt Solution

The first experiment was done to assess planar PCB-based MAS corrosion detection capabilities. In addition, it was aimed to check whether this planar PCB-based MAS is operating like existing CMAS probes or not. This is achieved by comparing planar PCB-based MAS results with published CMAS data. Fig. 4.1 show the corrosion currents measured from 7 out of 10 functioning electrodes of PCB-based MAS. Electrode 1 (E1) produced the highest anodic current. The negative (anodic) and positive (cathodic) currents in Fig. 4.1 showed that this planar PCB-based MAS works on the same principle as that of CMAS (for details of working principle see section 2.4). This production of

anodic and cathodic currents also shows that planar PCB-based MAS is detecting corrosion.

By using Eq (7) and Eq (11) the CR_{max} of Cu in 3%wt sea salt solution was obtained and plotted in Fig. 4.2. The CR_{max} started around 300 µm/yr and rose to nearly 1000 µm/yr but on Day 4 dropped again. It then became high and this fluctuating trend continued until Day 10 with maximum CR_{max} reaching to ~7000 µm/yr.

This corrosion rate is believed to be inaccurate because compared to published data [45]-[47], the CR_{max} of Cu in 3%wt sea salt solution measured by CMAS Cu probes is in the range of 80µm/yr as shown in Fig. 4.3 (the corrosion rate graph is very dense in Fig. 4.3 because the corrosion rate was measured at an interval of 20-600 seconds). However, the CR_{max} obtained from planar PCB-based MAS is ~7000µm/yr. Corrosion is a random natural process and the experimental conditions of every experiment can never be exactly the same. Therefore, a difference of a few hundred micrometers is always tolerable in comparing corrosion rates from different techniques. However, this huge difference of ~6000 µm/yr in the compared results indicated some discrepancy. That could be attributed to the corroding Cu traces. The expalantion is that the corrosion current obtained is believed to be from the electrodes. However, although Cu traces being relatively smaller in width (10 mils), their corrosion produces current that supplement the existing corrosion currents. Since corrosion current (anodic current) is proportional to the corrosion rate. The supplemented corrosion current produces higher corrosion rates.

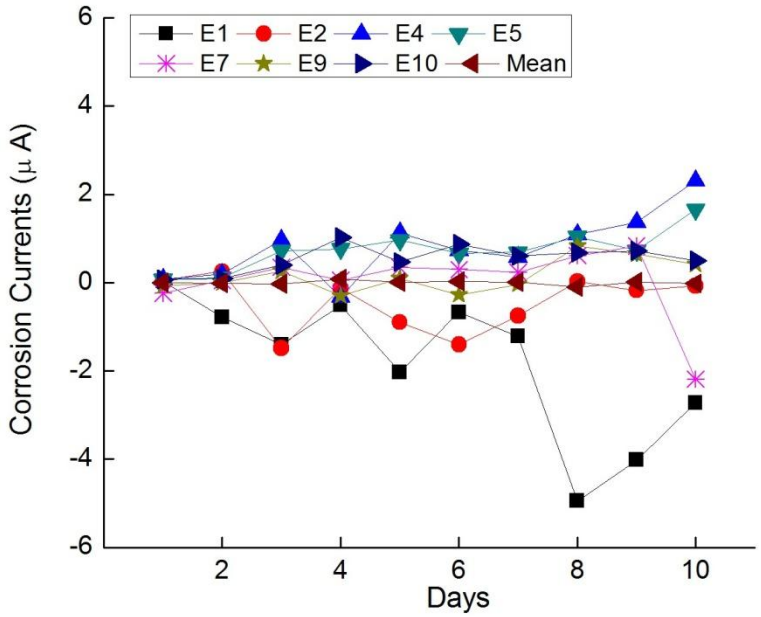

Fig. 4.1 Corrosion currents obtained from PCB-based MAS with Cu traces exposed to the corrosive environment along with the electrodes.

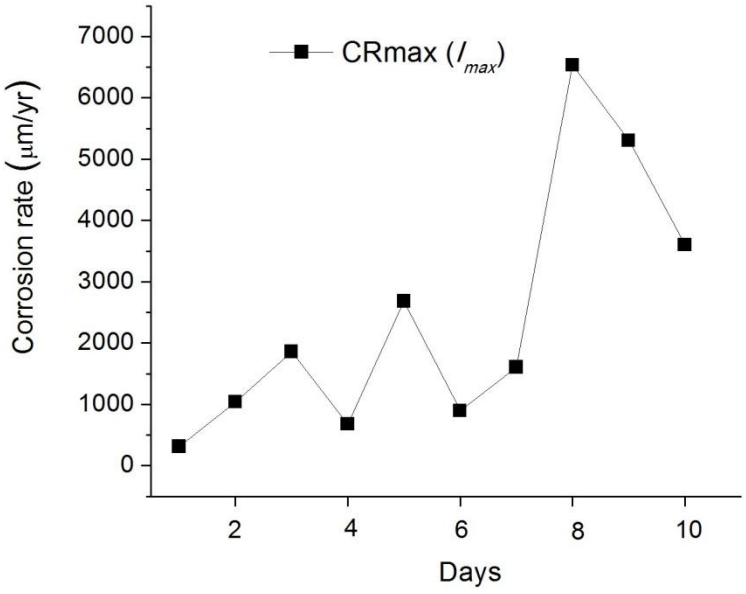

Fig. 4.2 Real time corrosion rate calculated from the maximum anodic current is plotted against time.

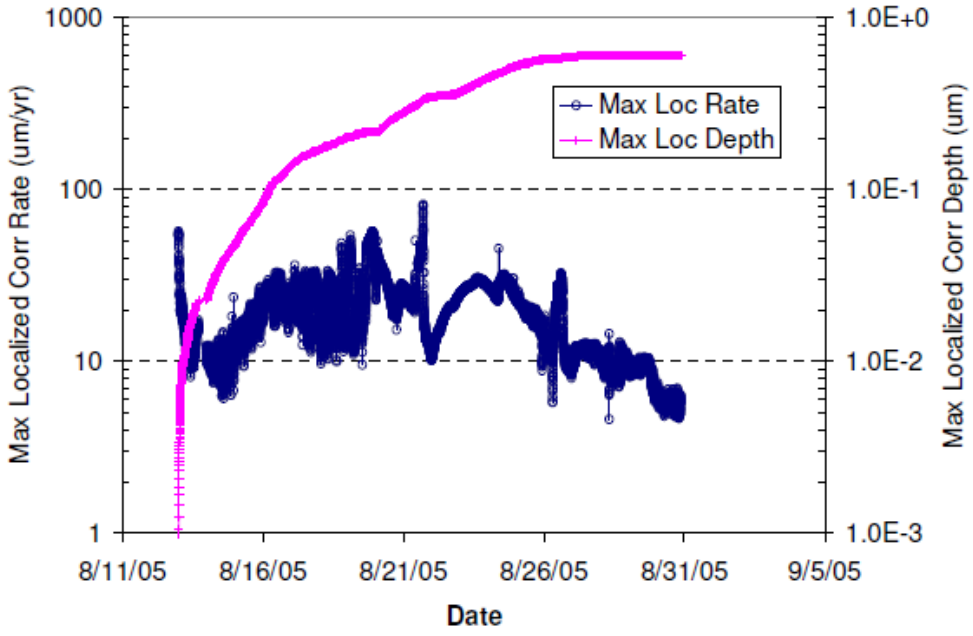

Fig. 4.3 CMAS probe monitored Cu corrosion rate taken from [45].

4.1.2 Acrylic Coated PCB-based MAS in Sea Salt Solution

Another similar experiment was run but with the Cu traces covered with acrylic conformal coating. Fig. 4.4 shows the corrosion currents measured from 10 electrodes of PCB-based MAS with Cu traces coated with acrylic conformal coating. Fig. 4.5 shows only the anodic currents.

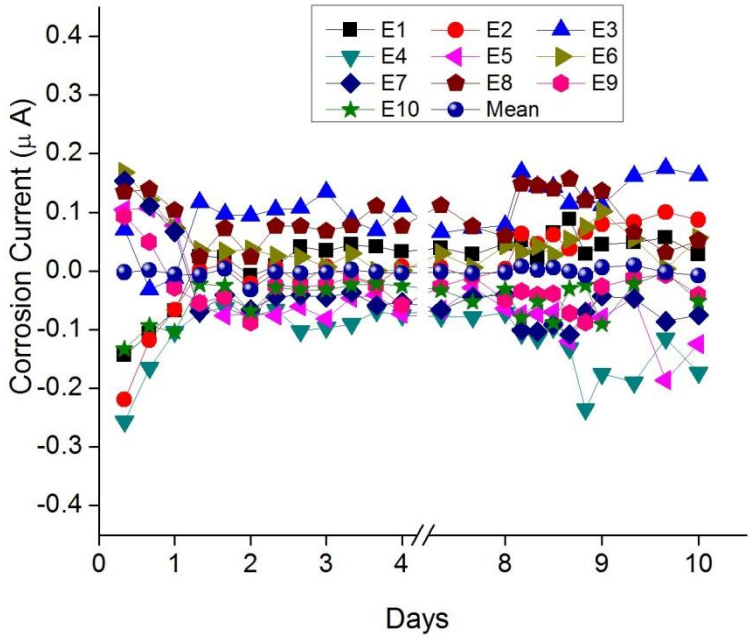

Fig. 4.4 Corrosion currents obtained using PCB-based MAS in sea salt solution. The Cu traces are covered with acrylic conformal coating.

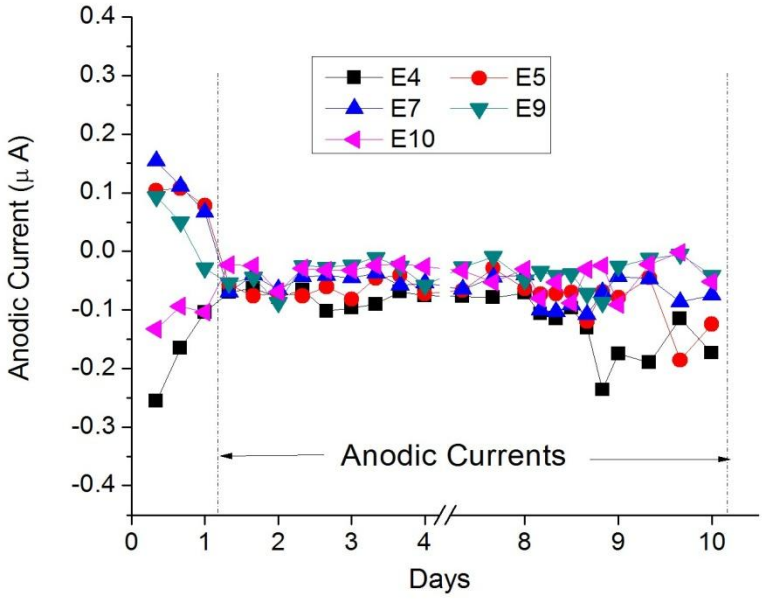

Fig. 4.5 Anodic currents of acrylic coated PCB-based MAS in sea salt solution.

According to literature [30] the corrosion currents (anodic and cathodic) should be almost in the same range. It means that by following kirchoff's current law, the anodic and

cathodic currents should compensate each other by giving a mean of zero. Exact zero mean is an ideal condition. In practical situations noise, offset currents may deviate the mean from zero. However, as long as the corrosion currents are in the same range, small deviation of mean is acceptable. In Fig. 4.4, the currents were in the range of ~-0.25μA to ~2 μA giving a mean of nearly zero at almost every measurement. In Fig. 4.5, out of 10 electrodes 5 electrodes showed the anodic behaviour. Electrode 4 (E4) gave the maximum anodic current most of the time except at a couple of points where Electrode 5 (E5) became the maximum anodic current. An interesting point to note over here is that the maximum anodic current is proportional to the corrosion rate (see (5)), therefore the trend of maximum anodic current and corrosion rate is same. If only the trend of corrosion is to be monitored and not the actual corrosion rate e.g. to check if corrosion is increasing or decreasing. Then it can be seen by observing the trend of the maximum anodic current only. In this case if seen upside down, E4 replicates the corrosion trend.

The CR_{max} of Cu in 3% wt sea salt solution obtained as a function of time is plotted in Fig. 4.6.

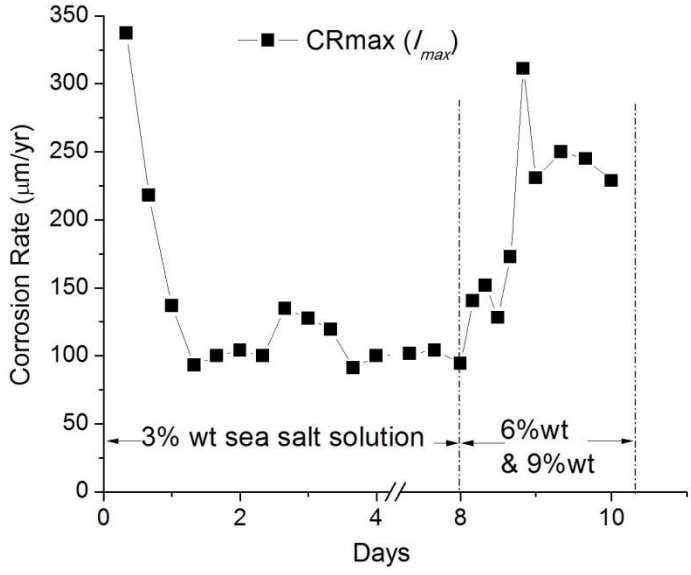

Fig. 4.6 CR_{max} of Cu in sea salt solution obtained by using maximum anodic current.

The corrosion rate is calculated using Eq (11) and Eq (7) with I^{a}_{max} being the most negative anodic current obtained from the measured corrosion currents. It is interesting to

note that the first few initial corrotion rates in Fig. 4.6 are high starting from ~350 µm/yr but from Day 2 onwards it decreases gradually to a more stable value of ~100 µm/yr. This is because when the polished bare Cu electrodes touched the corrosive sea salt solution they corroded vigorously. However, the corrosive activity slowed down in time due to built up of corrosion products. It was also observed that the corrosion rate from Day 4 until Day 8 did not changed much. On Day 8 when the concentration of sea salt solution is increased from 3% wt to 6% wt and 9% wt, there is a sudden rise of corrosion rate from ~100µm/yr to ~150µm/yr and then to ~300µm/yr. This corresponding change in corrosion rates suggests that PCB-based MAS efficiently detects the change in the corrosive environment.

Fig. 4.7 also shows the corrosion rate of Cu but it is calculated by using Eq (7) and Eq (12), which is by taking three times standard deviation (3σ) of all the anodic currents and then calculating the corrosion rate. The comparison of corrosion rates shown in Fig. 4.6 and Fig. 4.7 respectively can be seen in Fig. 4.8.

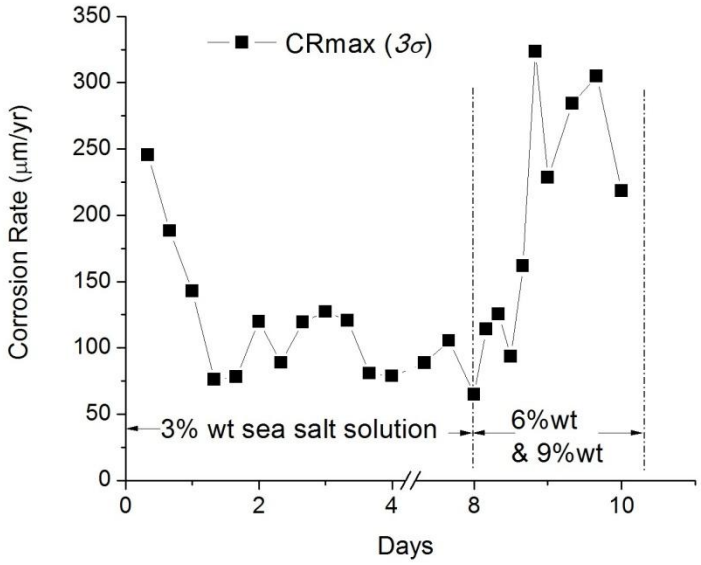

Fig. 4.7 CR_{max} of Cu in sea salt solution obtained by using three times standard deviation of all the anodic currents at that instant.

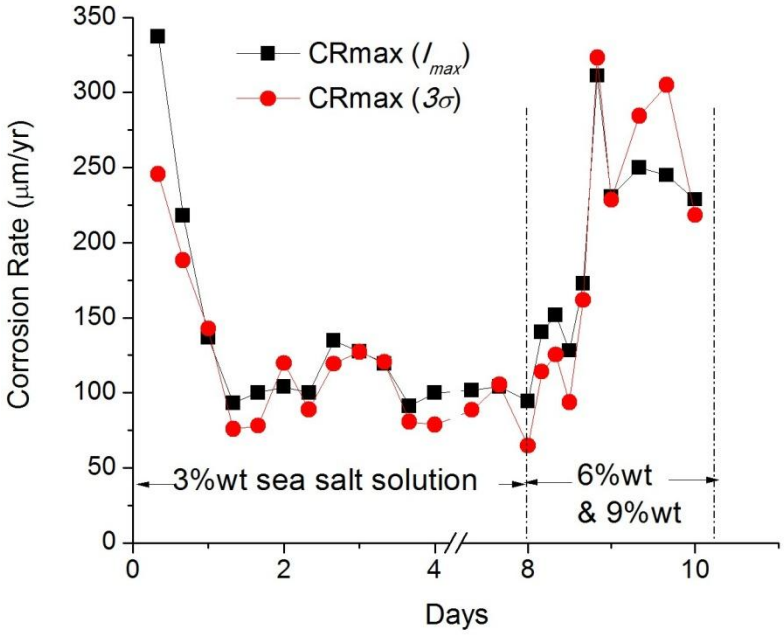

Fig. 4.8 Comparison of CR_{max} obtained from maximum anodic currents versus the CR_{max} obtained from three times standard deviation of anodic currents.

In statistics, 3σ represent 99% of confidence level for normal distribution. In simple words the 3σ of all anodic currents represent that we are 99% confident that the measured maximum anodic current is the maximum value. This means that the 3σ of all anodic currents should be equal to or less than the measured maximum anodic current, I_{max}.

It is seen that by using acrylic conformal coating, the CR_{max} of Cu measured by PCB-based MAS using Eq (11) and Eq (12) has the same order of magnitude as the CR_{max} of Cu measured by Cu CMAS probe [45], [46] and the corrosion rate of Cu reported in literature [47]. In addition, PCB-based MAS efficiently detects change in corrosive environment by providing corresponding corrosion rates.

4.2 Effects of Conformal Coatings on PCB-based MAS Performance

Once the corrosion rate detection capability of PCB-based was assessed, the effect of different types of conformal coatings on PCB-based MAS performance in different corrosive solutions was tested. Acrylic, cyanoacrylate and epoxy are used as the conformal coatings for coating Cu traces and NaCl and HCl are used as the corrosive solutions. Six samples of PCB-based MAS are tested in this experiment. Cu traces of three samples were coated with each mentioned coating and tested in NaCl solution, while the other three samples were similarly coated with each conformal coating and tested in HCl solution. The solution concentration of NaCl solution was changed on Day 8, 16 and 24 from 0.5M to 2M, 4M and 6M respectively. However, the HCl concentration was changed on Day 8 from 0.5M to 2M.

First the results from PCB-based MASs tested in NaCl are discussed followed by the results in HCl solution.

4.2.1 Effects Observed in NaCl Solution

4.2.1.1 Acrylic Conformal Coating

Fig. 4.9 show the anodic currents obtained from acrylic coated PCB-based MAS in NaCl solution. E1, E4 and E6 showed maximum anodic activity. Fig. 4.10 shows the CR_{max} of acrylic-coated PCB based MAS in NaCl solution. The CR_{max} calculated using three times standard deviation of all anodic currents is also plotted and is shown in Appendix A1.

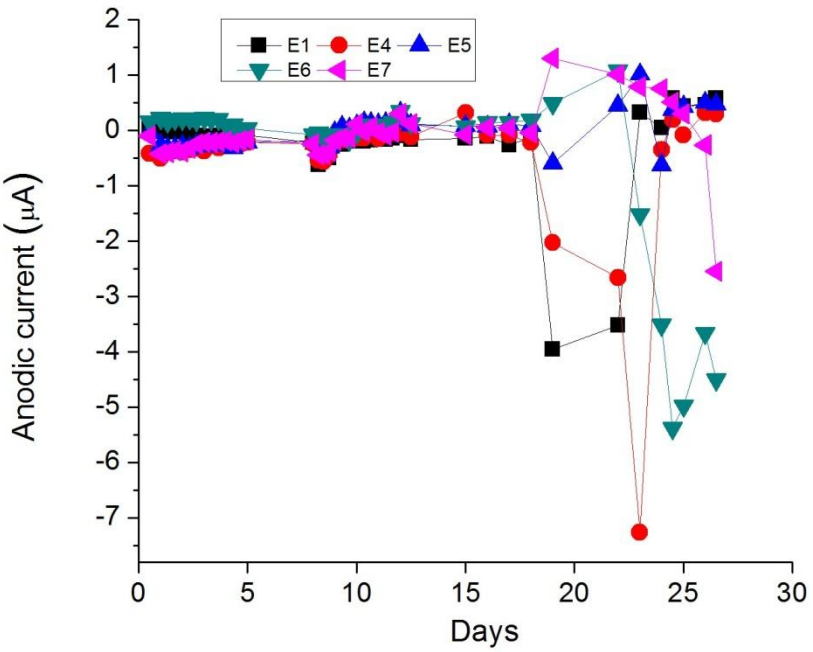

Fig. 4.9 Anodic currents of acrylic coated PCB-based MAS tested in NaCl solution.

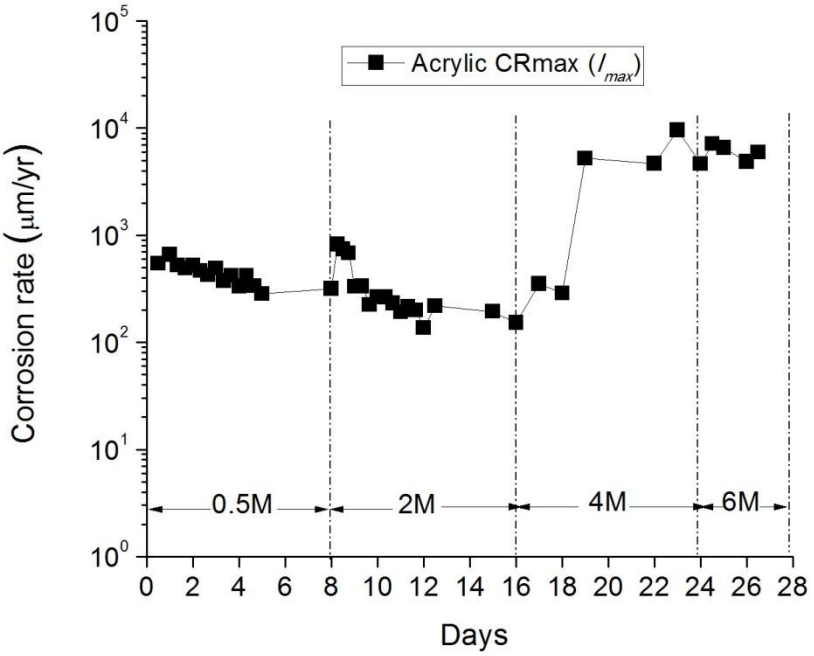

Fig.4.10 CR_{max} of Cu in NaCl solution obtained using acrylic coated PCB-based MAS.

The CR_{max} of Cu shown in Fig. 4.10 started around 500 µm/yr and settled to ~300 µm/yr in the course of eight days. The initial high CR_{max} is expected due to the polished bare Cu electrodes reacting with the corrosive solution. On Day 8 the solution concentration was changed from 0.5M to 2M NaCl solution. As soon as the concentration was changed, the acrylic coated PCB-based MAS produced high CR_{max} of ~900 µm/yr which settled to ~200 µm/yr. However, a very slight change of CR_{max} was observed when solution concentration was changed from 2M to 4M NaCl solution with CR_{max} rising to ~350 µm/yr. Day 18 onwards the CR_{max} increased very rapidly reaching to ~9500 µm/yr and stayed around ~7000 µm/yr until Day 28. Even the change in concentration on Day 24 from 4M to 6M was barely detected. From this trend, it is gathered that Day 18 onwards the acrylic conformal coating started to fail to protect Cu traces against corrosion. This resulted in very high corrosion rates. Though the concentration of NaCl was also very high (4M and 6M) suggesting high corrosion rates. However, this sudden increase of corrosion rate was not proportionate with the previous increase in corrosion rates with change in concentration.

4.2.1.2 Cyanoacrylate Conformal Coating

Fig. 4.11 show the anodic currents obtained from cyanoacrylate coated PCB-based MAS. Out of 10 electrodes 4 electrodes showed anodic activity with E2, E5 and E10 showing the maximum anodic current in different weeks. Fig. 4.12 show the CR_{max} of Cu obtained from cyanoacrylate coated PCB-based MAS in NaCl solution. In addition, graph of CR_{max} (3σ) is also plotted but shown in Appendix A2.

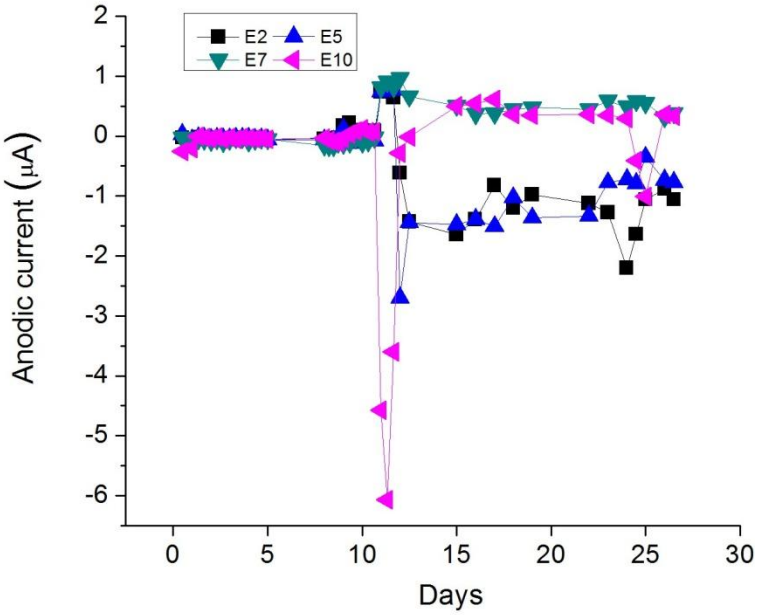

Fig. 4.11 Anodic currents of cyanoacrylate coated PCB-based MAS tested in NaCl solution.

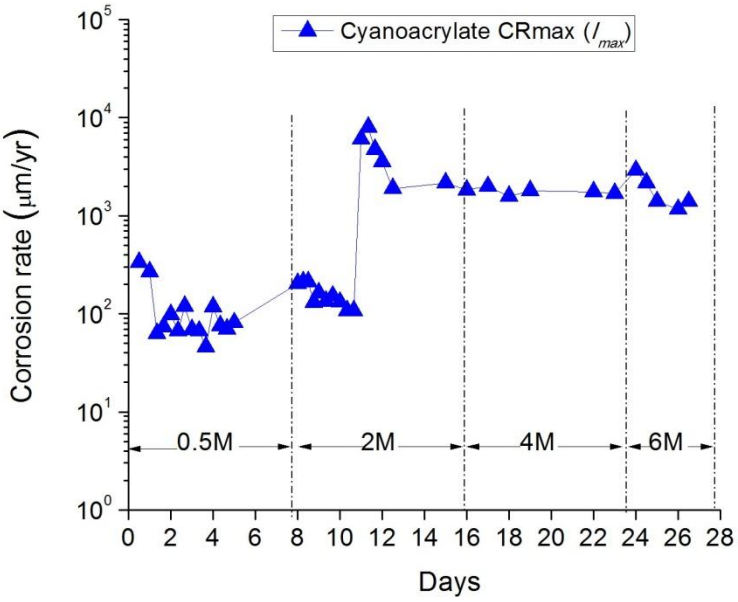

Fig. 4.12 CR_{max} of Cu in NaCl solution obtained using cyanoacrylate coated PCB-based MAS.

In Fig. 4.12, the initial CR_{max} of Cu in 0.5M NaCl was ~300 µm/yr which settled around ~80 µm/yr. The CR_{max} increased to ~200 µm/yr and settled around ~100 µm/yr when the solution concentration was changed from 0.5M to 2M on Day 8. However, Day 11 onwards the CR_{max} increased vigourously reaching a value of ~8000 µm/yr, it dropped back to ~1500 µm/yr on Day 12. It remained ~1500 µm/yr through out the 4M concentration. It then changed to ~3000 µm/yr when the solution concentration was changed from 4M to 6M. The sudden rise of CR_{max} on Day 11 suggests that the cyanoacrylate layer was compromised. However, the CR_{max} lowered on Day 12 onwards but it was still on the higher side suggesting that the cyanoacrylate coating could resist until 2M NaCl concentration after that it may fail to protect the Cu traces against corrosion.

4.2.1.3 Epoxy Conformal Coating

The anodic currents obtained from epoxy coated PCB-based MAS in NaCl solution are shown in Fig. 4.13, while the CR_{max} obtained is shown in Fig. 4.14 (graph of CR_{max} (3σ) is shown in Appendix A3).

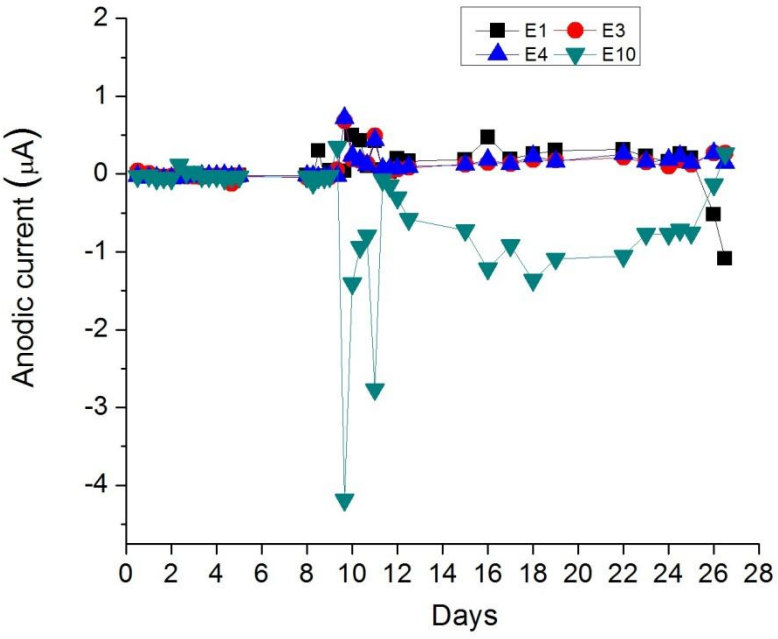

Fig. 4.13 Anodic currents of epoxy coated PCB-based MAS tested in NaCl solution.

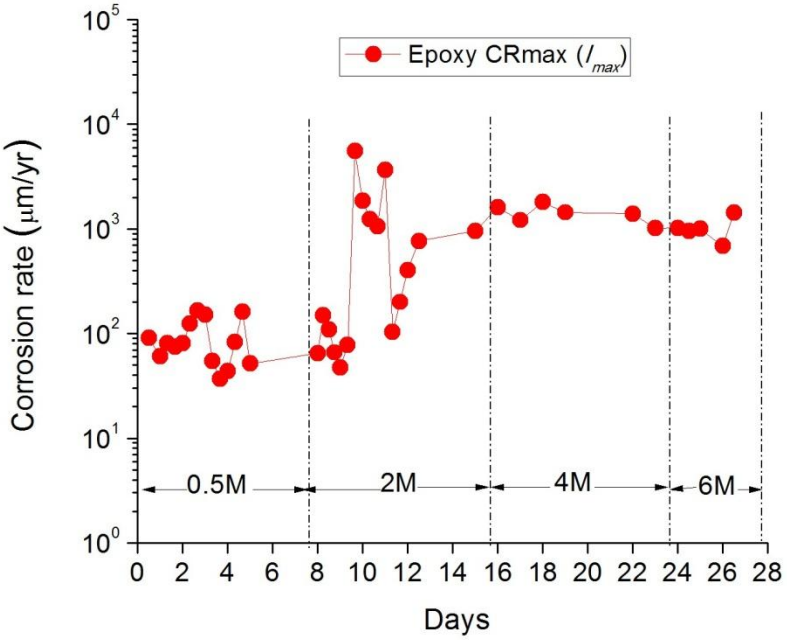

Fig. 4.14 CR_{max} of Cu in NaCl solution obtained using epoxy coated PCB-based MAS.

The CR_{max} of Cu obtained from epoxy coated PCB-based MAS in Fig. 3.14 remained in the range of ~150 μm/yr for eight days. When the solution concentration was changed from 0.5M to 2M the CR_{max} increased to ~200 μm/yr. There was a rapid increase in CR_{max} on Day 10 onwards to ~8000 μm/yr. This high rate however, decreased back to ~200 μm/yr rising again to remain ~1000 μm/yr until Day 28. The change in concentartion is barely detected after Day 16. This trend shows that epoxy functions properly by protecting the Cu traces against corrosion for 10 days until 2M NaCl solution. After that its performance is compromised which is apparent by sudden increase of CR_{max} on Day 10.

4.2.1.4 Comparison of Three Conformal Coatings

The mentioned results of three conformal coatings are compared in Fig. 4.15.

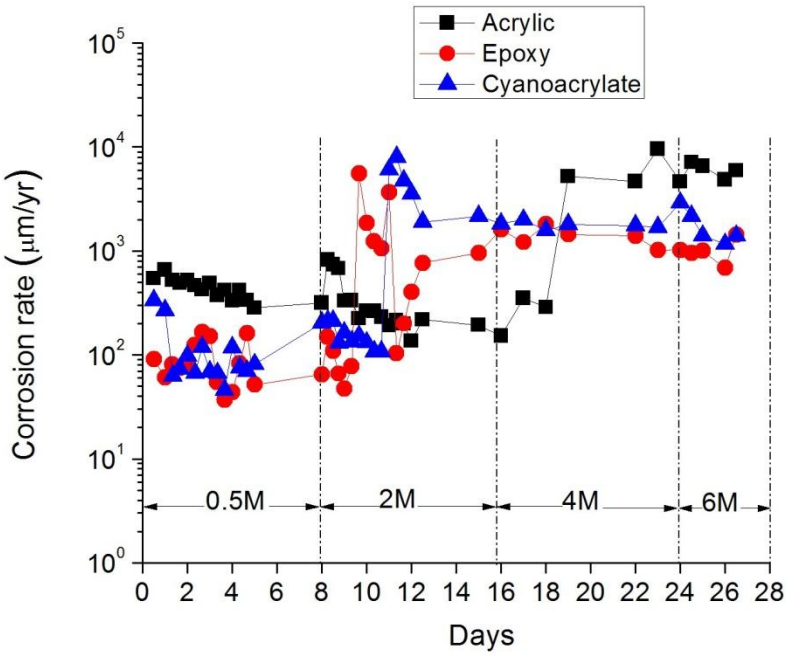

Fig. 4.15 Comparison of all three conformal coated PCB-based MAS results in NaCl solution.

In this comparison it is clearly seen that epoxy and cyanoacrylate initially inhibited corrosion which resulted in ~50% lower CR_{max} as compared to the acrylic coated PCB-based MAS. This inhibition property of cyanoacrylate and epoxy lasted for 10 and 11 days respectively. After that the sudden increase of data points suggest that the Cu traces were not properly protected by the two respective coatings which resulted in very high CR_{max}. Acrylic conformal coating on the other hand, did not inhibit corrosion but it worked efficiently until Day 18. After that there was a sudden increase in the CR_{max} which was not proportionate with the previous increases. This shows that although cyanoacrylate and epoxy inhibits corrosion which can prolong the sensor life but 2M NaCl solution is the maximum concentration that these conformal coatings can resist until ~10 days. Acrylic although does not inhibits corrosion but its protection propety for Cu traces against corrosion is 44% longer than the former two coatings. It also can

withstand upto 4M NaCl solution which is highly corrosive. Therefore, cyanoacrylate and epoxy can prolong sensor lifetime by inhibiting corrosion but their failure limit is 2M NaCl solution. Acrylic, however does not inhibit corrosion but it can withstand upto 4M NaCl solution.

4.2.2 Effects Observed in HCl Solution

4.2.2.1 Acrylic Conformal Coating

Anodic currents obtained from acrylic coated PCB-based MAS in HCl solution are shown in Fig. 4.16. E1 and E2 produced the maximum anodic currents. Fig. 4.17 shows the CR_{max} obtained using acrylic coated PCB-based MAS and graph of CR_{max} (3σ) is shown in Appendix A4.

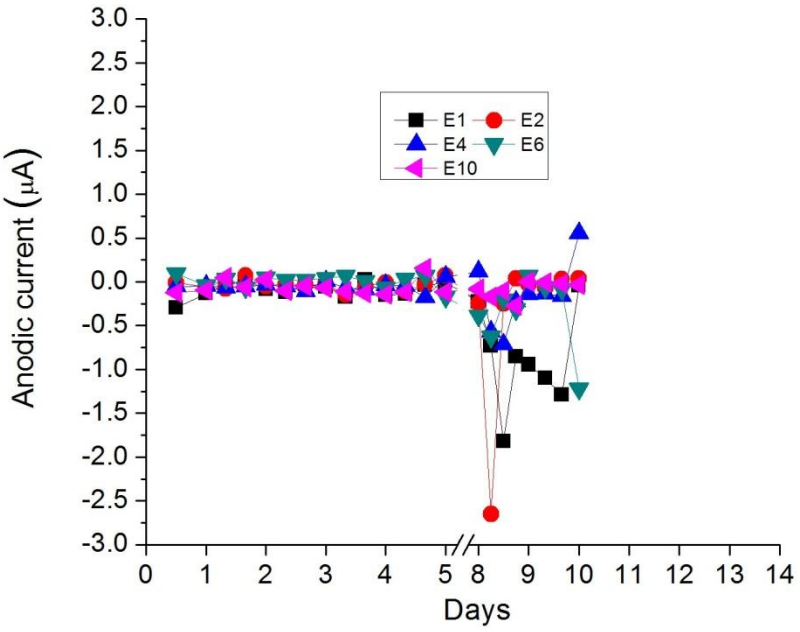

Fig. 4.16 Anodic currents of acrylic coated PCB-based MAS tested in HCl solution.

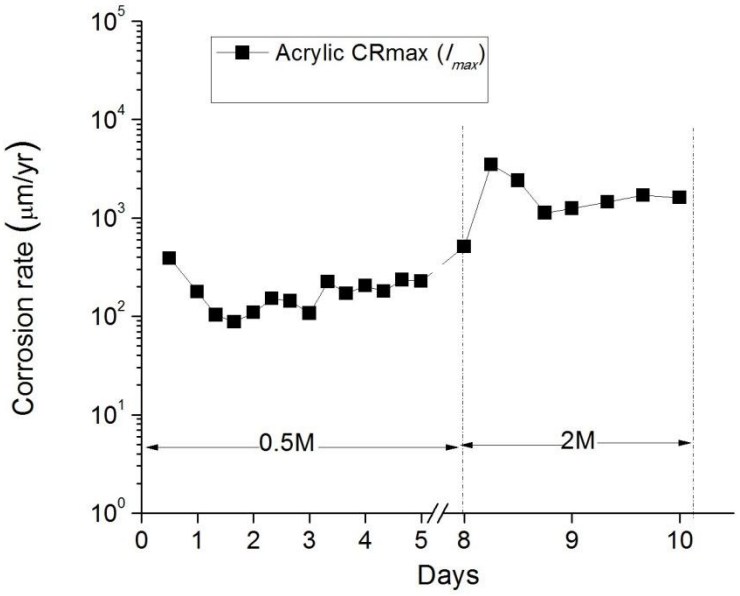

Fig. 4.17 CR_{max} of Cu in HCl solution obtained using acrylic coated PCB-based MAS.

As shown in Fig. 4.17, the CR_{max} of Cu in 0.5 HCl started with ~400 μm/yr and stabilizes at ~200 μm/yr. The initial high CR_{max} is expected due to the polished bare Cu electrodes reacting with the corrosive solution. The CR_{max} remained ~200 μm/yr for seven days indicating that the electrochemical process between Cu and HCl has reached equilibrium. On Day 8 the HCl concentration was changed from 0.5M to 2M. As expected the MAS produces a high CR_{max} of ~3500 μm/yr settling to ~2000 μm/yr till Day 9, indicating that it detected the increased intensity of the corrosive environment. On Day 10, however, all the electrodes were consumed by the corrosive acidic solution as seen in Fig. 4.18. The thickness of the electrodes consumed by the corrosive solution in nine days is calculated by averaging the deduced corrosion rates and it comes out to be ~14.5 μm. The actual thickness of the electrodes was ~16 μm. Since the calculated thickness is based on average corrosion rates ,therefore a difference of ~1.5 μm can be seen. However, the close agreement between the electrode thickness consumed by the corrosive solution and the actual electrode thickness suggests that the deduced CR_{max} is correct.

Fig. 4.18 Acrylic coated PCB-based MAS after 10 days exposure to HCl solution.

4.2.2.2 Cyanoacrylate Conformal Coating

Fig. 4.19 shows the anodic currents obtained from cyanoacrylate coated PCB-based MAS. E10 dominated all the anodic currents by producing maximum anodic current. The CR_{max} obtained from cyanoacrylate coated PCB-based MAS is plotted in Fig. 4.20 and graph of CR_{max} (3σ) is shown in Appendix A5.

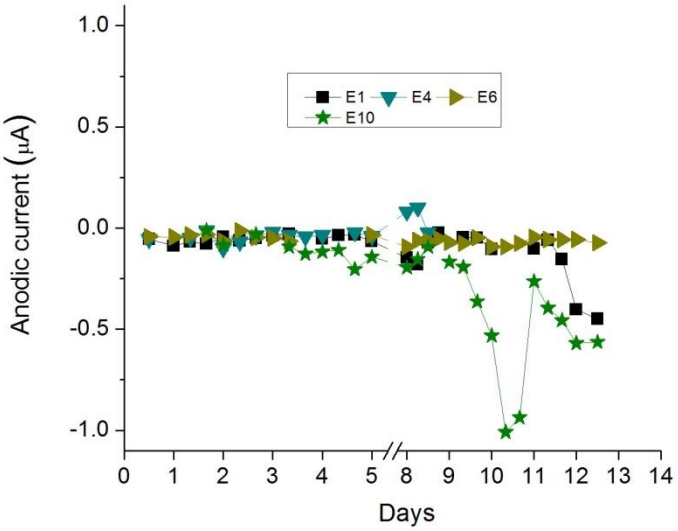

Fig. 4.19 Anodic currents of cyanoacrylate coated PCB-based MAS tested in HCl solution.

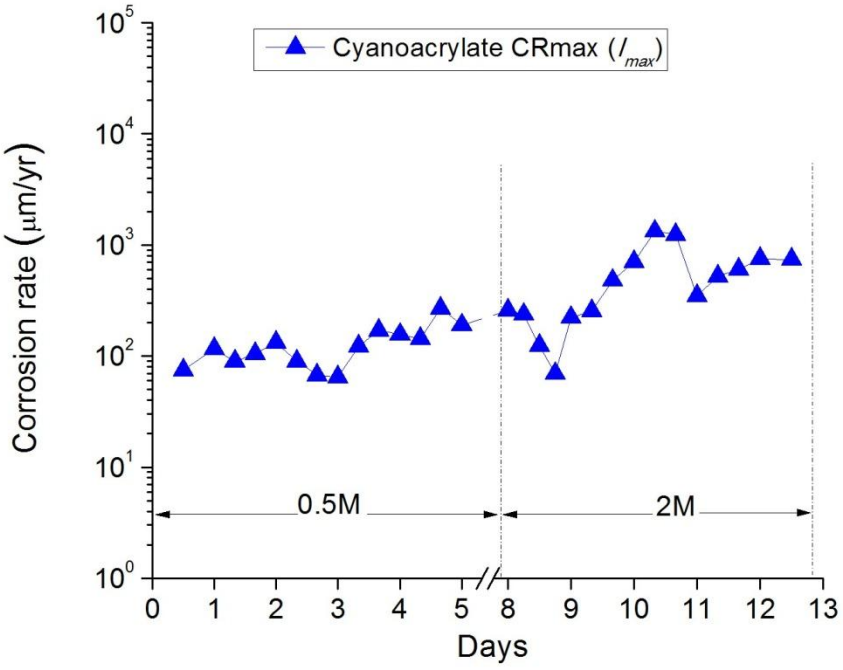

Fig. 4.20 CR_{max} of Cu in HCl solution obtained using cyanoacrylate coated PCB-based MAS.

In Fig. 4.20, the CR_{max} of Cu in 0.5M HCl solution started with ~100 µm/yr and remained in the range of ~60 µm/yr to ~200 µm/yr in the time period of seven days. The change in concentration of HCl solution from 0.5M to 2M did not produce much effect on the CR_{max} either. However, on Day 10 there was an increase in the CR_{max} rising to ~1000 µm/yr but it again dropped to ~600 µm/yr until Day 13 when the electrodes of the PCB-based MAS were consumed completely by the 2M HCl solution as seen in Fig. 4.21.

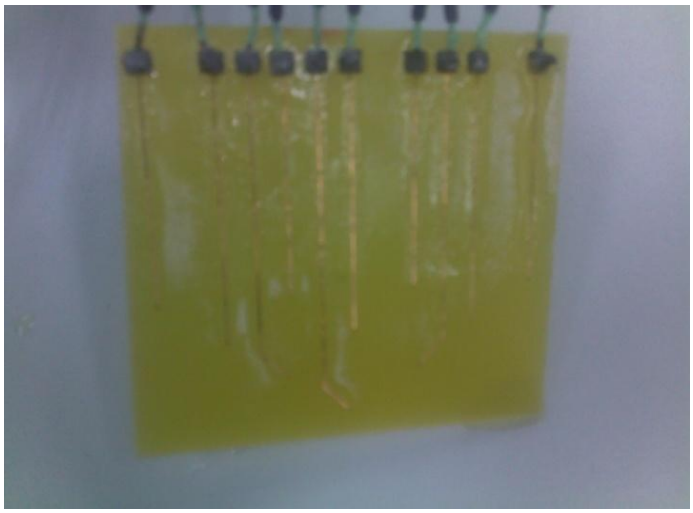

Fig. 4.21 Cyanoacrylate coated PCB-based MAS after 13 days exposure to HCl solution.

4.2.2.3 Epoxy Conformal Coating

Fig. 4.22 shows the anodic currents obtained from epoxy coated PCB-based MAS. E2 and E10 showed the maximum anodic currents. The CR_{max} obtained using epoxy coated PCB-based MAS is shown in Fig. 4.23 and graph of CR_{max} (3σ) is shown in Appendix A6.

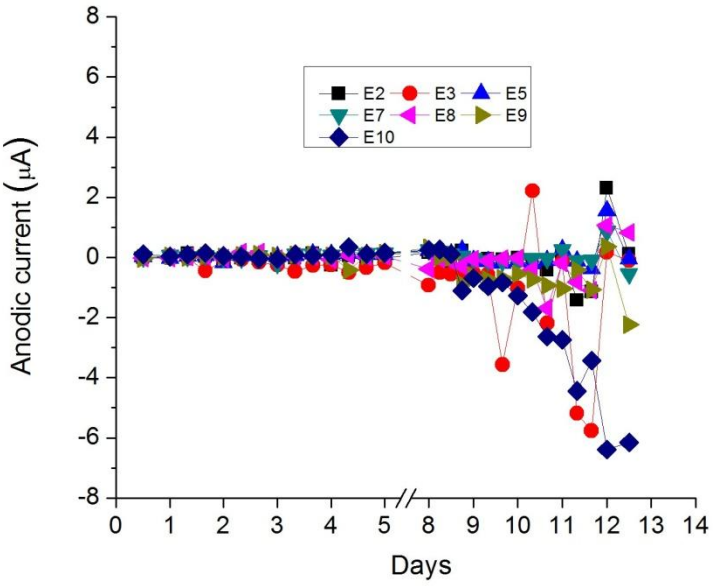

Fig. 4.22 Anodic currents of epoxy coated PCB-based MAS tested in HCl solution.

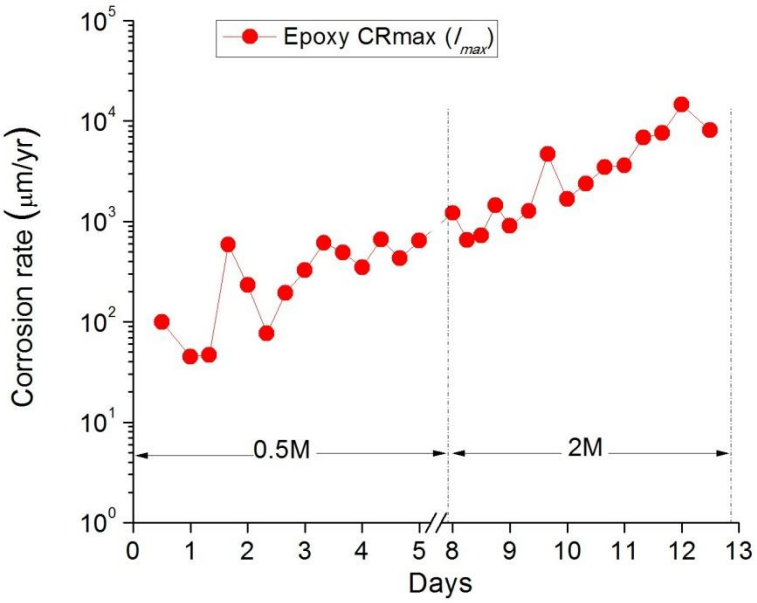

Fig. 4.23 CR_{max} of Cu in HCl solution obtained using epoxy coated PCB-based MAS.

Fig. 4.23 shows the CR_{max} obtained from PCB-MAS coated with epoxy conformal coating, the CR_{max} started from ~100 µm/yr and settles around ~50 µm/yr. After Day 1 the CR_{max} fluctuates and shows an increasing trend. Even the change in concentration of the HCl solution on Day 8 is barely detected and the CR_{max} continues to fluctuate until Day 9. There is a constant increase in CR_{max} Day 9 onwards until Day 12. On Day 9 visual inspection showed that epoxy started to peel off exposing the underlying Cu traces as shown in Fig. 4.24. It is believed that this could have resulted in the extremely high CR_{max} observed from Day 10 onwards. This peeling off of epoxy could also explain the fluctuations in CR_{max} after Day1. This is because the peeling off was visible on Day 9 but the process may have started much earlier with corrosive solution seeping under the epoxy coating, and the fluctuations suggest it may be after Day 1.

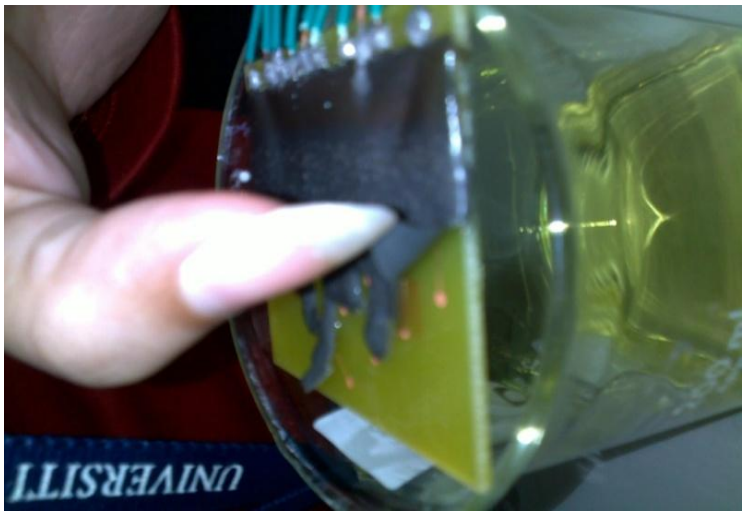

Fig. 4.24 Epoxy chipping off on Day 9 exposing the Cu traces.

4.2.2.4 Comparison of Three Conformal Coatings

Fig. 4.25 shows the comparison of the corrosion rates obtained from PCB-based MAS coated with acrylic and epoxy conformal coatings

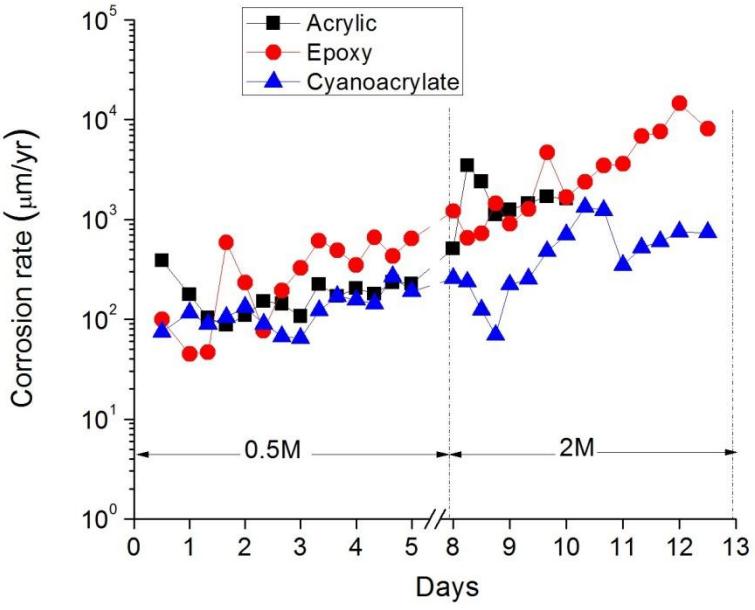

Fig. 4.25 Comparison of all three conformal coated PCB-based MAS results in HCl solution.

On Day 1 the CR_{max} of epoxy coated MAS is ~300 µm/yr below than that of acrylic, while cyanoacrylate also maintains a lower steady graph as compared to acrylic suggesting that epoxy and cyanoacrylate were inhibiting corrosion. However, as the peeling process of epoxy started the CR_{max} increased and fluctuated and showed an increasing trend through out the two week period. Cyanoacrylate steadily inhibited corrosion even the change in solution concentration did not produce much effect as seen in the graph on Day 8. However, it is seen that on Day 10 cyanoacrylate gave slightly higher CR_{max} but again returned to a lower value of ~600 µm through out until Day 13 when the electrodes were completely consumed. Another interesting point is the lifetime of the sensor. It is clearly shown in Fig. 4.23 that the lifetime of PCB-based MAS coated with epoxy and cyanoacrylate is 30% more than the one coated with acrylic due to the inhibition property of former two coatings.

4.2.3 Comparison with EIS Results

In this work EIS was used to obtain corrosion rate of Cu in the same concentrations of corrosive solutions in which PCB-based MAS was tested. Same FR486 UV copper clad laminate board was in EIS measurements which was used to make PCB-based MAS. Since EIS provides estimated corrosion rates, it is usually slightly higher than the real time corrosion rates. Nonetheless, the estimated corrosion rate that can be obtained in almost a minute from EIS can provide some indication of the accuracy of our sensor. The highest CR_{max} obtained from each PCB-based MAS in each concentration in section 4.2 is compared with EIS corrosion rates in that concentration. This way the comparison would be between the corrosion rates obtained from PCB-based MAS and the ones obtained from EIS. Since each PCB-based MAS was coated with a different conformal coating the comparison will also show the effect of the coatings on the results of PCB-based MAS. Summary of this comparison in shown in Table 4.1.

Table 4.1 Comparison of PCB-based MAS and EIS corrosion rates.

Solution	Concentration	Acrylic CR (µm/yr)	Cyanoacrylate CR (µm/yr)	Epoxy CR (µm/yr)	EIS CR (µm/yr)
NaCl	0.5M	~500	~300	~150	664
	2M	~900	~8000	~8000	1811
	4M	~9000	~1500	~1000	5124
	6M	~7000	~3000	~1000	11117
HCl	0.5M	~400	~100	~1000	1213
	2M	~3500	~1000	~10000	5937

As seen in Table 4.1, in 0.5M NaCl the acrylic coated PCB-based MAS gave ~500 µm/yr as the highest CR_{max} while cyanoacrylate and epoxy provided relatively lower CR_{max} of ~300 µm/yr and ~150 µm/yr respectively. If compared, these three results lie in the same range as that of EIS corrosion rate. However, the low corrosion rates by cyanoacrylate and epoxy clearly indicates the corrosion inhibition property of both coatings. In 2M NaCl, it is observed that cyanoacrylate and epoxy coating failed to protect the Cu traces, which resulted in high corrosion rates of ~8000 µm/yr. Whereas, acrylic remained intact in 2M NaCl providing comparable results with EIS. However, acrylic coating failed to provide protection to Cu traces in 4M NaCl. The corrosion rates of cyanoacrylate and epoxy are in the range of EIS results in 4M and 6M concentartions but they cannot be believed as realiable due to the failure of two coatings observed at 2M concentration.

In 0.5M HCl solutions acrylic and cyanoacrylate coated PCB-based MAS provided comparable CR_{max} with EIS corrosion rates. In addition, the inhibition property of cyanoacrylate can be seen by lower CR_{max} of ~100 µm/yr. However, as discussed in previous section epoxy could not withstand the HCl solution and chipped off exposing the Cu traces (see Fig. 4.23 and Fig.4.24), resulting in high corrosion rates. In 2M HCl, acrylic and cyanoacrylate provided a CR_{max} of ~3500 µm/yr and ~1000 µm/yr respectively which lie in the same range as that of EIS corrosion rate. Epoxy maintained the same trend of very high CR_{max} in 2M concentration as well clearly showing its ineffectiveness in HCl solution.

4.3 Reliability and Repeatability of PCB-based MAS

The third experimental setup was run to test the reliability and repeatability of PCB-based MAS. In order to check reliability, three samples of PCB-based MAS with Cu traces covered with acrylic conformal coating were tested in 3% wt sea salt solution. The solution concentration was changed from 3% wt to 9% wt sea salt solution on Day 8. The repeatability is checked by comparing the CR_{max} obtained from these three samples with the already obtained CR_{max} of Cu in 3% wt sea salt solution in the first experiment.

4.3.1 Sample 1

Fig. 4.26 shows the anodic currents obtained from sample 1 of PCB-based MAS tested in 3% wt sea salt solution. E10 produced the maximum anodic current. The CR_{max} calculated using this maximum anodic current is shown in Fig. 4.27. the graph showing CR_{max} (3σ) is plotted in Appendix A7).

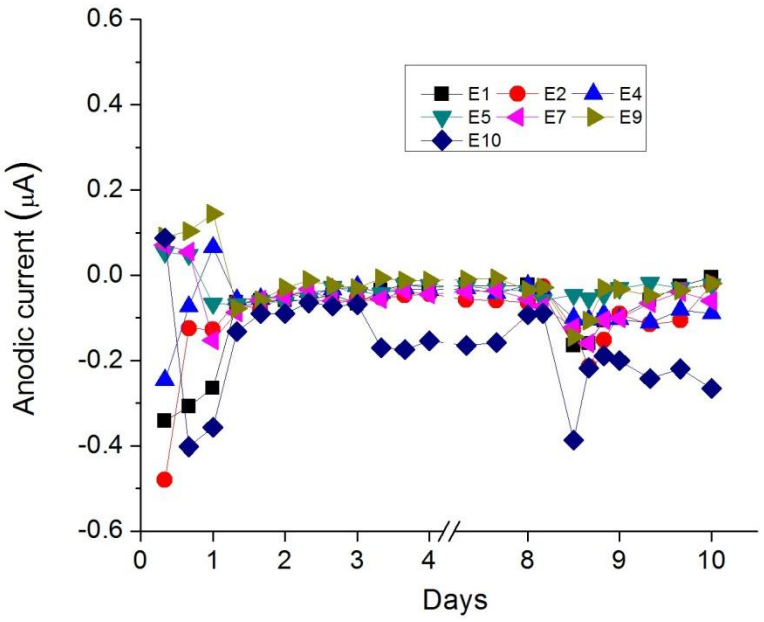

Fig. 4.26 Anodic currents of sample 1 of PCB-based MAS tested in sea salt solution.

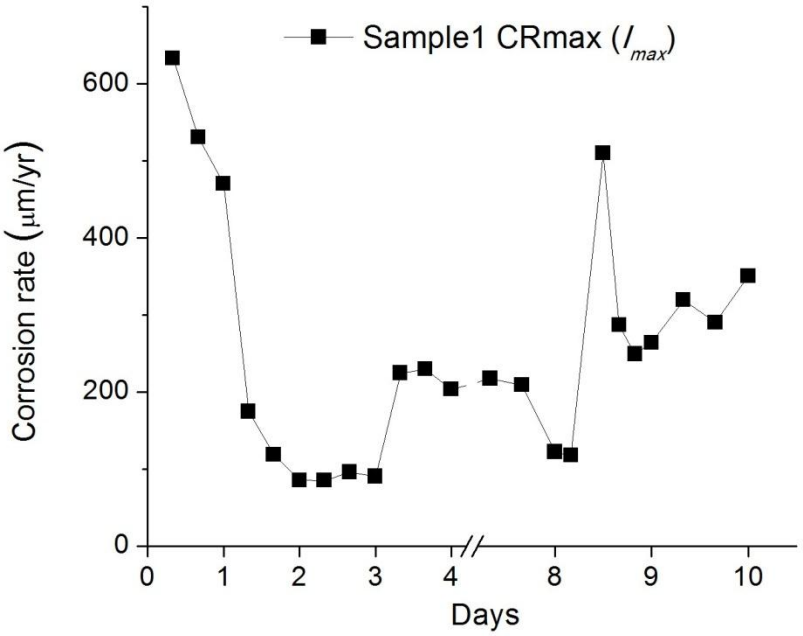

Fig. 4.27 CR_{max} obtained from sample 1.

4.3.2 Sample 2

Fig. 4.28 shows the anodic currents obtained from sample 2 of PCB-based MAS tested in 3% wt sea salt solution. E1 produced the maximum anodic current. The CR_{max} calculated using this maximum anodic current is shown in Fig. 4.29. Graph of CR_{max} (3σ) is shown in Appendix A8.

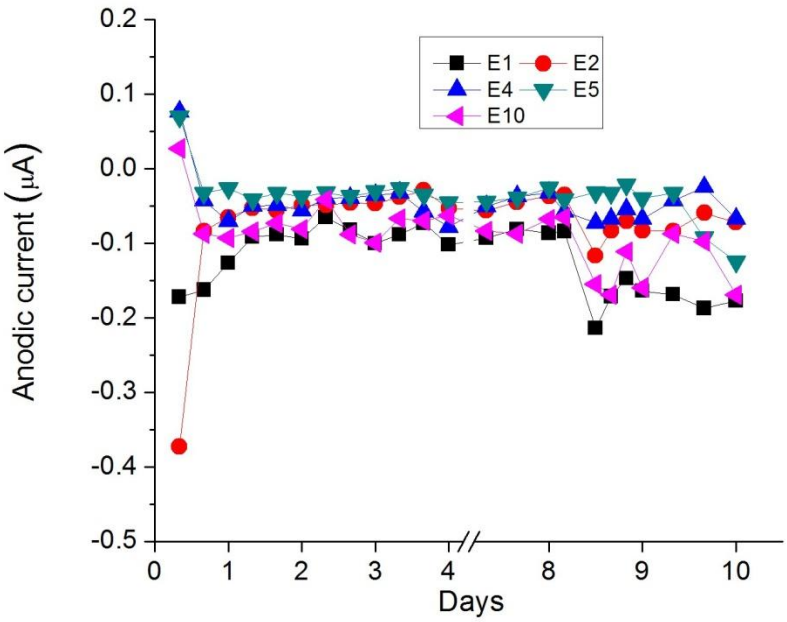

Fig. 4.28 Anodic currents of sample 2 of PCB-based MAS tested in sea salt solution.

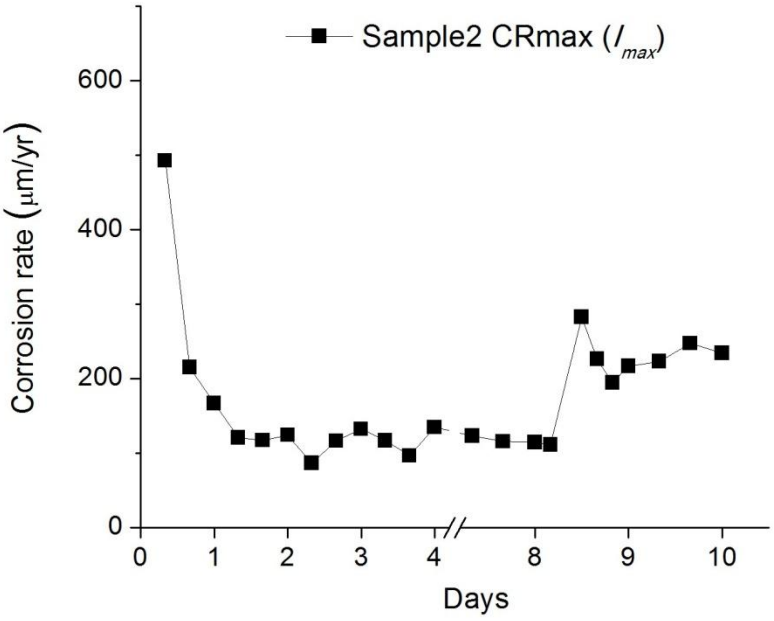

Fig. 4.29 CR_{max} obtained from sample 2.

4.3.3 Sample 3

Fig. 4.30 shows the anodic currents obtained from sample 3 of PCB-based MAS tested in 3% wt sea salt solution. E5 produced the maximum anodic current. The CR_{max} calculated using this maximum anodic current is shown in Fig. 4.31. Graph of CR_{max} (3σ) is shown in Appendix A9.

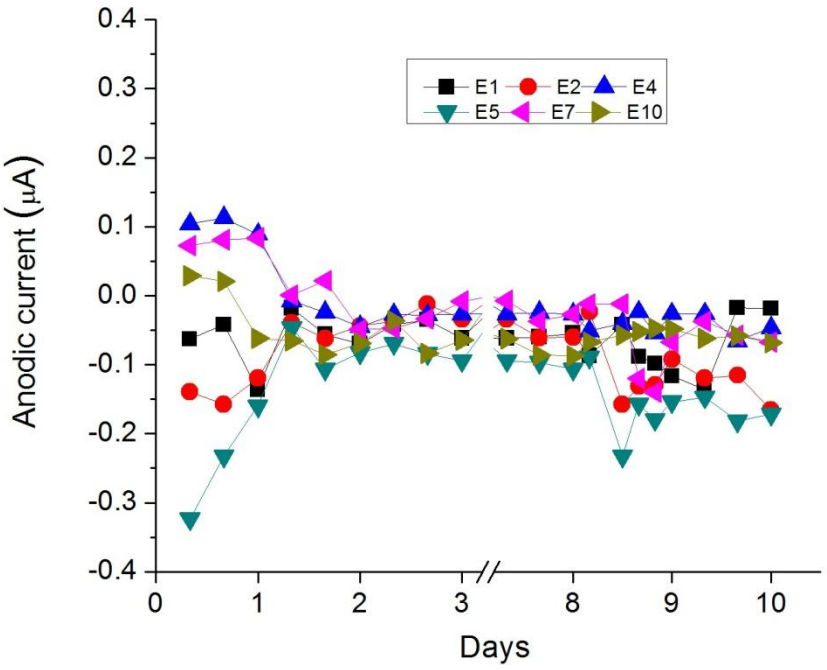

Fig. 4.30 Anodic currents of sample 3 of PCB-based MAS tested in sea salt solution.

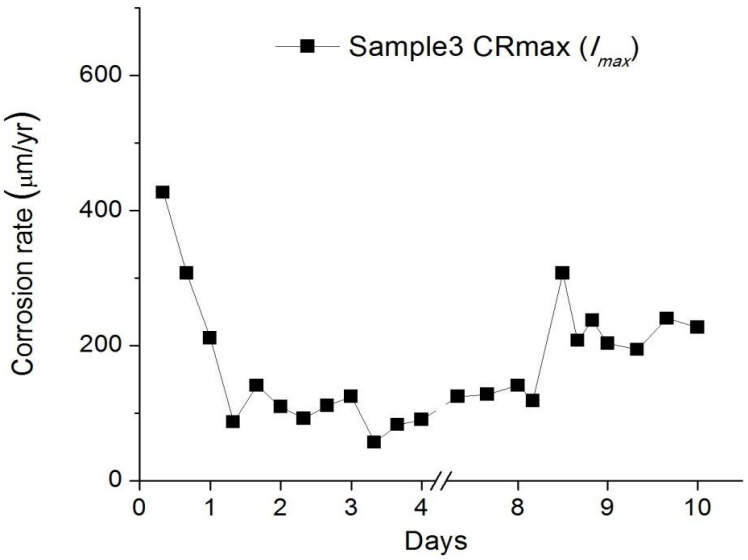

Fig. 4.31 CR_{max} obtained from sample 3.

4.3.4 Reliability

Fig. 4.32 shows the comparison of CR_{max} of Cu in sea salt solution obtained from three samples of PCB-based MAS. Reliability of PCB-based MAS is assessed by calculating the correlation between CR_{max} of the three tested samples. Correlation is a very useful statistical parameter used to measure the relationship between two variables. It is represented by correlation coefficient, r. For two set of data e.g. X and Y, r is the sum of the differences between values of X and the mean of X divided by the standard deviation of X, times the sum of the differences between values of Y and the mean of Y divided by the standard deviation of Y, all divided by the number of sample minus 1. The value of r is from -1 to 1. If r = -1, then that means the set of correlated data is opposite to each other. If r = 1, this means that the data completely match each other [42], and if r = 0 then that means no correlation exixts between the set of data. Therefore, the more r is closer to one the more two set of data are closely matched to each other. In our case since all the matched set of data was positive or the values were above zero, therefore, the range of r considered was from 0 to 1. Table 4.2 shows the correlation coefficient calculated among the three samples. It is calculated for CR_{max} of each sample after Day 1 because it is

known that the first few values of CR_{max} are due to the bare polished Cu electrodes touching the corrosive solution.

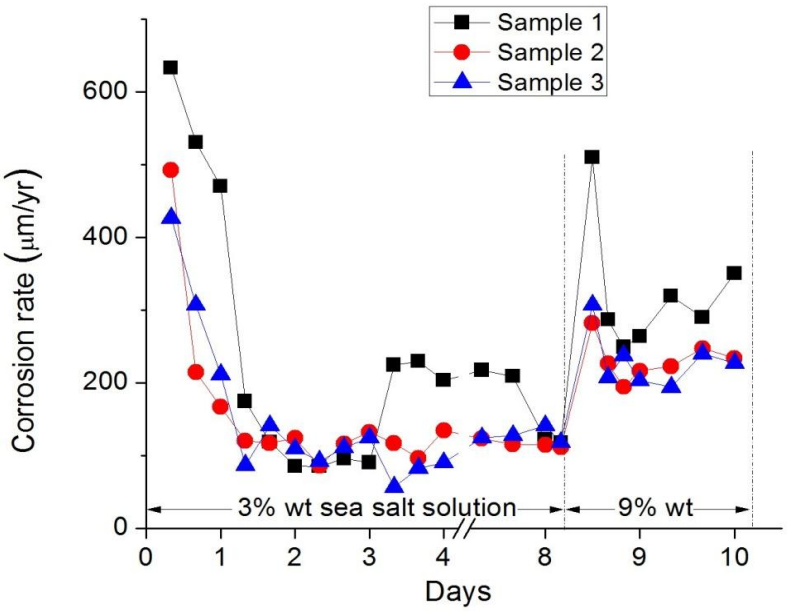

Fig. 4.32 CR_{max} comparison of three samples to verify reliability.

Table 4.2 Correlation among three samples of PCB-based MAS is calculated by finding the correlation coefficient to check reliability of PCB-based MAS.

Sample	Correlation Coefficient (r)
Sample 1-Sample 2	0.85
Sample 1-Sample3	0.76
Sample 2-Sample3	0.93

Although the graphs in Fig. 4.32 appears in close agreement however, it is only after statistical analysis that we can determine the real degree of compatibility of these graphs. As mentioned earlier Table 4.2 show the correlation coefficient calculated for each sample. The correlation was calculated between the CR_{max} of sample 1 and sample 2 and it resulted in r = 0.85. Similarly, between sample 1 and sample 3, r = 0.76 and between sample 2 and sample 3, the r = 0.93. The correlation of sample 1 and sample 3 is

acceptable however, it is slightly lower than the other two correlations. This can be attributed to the slight rise of CR_{max} of sample 1 on Day 3 onwards. This slight rise can be due to any experimental setup upset or a very small puncture in the acrylic conformal coating which was not visible or detected during pre-test examination.

The correlation coefficients for three samples in Table 4.2 show that all three samples provided CR_{max} in the same range which shows that PCB-based MAS can produce reliable results.

4.3.5 Repeatability

Fig. 4.33 shows the CR_{max} obtained from three mentioned samples plotted in comparison with reference data points which is the CR_{max} of the first experiment (see section 4.1.2 and Fig. 4.6). In order to check the repeatability of PCB-based MAS the obtained CR_{max} from each sample is correlated with the CR_{max} of reference sample in Fig. 4.33. The resultant correlation coefficients are shown in Table 4.3.

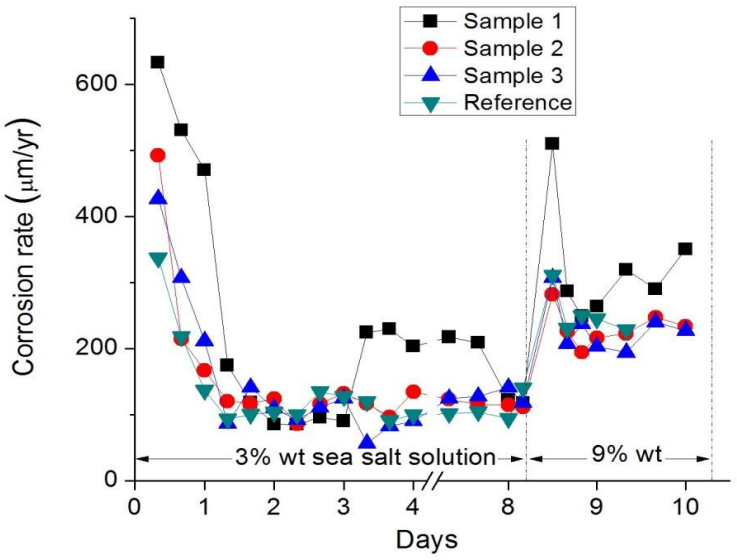

Fig. 4.33 CR_{max} comparison of three samples with a reference graph to verify repeatability.

Table 4.3 Correlation of three samples of PCB-based MAS with a reference sample is calculated by finding the correlation coefficient to check repeatability of PCB-based MAS.

Sample	Correlation Coefficient (r)
Sample 1-Ref	0.78
Sample 2-Ref	0.95
Sample 3-Ref	0.92

As seen in the Table 4.3 the correlation of sample 1 with the reference results is r = 0.78. In addition, the correlation coefficient of sample 2 and sample 3 with reference graph is r = 0.95 and r = 0.92 respectively. The sample 1 produced repeatable results however, slightly less repeatable than sample 2 and sample 3 due to the slightly higher CR_{max} observed on Day 3 onwards explained in the previous section. The close to 1 value of correlation coefficients for all three samples suggest that PCB-based MAS can produce repeatable results.

CHAPTER 5

CONCLUSION AND RECOMMENDATIONS

5.1 Conclusion

A planar PCB-based MAS for corrosion monitoring is developed in this work. It is fabricated using typical PCB processes. It works on the same working principle as that of CMAS with the exception of being planar and miniaturized. Once fabricated, this PCB-based MAS with Cu traces covered with acrylic conformal coating was tested in sea salt solution and it provided acceptable corrosion rates with published data. In addition, it detected the change in the corrosive environment when solution concentration was changed from 3% wt to 6% wt and 9% wt sea salt solution.

It was observed through initial characterization that the Cu traces in PCB-based MAS must be shielded against corrosive solution in order to get desirable results. Therefore, three types of conformal coatings namely; acrylic, cyanoacrylate and epoxy were used to cover the Cu traces of PCB-based MAS and then tested in NaCl and HCl solution. In NaCl solution, it is found that acrylic protects Cu traces efficiently until 18 days and can resist a concentration of 4M NaCl solution. Cyanoacrylate and epoxy on the other hand, inhibits corrosion, a property which can be used to prolong sensor life but can resist a concentration of maximum 2M NaCl. After this concentration, cyanoacrylate and epoxy fail to protect the Cu traces against corrosive solution. Although acrylic does not provide inhibition of corrosion but it is more resistant against NaCl solution at higher concentrations (until 4M). If less than 2M concentrations of NaCl are used then cyanoacrylate and epoxy function properly also providing corrosion inhibition which can be helpful in prolonging sensor life. In HCl solution, it is shown that the PCB-based MAS is a robust sensor that can work in a highly corrosive environment. However, its

lifetime is short due to the limited thickness of the sensing electrodes. If acrylic is used as a conformal coating, the MAS may only last barely more than a week but the corrosion rate deduced is within an acceptable range. However, if cyanoacrylate and epoxy is used, the PCB-based MAS may last longer, but in case of epoxy it deduces a misleading corrosion rate. The misleading corrosion rate is due to the peeling off of the epoxy coatings. To sum up, PCB-based MAS can work in both acidic (HCl) and basic (NaCl) environments and with an appropriate conformal coating, the accuracy and the lifetime of the sensor can be optimized.

It is very necessary to assess the ability of a sensor to produce reliable and repeatable results. Therefore, reliability and repeatability of PCB-based MAS was also checked in this work. By applying statistical analysis like finding the correlation coefficient among three samples of PCB-based MAS tested in sea salt solution, it was seen that PCB-based MAS can produce reliable results. In addition, the repeatability of PCB-based MAS is also checked against a reference data and again by using correlation, it was found that PCB-based MAS can produce repeatable results.

5.2 Recommendations

- Optimization of the PCB-based MAS, like introducing more electrodes, implementation of interfacing and read out circuit is suggested for future enhancement. As an alternative, dual layer PCB can be considered to avoid contact of Cu traces with the corrosive liquid without the need of a conformal coating altogether. Field tests like testing of PCB-based MAS in actual corrosive environments are also suggested for future work.
- There is a need to further study the effects of different conformal coatings on PCB-based MAS performance in detail. The adhesion of the epoxy coating including the adhering technique as well as the epoxy materials itself must be also studied in detail.
- Further miniaturization of the PCB-based MAS using CMOS compatible processes and using ideal metals as sensing elements should also be considered.

APPENDIX A

GRAPHS

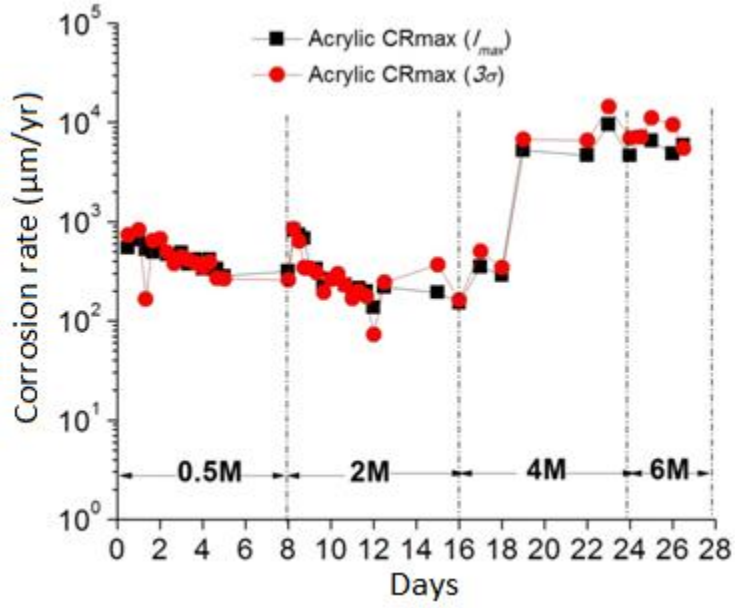

A1: Comparison of CR_{max} (I_{max}) and CR_{max} (3σ) obtained from acrylic coated PCB-based MAS in NaCl solution.

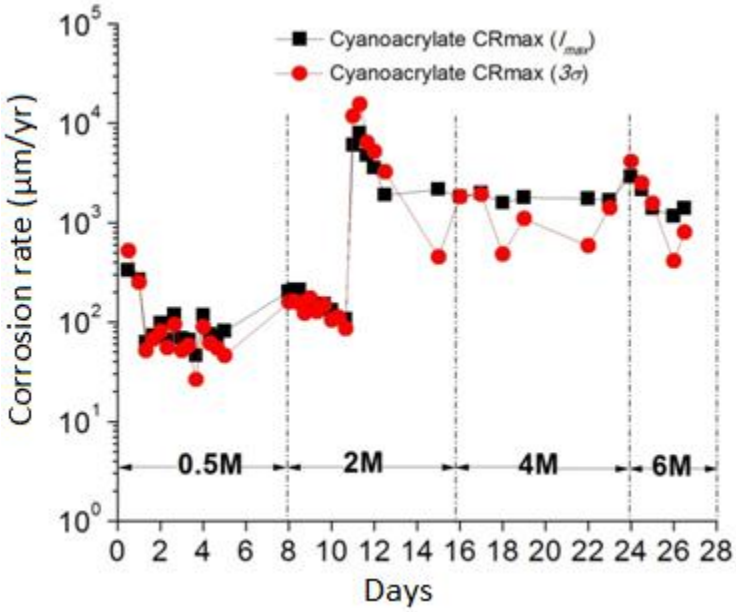

A2: Comparison of CR_{max} (I_{max}) and CR_{max} (3σ) obtained from cyanoacrylate coated PCB-based MAS in NaCl solution.

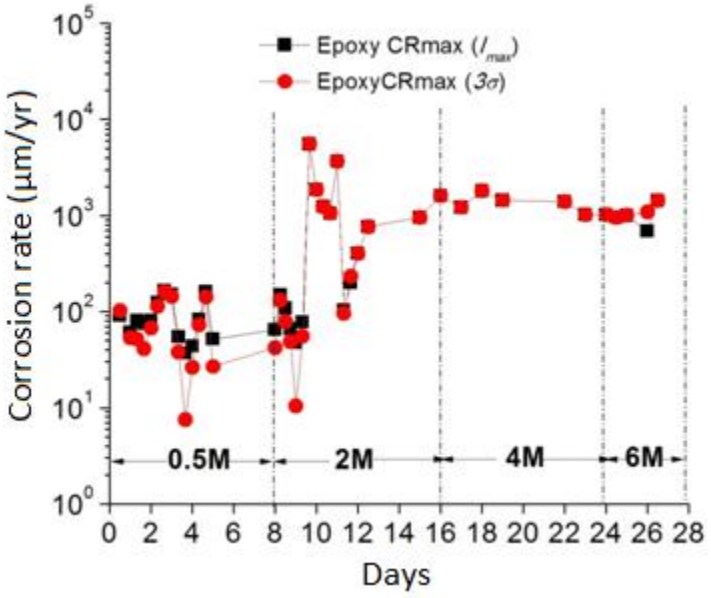

A3: Comparison of CR_{max} (I_{max}) and CR_{max} (3σ) obtained from epoxy coated PCB-based MAS in NaCl solution.

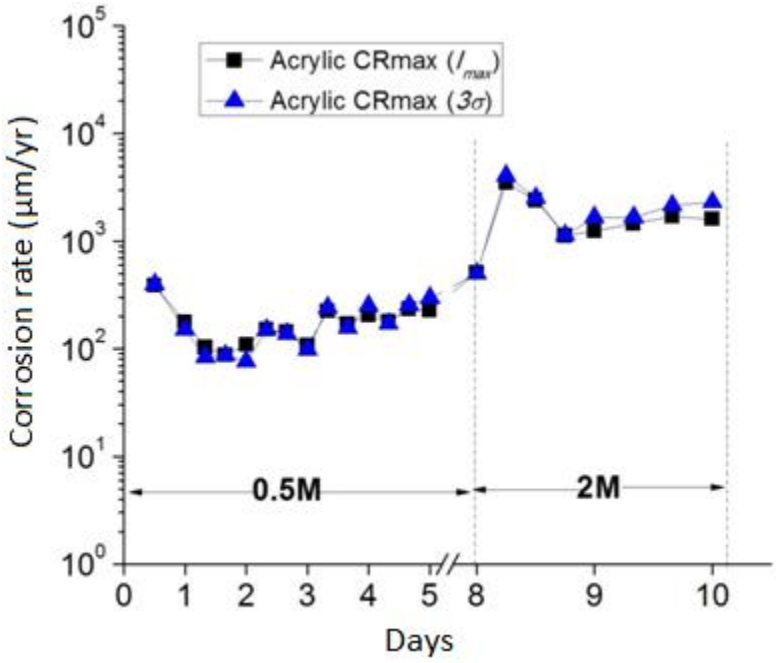

A4: Comparison of CR_{max} (I_{max}) and CR_{max} (3σ) obtained from acrylic coated PCB-based MAS in HCl solution.

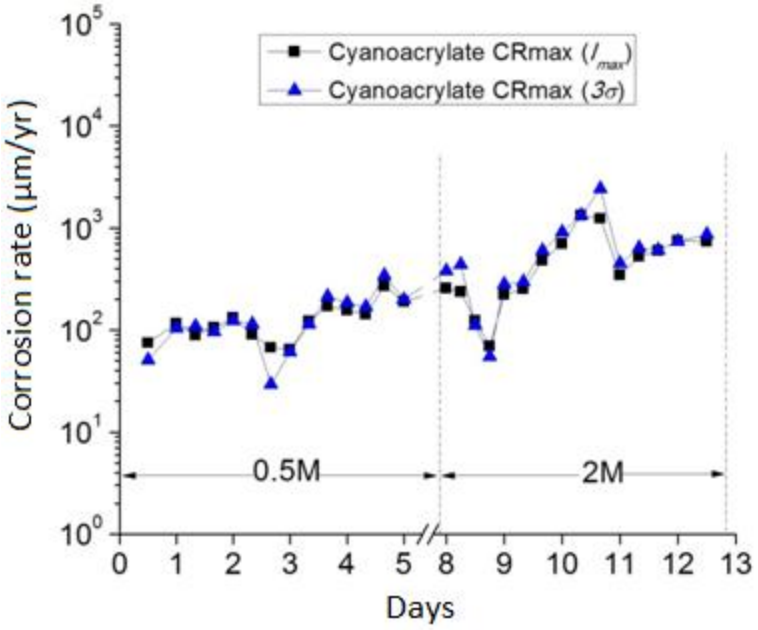

A5: Comparison of CR_{max} (I_{max}) and CR_{max} (3σ) obtained from cyanoacrylate coated PCB-based MAS in HCl solution.

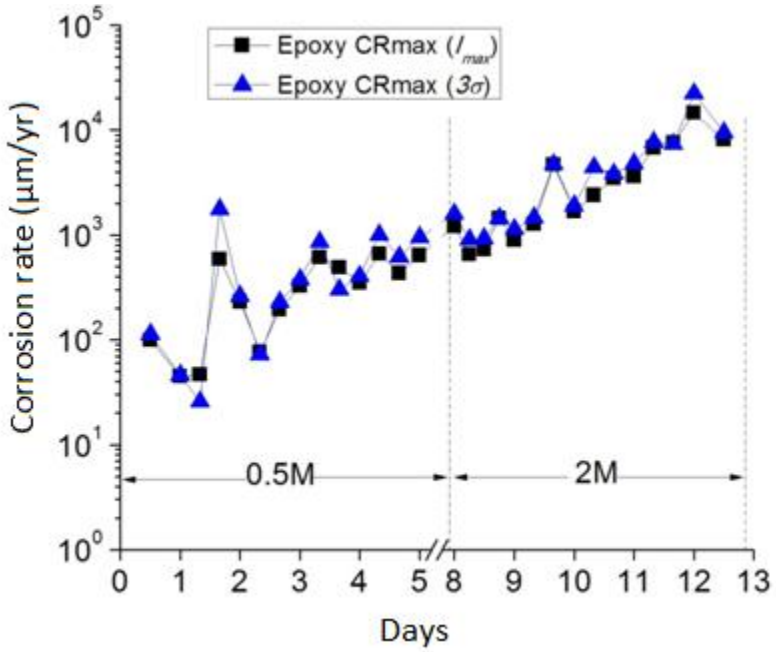

A6: Comparison of CR_{max} (I_{max}) and CR_{max} (3σ) obtained from epoxy coated PCB-based MAS in HCl solution.

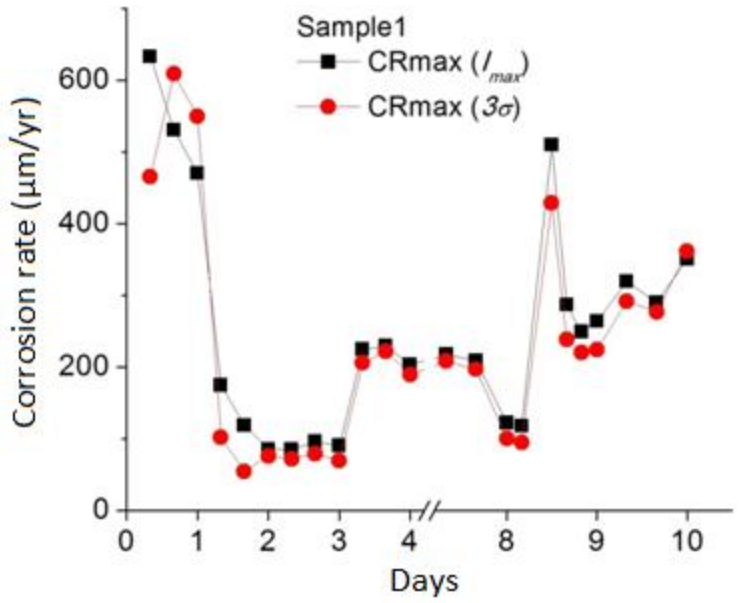

A7: Comparison of $CR_{max}(I_{max})$ and $CR_{max}(3\sigma)$ obtained from acrylic coated PCB-based MAS sample 1 tested in sea salt solution.

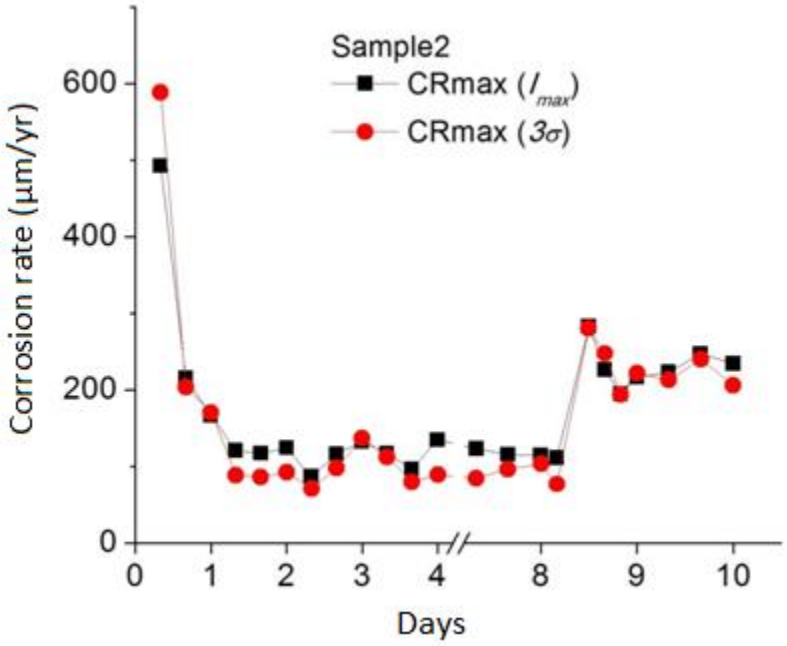

A8: Comparison of $CR_{max}(I_{max})$ and $CR_{max}(3\sigma)$ obtained from acrylic coated PCB-based MAS sample 2 tested in sea salt solution.

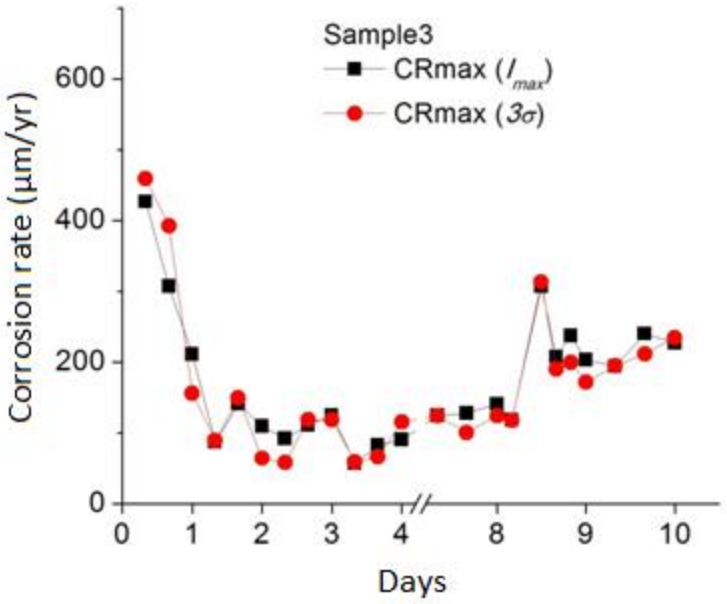

A9: Comparison of CR_{max} (I_{max}) and CR_{max} (3σ) obtained from acrylic coated PCB-based MAS sample 3 tested in sea salt solution.

REFERENCES

[1] Gretchen A. Jacobson, "A Natural but Controllable Process," MP editorial, *Supplement to Materials Performance*, pp. 3-3, 2002.

[2] G. H. Koch, M. P. H. Brongers, N. H. Thompson, Y. P. Virmani and J. H. Payer, "Corrosion Cost and Preventive strategies in the United States," FHWA-RD-01-156 (Springfield, VA: National Technical Information Service, 2001).

[3] R. Bolt, "Database Reflects Recent Trends in European Gas Pipeline Failures," *Oil and Gas Journals*, vol. 99, issue 1, January 01, 2001.

[4] R. Winston Revie, *Uhlig's Corrosion Handbook*, 2nd Ed., John Wiley & Sons, 2005.

[5] Pipeline Accident Report, "Natural Gas Pipeline Rupture and Fire Near Carlsberg, New Mexico August 19, 2000," National Transportation Safety Board, Washington, D.C, 2003.

[6] Einar Mattson, *Basic Corrosion Technology for Scientists and Engineers*, 2nd Ed., IOM Communications, 2001.

[7] Franklyn W. Pogge, *External Corrosion-Introduction to Chemistry*, 2nd Ed., American Water Works Association, 2004.

[8] Available: http://www.cdcorrosion.com/mode_corrosion/corrosion_uniform.htm

[9] Available: http://www.isa.org/Template.cfm?Section=Communities&template=/TaggedPage/DetailDisplay.cfm&ContentID=26843

[10] P. A. Schweitzer, *Corrosion Engineering Handbook*, Marcel Dekker, 1996.

[11] W. H. Ailor, *Handbook on Corrosion Testing and Evaluation*, Volume 1970, J. Wiley, 1971.

[12] Available: http://www.cosasco.com/corrosometer-internal-corrosion-monitoring-system-corrosometer-electronic-corrosion-control-probes-c-104_9-l-en.html

[13] R. Baboian, *Corrosion Tests and Standards: Application and Interpretation*, 2nd Ed., ASTM International, 2005.

[14] P. R. Roberge, *Handbook of Corrosion Engineering*, McGraw-Hill Professional, 2000.

[15] L. Yang, *Techniques for Corrosion Monitoring*, Woodhead Publishing Limited, 2008.

[16] Available: http://www.argentumsolutions.com/wiki/en/Polarization_Resistance_Technique

[17] G. Rocchini, "Corrosion Rate Monitoring by Linear Polarization Method," *Corrosion Science*, vol. 34, pp. 2031-2044, December 1993.

[18] M. Kouril, P. Novak and M. Bojko, "Limitations of the Linear Polarization Method to Determine Stainless Steel Corrosion Rate in Concrete Environment," *Corrosion Science*, vol. 28, pp. 220-225, March 2006.

[19] D. C. Silverman and J. E. Carrico, "Electrochemical Impedance Technique - A Practical Tool For Corrosion Prediction", *Corrosion*, vol. 44, pp. 280, 1988.

[20] P. R. Roberge, *Corrosion Inspection and Monitoring*, Wiley-Interscience, 2007.

[21] A. Groysman, *Corrosion for Everybody*, Springer, 2009.

[22] Dr. R.A. Cottis, "An Evaluation of Electrochemical Noise for the Estimation of Corrosion Rate and Type", *Corrosion/2006*, paper no. 06432, NACE international 2006.

[23] R. A. Cottis, "The Significance of Electrochemical Noise Measurements on Asymmetric Electrodes," *Electrochimica Acta*, vol. 52(27), pp. 7585-7589, 2007.

[24] S. CHO, J. Jungho PAK, J. HONG, Y. KIMPAK, "Fabrication of a Multi-Electrode Array DNA Sensor for Electrochemical Genotyping," *Journal of the Korean Society*, vol. 41, pp. 1054-1057.

[25] M. W. Jung, D. W. Kim, R. A. Jeong, H. C. Kim, "Needle-type Multielectrode Array Fabricated by MEMS Technology for the Hypodermic Continuous Glucose Monitoring System," 26th IEEE EMBS, San Francisco, CA, USA, September 1-5, 2004.

[26] P. Schiessl, United States Patent 5,015,355, "Corrosion Measuring Cell," May 14, 1991.

[27] L. Yang and N. Sridhar, "Coupled Multielectrode Array Systems and Sensors For Real Time Corrosion Monitoring – A Review," *Corrosion/2006*, paper no. 06681, NACE International 2006.

[28] Z. Qingdong, Z. Zhao, "Study of Anti-Contamination Performance of Temporarily Protective Oil Coatings Using Wire Beam Electrodes," *Corrosion Science*, vol. 44, pp. 2777-2787, 2002.

[29] Y. J. Tan, "Wire Beam Electrode: A New Tool for Studying Localised Corrosion and Other Heterogeneous Electrochemical Processes," *Corrosion Science*, vol. 41, pp. 229-247, 1999.

[30] L. Yang, N. Sridhar, and D. S. Dunn, "An In-Situ Galvanically Coupled Multielectrode Array Sensor for Localized Corrosion," *Corrosion*, vol. 58, pp. 1004-1014, 2002.

[31] L. Yang, N. Sridhar, C. Sean Brossia, Darrell S. Dunn, "Evaluation of the Coupled Multielectrode Array Sensor as a Real Time Corrosion Monitor," *Corrosion Science*, vol. 47, pp. 1794-1809, 2005.

[32] L. Yang and N. Sridhar, "Coupled Multielectrode Online Corrosion Sensor," *Materials Performance*, vol. 42, pp. 48-52, 2003.

[33] X. Sun, "Online Monitoring of Corrosion under Cathodic Protection Conditions Utilizing Coupled Multielectrode Array Sensors," *Corrosion/2004*, paper no. 04094, NACE international 2004.

[34] L. Yang and D. Dunn, "Evaluation of Corrosion Inhibitors in Cooling Water Systems Using a Coupled Multielectrode Array Sensor," *Corrosion/2002*, paper no. 02004, NACE international 2002.

[35] L. Yang, N. Sridhar, and G. Cragnolino, "Comparison of Localized Corrosion of Fe-Ni-Cr-Mo Alloys in Concentrated Brine Solutions Using Coupled Multielectrode Array Sensors, " *Corrosion/2002*, paper no. 02545, NACE international 2002.

[36] X. Sun and L. Yang , "Real-Time Monitoring of Localized and General Corrosion Rates in Drinking Water Utilizing Coupled Multielectrode Array Sensors," *Corrosion/2006*, paper no. 06094, NACE international 2006.

[37] A. Anderko, N. Sridhar, C.S. Brossia, D.S. Dunn, L.T. Yang, B.J. Saldanha, S.L. Grise and M.H. Dorsey, "An Electrochemical Approach to Predicting and Monitoring Localized Corrosion in Chemical Process Streams," *Corrosion/2003*, paper no. 03375, NACE international 2003.

[38] C.S. Brossia and L. Yang , "Studies of Microbiologically Influenced Corrosion Using a Coupled Multielectrode Array Sensor," *Corrosion/2003*, paper no. 03575, NACE international 2003.

[39] X. Sun, "Real-Time Monitoring of Corrosion in Soil Utilizing Coupled Multielectrode Array Sensors." *Corrosion/2005*, paper no. 05381, NACE international 2005.

[40] N. Sridhar, L. Yang and F. Song, "Application of Multielectrode Array Sensor to Study Dew point Corrosion in High Pressure Natural Gas Pipeline Environments," *Corrosion/2006*, paper no. 06673, NACE international 2006.

[41] L. Yang and X. Sun, "A Method to Reduce the Internal Current Effect on Localized Corrosion Measurements with Coupled Multielectrode Array Sensor," *Corrosion/2008*, paper no. 08395, NACE international 2008.

[42] R. E. Walpole, R. Myers, S. L. Myers, *Probability and Statistics for Engineers & Scientists*, Pearson Prentice Hall, 2006.

[43] AL Williams, *Build Your Own Printed Circuit Board*, McGraw-Hill, 2004.

[44] J. Varteresian, *Fabricating Printed Circuit Boards*, Newnes, 2002.

[45] X. Sun and L. Yang, "Real-Time Monitoring of Localized and General Corrosion Rates in Simulated Marine Environments Using Coupled Multielectrode Array Sensors," *Corrosion/2006*, paper no. 06284, NACE international 2006.

[46] X. Sun and L. Yang, "Real Time Monitoring of Crevice Corrosion Propagation Rates in Simulated Seawater Using Multielectrode Array Sensors," *Corrosion/2006*, paper no. 06679, NACE international 2006.

[47] P. A. Schweitzer, *Corrosion Resistance Tables*, 4th Ed., Part C, P-Z, Marcel Dekker, Inc, 1995.